

**République Algérienne Démocratique Et Populaire**  
**Ministère de l'enseignement supérieur**  
**Et de la recherche scientifique**  
**Université Ferhat Abbas de Sétif-1-**



## **Thèse**

Présentée à la faculté des sciences  
Département d'informatique  
En vue de l'obtention du diplôme de

### **Doctorat en sciences**

#### **Ecole Doctorale**

Sciences et Technologies de l'Information et de la Communication  
Option : Ingénierie des systèmes informatiques

**Par**

M. Abdelouahab ATTIA

## **Thème**

**Fusion et fouille d'informations multimodales EEG/IRMf :  
application à l'étude de l'activité cérébrale**

Soutenu le : 03/03/2018 devant le jury compose de :

<b>Président :</b>	Mohamed SAIDI	MCA	Université Ferhat Abbas Sétif 1
<b>Rapporteur :</b>	Abdelouahab MOUSSAOUI	Prof.	Université Ferhat Abbas Sétif 1
<b>Examineurs :</b>	Salim CHIKHI	Prof.	Université Constantine 2
	Med Chaouki BATOUCHE	Prof.	Université Constantine 2
<b>Invités :</b>	Youssef CHAHIR	Prof.	U. de Caen basse-normandie
	Mohand Tahar KECHEDI	Prof.	U. Colledge Dublin, Irlande

## **Acknowledgement**

It is a great pleasure to thank many people who made this dissertation possible. My deepest gratitude goes to my supervisor Pr. Abdelouahab MOUSSAOUI for his encouragement, support and for his valuable comments that helped to improve my work. I have been fortunate to have a supervisor who gave me the freedom to explore on my own and at the same time the guidance to recover when my steps faltered. I would like also to thank the examiners who saved no time to read and evaluate this work. I owe my gratitude to my colleague Miss FAID for reading and correcting parts of my thesis and for the countless hours of supporting and caring she provided. Special thanks go to all my friends for their support. I wish also to thank my entire family for providing a supporting environment for me.

Abdelouahab ATTIA  
July 1, 2017

## ***Table of contents***

<b>List of abbreviation</b>	<b>I</b>
<b>List of Figures</b>	<b>II</b>
<b>List of Tables</b>	<b>IV</b>
<b>Introduction</b>	<b>1</b>
<b>I Chapter I <i>Functional Cerebral Anatomy Mapping</i></b>	<b>5</b>
<b>I.1 Introduction</b>	<b>5</b>
<b>I.2 Brain structure</b>	<b>6</b>
I.2.1 The cerebrum	7
I.2.2 Brainstem	9
I.2.3 The cerebellum	11
<b>I.3 Basic Functions of the brain</b>	<b>11</b>
<b>I.4 Metrics of the cerebral activity</b>	<b>12</b>
I.4.1 Electrical activity	12
I.4.2 Metabolic activity	14
I.4.3 Metabolic activity and the cerebral blood flow	16
I.4.4 Couplings between different activities	16
<b>I.5 Exploration techniques of the brain activity</b>	<b>17</b>
I.5.1 Magnetic Resonance Imaging (MRI)	18
I.5.2 EEG (Electroencephalography)	19
I.5.3 Magneto encephalography (MEG)	20
I.5.4 Functional Magnetic Resonance Imaging (fMRI)	21
<b>I.6 Characteristics of the different functional exploration techniques</b>	<b>22</b>
I.6.1 Spatial resolution	22
I.6.2 Temporal Resolution	22
I.6.3 Invasiveness degree	22
<b>I.7 Conclusion</b>	<b>23</b>
<b>II Chapter II <i>EEG Electroencephalogram</i></b>	<b>25</b>
<b>II.1 Introduction</b>	<b>25</b>
<b>II.2 Historical background</b>	<b>25</b>
<b>II.3 Conducting and performing an experiment EEG</b>	<b>27</b>
<b>II.4 The rhythmic activity</b>	<b>29</b>
<b>II.5 Evoked Potentials</b>	<b>31</b>

II.5.1	The visual evoked potentials (VEP)	32
II.5.2	The Auditory Evoked Potentials (AEP)	33
II.5.3	Somatosensory evoked potentials (SEPs)	34
II.5.4	Cognitive Evoked Potentials:	35
<b>II.6</b>	<b>Types of electrodes</b>	<b>36</b>
<b>II.7</b>	<b>Position of electrodes</b>	<b>36</b>
<b>II.8</b>	<b>EEG principales</b>	<b>38</b>
<b>II.9</b>	<b>Conclusion</b>	<b>39</b>
<b>III</b>	<b>Chapter III <i>Functional Magnetic Resonance Imaging</i></b>	<b>40</b>
<b>III.1</b>	<b>Introduction</b>	<b>42</b>
<b>III.2</b>	<b>History of fMRI</b>	<b>43</b>
<b>III.3</b>	<b>Magnetic resonance imaging (MRI)</b>	<b>44</b>
<b>III.4</b>	<b>Blood oxygen level dependent (BOLD)</b>	<b>46</b>
<b>III.5</b>	<b>Hemodynamic Response Function</b>	<b>48</b>
<b>III.6</b>	<b>Guidelines and Design for fMRI experimental studies</b>	<b>49</b>
III.6.1	Blocked design:	50
III.6.2	Event-related design	51
III.6.3	Mixed designs	52
	Blocked Design	53
	Event- related design	53
	Mixed design	53
<b>III.7</b>	<b>The Principle of The General Linear Model</b>	<b>53</b>
<b>III.8</b>	<b>Conclusion</b>	<b>55</b>
<b>IV</b>	<b>Chapter IV State of the art of EEG/ fMRI information fusion</b>	<b>57</b>
<b>IV.1</b>	<b>Introduction</b>	<b>57</b>
<b>IV.2</b>	<b>State of the art of fMRI-EEG fusion methods</b>	<b>58</b>
IV.2.1	Asymmetric approaches	59
IV.2.2	EEG/fMRI SYMMETRICAL FUSION	62
<b>IV.3</b>	<b>EEG FMRI INFORMATION FUSION APPLICATIONS</b>	<b>63</b>
IV.3.1	fMRI-EEG in epilepsy	63
IV.3.2	fMRI- EEG for sleep study	64
IV.3.3	fMRI-EEG and evoked potentials	64
IV.3.4	fMRI-EEG and spontaneous rhythmic activity	65
<b>IV.4</b>	<b>CONCLUSION</b>	<b>65</b>

<b>V</b>	<b>Chapter V Contribution: Dempster Shafer theory in EEG/ fMRI information fusion</b>	<b>66</b>
<b>V.1</b>	<b>Introduction</b>	<b>67</b>
<b>V.2</b>	<b>An Efficient fMRI Data Clustering Method using PHA Algorithm and Dynamic Time Warping</b>	<b>68</b>
V.2.1	Dynamic time warping	68
V.2.2	PHA algorithms	70
V.2.3	Proposed approach	71
V.2.4	Experiment and result	72
<b>V.3</b>	<b>Approaches based on Dempster-Shafer Theory of Evidence</b>	<b>79</b>
V.3.1	The Dempster-Shafer Theory of Evidence	80
V.3.2	Proposed Method	82
V.3.3	Computing the basic belief assignments and the belief measure	83
V.3.4	Separating the activated voxels from the non-activated ones	84
<b>V.4</b>	<b>Evaluation metrics and proposed algorithm</b>	<b>85</b>
V.4.1	Evaluation metrics	85
V.4.2	Algorithm DS-fMRI analysis	86
<b>V.5</b>	<b>Results and Discussion</b>	<b>86</b>
V.5.1	Artificial data	87
V.5.2	Real fMRI Dataset	89
V.5.3	Comparison with GLM method	91
<b>V.6</b>	<b>EEG fMRI fusion using Dempster shafer theory</b>	<b>94</b>
V.6.1	JointICA method	94
V.6.2	The Proposed Method	95
V.6.3	Experiments and results	97
<b>V.7</b>	<b>Conclusion</b>	<b>106</b>
	Final conclusion	<b>108</b>
	References	

---

## *List of abbreviation*

<b>Abbreviation</b>	<b>Meaning</b>
AEP	<i>Auditory Evoked Potentials</i>
ATP	<i>Adenosine triphosphate</i>
BBA	<i>Basic Belief Assignment</i>
Bel	<i>Belief function</i>
BOLD	<i>Blood Oxygen Level Dependent</i>
CBF	<i>Cerebral blood flow</i>
CEP	<i>Cognitive Evoked Potentials</i>
CNS	<i>central nervous system</i>
CT	<i>Computerized Tomography</i>
DS	<i>Dempster Shafer theory</i>
DSM	<i>Distributed Source Model</i>
dHb	<i>deoxygenated hemoglobin</i>
ECD	<i>Equivalent Current Dipole</i>
EEG	<i>Electroencephalogram, Electroencephalography</i>
ERP	<i>Event-Related Potentials</i>
EPSP	<i>excitatory postsynaptic potential</i>
EP	<i>evoked potentials</i>
Ft	<i>femto-tesla</i>
fMRI	<i>Functional Magnetic Resonance</i>
FAR	<i>false activation rate</i>
FDR	<i>False Discovry Rate</i>
FDI	<i>Freedom from Distractibility Index</i>
GLM	<i>General Linear Mode</i>
GE	<i>gradient-echo</i>
GSM	<i>Gaussian Source Model</i>
HbO <sub>2</sub>	<i>oxygenated hemoglobin</i>
HDR	<i>Hemodynamic response</i>
HRF	<i>Hymodynamic Response function</i>
IBS	<i>Intermittent Bright Simulation test</i>
ICA	<i>Independent Component Analysis</i>
IED	<i>Interictal Epileptic Discharges</i>
IPSP	<i>inhibitory postsynaptic potential</i>
ISI	<i>inter-stimulus interval</i>
MEG	<i>Magneto encephalography</i>
MRI	<i>Magnetic Resonance Imaging</i>
NMR	<i>Nuclear Magnetic Resonance</i>
PHA	<i>potential-based hierarchical agglomerative</i>
PET	<i>Positron Emission Tomography</i>
PI	<i>Plausibility</i>
PCA	<i>Principal Component Analysis</i>
RCBF	<i>regional Cerebral Blood Flow</i>
ROC	<i>receiver operating characteristics curve</i>
RF	<i>Radiofrequency</i>
ROI	<i>region of interest</i>
SQUID	<i>Superconducting Quantum Interference Devices</i>
SEPs	<i>Somatosensory evoked potentials</i>
SNR	<i>signal to noise ratio</i>
SPM	<i>Statistical Parametric Mapping</i>
TAR	<i>True activation rate</i>
TR	<i>Repetition time</i>
TE	<i>time to echo</i>
VEP	<i>Visual Evoked Potentials</i>
2D	<i>Two dimension</i>
3D	<i>Three dimension</i>

## List of figure

FIGURE I-1 LOCALIZATION OF HUMAN HIGHER MENTAL FUNCTIONS AS PHRENOLOGY .....	6
FIGURE I-2 THE TWO CEREBRAL HEMISPHERES AND THEIR FUNCTIONS .....	7
FIGURE I-3 THE SUBDIVISIONS OF THE CORTEX.....	9
FIGURE I-4 : THE BRAINSTEM STRUCTURE .....	10
FIGURE I-5 : (A) THE CEREBELLUM (B) POSTER INFERIOR VIEW.....	11
FIGURE I-6 BASIC STRUCTURE OF A TYPICAL NEURON (SANEI & CHAMBERS, 2013).....	13
FIGURE I-7 : FUNCTION OF NEURONS(F.WENDLING,2008) .....	14
FIGURE I-8:THE DEFERENT MEASURES OF BRAIN FUNCTION .....	15
FIGURE I-9 MAGNETIC RESONANCE IMAGING.....	19
FIGURE I-10 : ELECTROENCEPHALOGRAPHY .....	19
FIGURE I-11:MEG MACHINE.....	21
FIGURE I-12 A COMPARATIVE DIAGRAM OF THE DIFFERENT FUNCTIONAL BRAIN IMAGING TECHNIQUES. ....	23
FIGURE II-1: THE FIRST EEG RECORDED BY HENS BERGER AND PUBLISHED IN 1929(BERGER, 1929) .....	26
FIGURE II-2 : EEG TECHNIQUE .....	26
FIGURE II-3 : TYPES OF SIGNALS.....	30
FIGURE II-4: STUDY OF VISUAL EVOKED POTENTIAL.....	33
FIGURE II-5 STUDY OF AUDITORY EVOKED POTENTIAL.....	34
FIGURE II-6 STUDY OF SOMATOSENSORY EVOKED POTENTIAL.....	34
FIGURE II-7 POSITION OF ELECTRODES IN 10/20 SYSTEM ( <a href="http://www.bem.fi/book/13/13.htm">HTTP://WWW.BEM.FI/BOOK/13/13.HTM</a> ).....	37
FIGURE IV-1: NUMBER OF PAPERS PER YEAR FOR EEG, FMRI, AND THEIR FUSION ( <a href="https://scholar.google.fr">HTTPS://SCHOLAR.GOOGLE.FR</a> ) .....	57
FIGURE IV-2: FORMALIZATION OF THE EEG/FMRI COUPLING-UNCOUPLING (DAUNIZEAU, LAUFS, & FRISTON, 2009) .....	59
FIGURE IV-3: INTEGRATION OF DATA- AND MODEL-DRIVEN FUSIONS. DESPITE THE INDIVIDUALITY BETWEEN THEM, THE INTEGRATION AND INTERACTION OF DATA AND MODEL MIGHT BE PROMISING FOR EEG/FMRI FUSION. ....	63
FIGURE IV-4: THE APPROACHES OF EEG-FMRI TECHNIQUES FUSION.....	64
FIGURE V-1: THE OPTIMAL WARPING PATH ALIGNING TIME SERIES.....	69
FIGURE V-2: FLOWCHART OF THE PROPOSED APPROACH .....	72
FIGURE V-3 SIMULATED FMRI DATA .....	73
FIGURE V-4:FAR AND TAR ON REGIONS STARTED BY K= 3 REGIONS TO K= 10.....	74
FIGURE V-5: TRUE AND FALSE ACTIVATION RATES BY T-TEST METHOD.....	74
FIGURE V-6: (A) ACTIVATED AREAS OF SIMULATED DATA BY PROPOSED APPROACH. (B) ACTIVATED AREAS OF SIMULATED DATA BY T-TEST .....	75
FIGURE V-7: (A) THE VARIOUS FALSE ACTIVATION RATE. – (B) THE TRUE ACTIVATION RATE .....	77
FIGURE V-8: FALSE DISCOVERY RATE AND TRUE ACTIVATION RATE OBTAINED BY GLM METHOD .....	78
FIGURE V-9: TRUE AND FALSE ACTIVATION RATE OBTAINED BY T-TEST METHOD.....	78
FIGURE V-10: SOME SLICES ILLUSTRATE THE ACTIVATED REGIONS: A) ACTIVATED AREAS BY T-TEST METHOD B) THE RESULT IS GENERATED BY GLM METHOD; C)THE RESULT OBTAINED BY PROPOSED METHOD .....	79
FIGURE V-11: BASICS MEASURES OF DEMPSTER-SHAFER THEORY OF EVIDENCE .....	81
FIGURE V-12: FLOWCHART OF THE PROPOSED MODEL FMRI ANALYSIS WITH DS.....	83

FIGURE V-13: FLOWCHART OF THE PROPOSED MODEL OF HRF.....	83
FIGURE V-14: THE PROJECTION OF THE INTRODUCED MODEL WITH FMRI DATA .....	84
FIGURE V-15: THE FMRI ARTIFICIAL DATA .....	87
FIGURE V-16: THE ACTIVATE VOXELS WITH FMRI ARTIFICIAL DATA BY THE PROPOSED APPROACH .....	88
FIGURE V-17: THE PLOTS SHOW THE FALSE ACTIVATION RATE AND THE POSITIVE ACTIVATION RATE USING BELIEF THRESHOLD.....	88
FIGURE V-18: TRUE AND FALSE ACTIVATION RATES BY T-TEST METHOD.....	89
FIGURE V-19: THE HISTOGRAM OF BELIEF MEASURES .....	90
FIGURE V-20: FALSE AND TRUE ACTIVATION RATE OBTAINED BY DS METHOD .....	91
FIGURE V-21: THE OBTAINED RESULT WITH GLM METHOD .....	92
FIGURE V-22: FALSE DISCOVERY RATE AND TRUE ACTIVATION RATE OBTAINED BY GLM METHOD .....	93
FIGURE V-23: SOME SLICES ILLUSTRATE THE ACTIVATED REGIONS: .....	933
FIGURE V-24: FIGURE SHOWS HOW TO DETECT THE INTERVAL A.....	94
FIGURE V-25: FMRI-EEG FUSION USING JOINT ICA. ....	95
FIGURE V-26: FLOWCHART OF THE EEG-FMRI DATA FUSION BASED ON DS METHODTHE CHART IS DEVIDED INTO THREE MAIN PARTS. THE BLUE PART CONCERNS PREPROCESS AND MODELSISATION OF FMRI DATA.THE GREEN PART IS ABOUT EEG DATA AND CONTAINS THREE STEPS; PREPROCESSING, EXTRACTING ERP AND MODELSISATION BY DS. THE RED PART DENOTES CLUSTERING EXTRACT ACTIVATED VOXELS .....	97
FIGURE V-27 : ARTIFICIAL FMRI AND ERP DATA(A) ARTIFICIAL FMRI DATA CONTAINS EIGHT SOURCES WHERE EACH SIMULATED SOURCE IS OF $60 \times 60$ IMAGE WITH 100 POINT COURSES (B) THE SELECTED ERP SIMULATION DATA GENERATED BY USING( EQUA. V.24) .....	99
FIGURE V-28: A) THE OBTAINED RESULTS BY PROPOSED METHOD THAT SHOW THE MIXED AREA IN EACH SLICE .....	100
FIGURE V-29: VARIATION IN THE NUMBER OF VOXELS BY NUMBER MAX OF CLUSTERS K.....	102
FIGURE V-30 :(A) ACTIVATED AREAS IN SOME SLICES BY PROPOSED METHOD (B) ACTIVATED AREAS IN SLICES BY JOINTICA METHOD, PROVIDED IN BOTH COULOR RED AND BLUE FOR EACH COMPENENT .....	103
FIGURE V-31 : NUMBER OF TRUE POSITIVES (A) AND FALSE POSITIVES (B) USING DIFFERENT THRESHOLDS (MEEG,FMRI). ....	104
FIGURE V-32 THE NUMBER OF (A) FALSE ACTIVATION RATE (B) BY USING SEVERAL P-VALUES .....	105
FIGURE V-33: ROC CURVES FOR THE COMPARISON OF JOINTICA AND THE INTRODUCED METHOD .....	105



## *List of table*

TABLE I-1: THE PRINCIPAL FUNCTIONS OF THE FOUR LOBES.....	8
TABLE I-2: THE STRUCTURE OF THE BRAINSTEM .....	10
TABLE II-1: TYPES OF EEG RECORDINGS .....	29
TABLE II-2: TYPICAL FREQUENCIES AND AMPLITUDES OF SYNCHRONIZED BRAINWAVES .....	30
TABLE II-3: TYPES OF CEREBRAL RHYTHMIC ACTIVITY .....	30
TABLE III-1: COMPARISON OF FMRI DESIGNS .....	53
TABLE V-1: AVERAGE OF TRUE ACTIVATION RATE AND FALSE ACTIVATION RATE OBTAINED BY APPLYING THE PROPOSED METHOD AND T-TEST METHOD TO THE ARTIFICIAL DATA SET .....	75
TABLE V-2 :AVERAGE OF TRUE ACTIVATION RATE AND FALSE ACTIVATION RATE OBTAINED BY APPLYING THE PROPOSED METHOD AND T-TEST AND GLM TO THE REAL DATA SET.....	78
TABLE V-3: AVERAGE OF TRUE ACTIVATION RATE AND FALSE ACTIVATION RATE OF THE DS METHOD AND T- TEST METHOD TO THE ARTIFICIAL DATA SET .....	89
TABLE V-4: AVERAGE OF TRUE ACTIVATION RATE AND FALSE ACTIVATION RATE OBTAINED BY APPLYING THE DS METHOD AND GLM TO THE REAL DATA SET .....	93
TABLE V-5: TRUE AND FALSE ACTIVATION RATES BY THE PROPOSED METHOD AND JOINTICA .....	101
TABLE V-6: AVERAGE OF TAR AND FAR OF THE PROPOSED METHOD AND JOINTICA TO THE SIMULATED DATASET. ....	101
TABLE V-7: RESULT OF $M_{EEG,FMRI}$ CLUSTERING BY PHA METHOD .....	102

# Introduction

---

The brain is the most complex fascinating portion of the human body. It has been a topic of interest for several centuries for both neuroscientists and philosophers. However, it is viewed until now as incomprehensible and needs further investigation to reveal its hidden secrets and to provide better understanding of its structure and function.

Localizing the brain function has been developed in the mid of 1800's by several clinicians such as Jackson and Broca (Finger, 2009). Typically, almost all the obtained information on the human brain was from subjects who had experienced severe head injuries, or who had a medical condition like mental disorders. Identifying to what extent the brain has been damaged and the degree of lost body function was a key element in deducing which area of the brain was in charge for which function. Sometimes, brutal neurological disorders were treated by taken away the brain areas. For instance, severe epilepsy was treated by splitting the corpus callosum which bonds the right and left cerebral hemispheres.

The recent advances in neuroimaging techniques have paved the way to better localize the extent of damage in patients' brain. Basically, the most common techniques used in exploring the brain are categorized into two main classes: (i) structural imaging modalities and (ii) functional imaging modalities. The earliest technique for imaging the brain structure was Computerized Tomography (CT) and recently a very useful tool has been developed, known as Magnetic Resonance Imaging (MRI). A variety of noninvasive functional neuroimaging techniques have been introduced to better examine the function of particular areas of the brain. Electroencephalography, known as (EEG), has been developed to provide a detailed study of the brain with new data on anatomical and functional correlation. EEG has gradually become a useful tool in revealing the secrets of the healthy brain functionality. Also, the emergence of Positron Emission Tomography (PET), Single Photon Emission Computed Tomography (SPECT), functional Magnetic Resonance Imaging (fMRI), and magnetoencephalography (MEG) has provided a shift in studying the brain and greatly improved our knowledge of brain function.

In the literature of exploring brain activity, both EEG and fMRI techniques have gained a considerable attention. These techniques have clearly shown their ability in measuring different attributes of brain function. On the one hand, EEG relies on measuring the electrical signals on the scalp of the patient resulting from responding to a stimulus. This technique provides high temporal resolution. On the other hand, fMRI depends on the principle of Blood Oxygenation Level Dependent, referred to as BOLD contrast, where the detection of the signal from desoxy-haemoglobin of venous blood enables to depict the brain active areas during the performance of a particular task. Due to the high spatial resolution it provides, fMRI has gradually become a useful tool in revealing a better insight to the brain activity and has been widely employed in various fields such as psychology, medicine...etc.

Although both fMRI and EEG separately have received a great attention of scientists, each of them suffers from some limitations. As regards fMRI, it is difficult to estimate the neural activity from hemodynamic response because fMRI data analysis relies on slow mechanisms such as blood flow, oxygen consumption and metabolism which yield only an indirect measure of evoked BOLD signals. Likewise, fMRI suffers from an ill-posed temporal inverse problem. On the other hand, the EEG modality suffers from spatial inverse problem. Besides, noise that results due to the unavoidable artefacts raised during the course of the experiment can completely obscure the signals detected by EEG and degrade the quality of the obtained images.

By combining fMRI and EEG modalities together, it has become possible to exploit the strengths and flaws of each modality. In line with this scope, several studies have been conducted on simultaneous EEG and FMRI data to provide a powerful technique capable to address the knowledge gap in the brain function research.

Simultaneous EEG-fMRI recording provides complementary information about the human systems, cognitive, and activities. EEG-fMRI applications are fast becoming a powerful paradigm to better understanding the nature of the cerebral activity with the enhanced spatiotemporal resolution it provides. More specifically, EEG-fMRI integration aims to pinpoint the neural sources activity for both diagnosis and presurgical planning. Primarily, both EEG and fMRI data measures the activity of neurons where the EEG is typical for the electrical activity and fMRI is concerned with the hemodynamic signal. It is worth to note that the evoked electromagnetic and metabolic responses which are

detected by both EEG and fMRI, are not essentially the result of the same primary neuronal processes.

In line with this scope, the focus of this thesis has been placed on EEG-fMRI fusion methods and techniques based on correlation. This work concentrates on how to fuse the different modalities and its application in times series dataset. It reveals what neuroimaging can provide to scientist and why simultaneous EEG-fMRI presents a challenge in EEG-fMRI fusion to explore brain functions and activities.

### Thesis Overview

The aim of this body of work is to produce a better understanding of the brain activity using simultaneous EEG-fMRI information fusion and data analysis. This knowledge is then employed in combining EEG and fMRI in such a way to obtain high quality results which in the future will allow yielding detailed exploration of neural activity and brain function. This project focuses on the EEG and fMRI modalities separately and combined EEG-fMRI data. The thesis is split into five chapters:

*Chapter one* aims to provide the reader with a brief review on the complex structure of the human brain. Also, it introduces the essential high functions of the brain in addition to the different measures of the brain functional activity. At last, it describes briefly the most common brain imaging techniques that have been developed so far in the literature.

*Chapter two* explores, in detail, the electroencephalography modality. At first, it sheds the light on the emergence of the EEG signals recordings to provide the unfamiliar reader with information background. Then, it describes how EEG experiments are conducted and how signal are recorded during the course of these experiments using different techniques. Also, this chapter considers rhythmic activity. The evoked potentials with its main types including the Visual Evoked Potentials (VEP), the Auditory Evoked Potentials (AEP), Somatosensory evoked potentials (SEPs) and Cognitive Evoked Potentials will be also discussed in this chapter. Beside it reviews the different types of electrodes; this chapter also introduces the way electrodes are positioned. Furthermore, EEG principles will be depicted as a separate section in this chapter. At last, brain electrical activity and modelling will be last focus of the chapter.

*Chapter three* is designed to describe the principles of Magnetic Resonance Imaging (MRI) and to introduce Blood Oxygen Level Dependent BOLD effect and a brief history of fMRI technique. The chapter illustrates in details the BOLD signal on which fMRI is

based. After this, the basic model to generate fMRI signal is described. Finally, the components of an fMRI experiment are discussed where the focus –in particular- has been placed on data analysis.

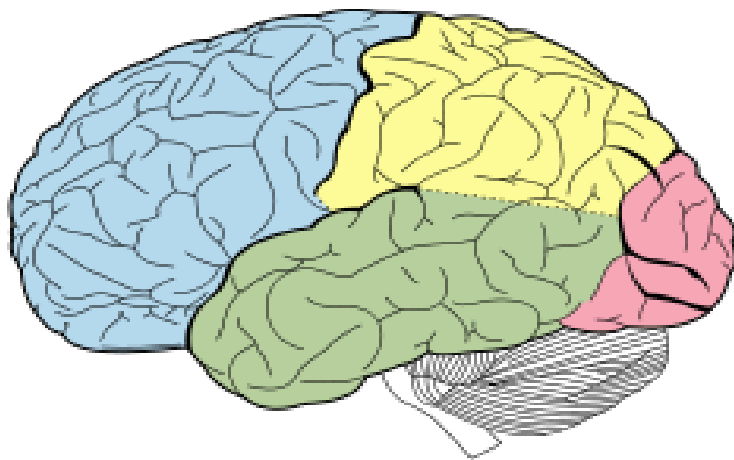
*Chapter four* describes the state of the art of EEG -fMRI data fusion techniques both asymmetric and symmetric approaches.

*Chapter five* describes the contribution of this work that consists of proposing a new framework based on Dempster Shafer theory of evidence in order to explore brain activity. The first contribution is about fMRI modality while the second is about a model of information fusion EEG and fMRI based on symmetric technique. These contributions are exposed in details with experiments and results.

The final conclusion includes concluding discussions and directions for future work. It provides a summary and the findings of the work presented on the issues tackled in this research.

## Chapter I

# *Functional Cerebral Anatomy Mapping*



## **I.1 Introduction**

The essence of analyzing the brain activity or the neuronal connectivity lies in understanding how the brain is structured. In the early of the 19<sup>th</sup> century, the brain's anatomy played an ambiguous role in the works designed to explore and understand how the human brain functions with the phrenology of Gall (Changeux, 1983), (Hämäläinen, Hari, Ilmoniemi, Knuutila, & Lounasmaa, 1993), (Hari & Kujala, 2009). Thus, It enables to understand the brain functioning and then partition it into regions where each region controls some tasks (perception, emotion, etc) (Figure I.1). In this context, several imaginary assumptions have been conducted.

In fact, Gall et al. have explained in their mapping the existence, since that time, of a reluctance that is still lasting today in establishing correlations between morphological cortical anatomy and function. Nevertheless, observing patients with focal brain lesions (Broca, 1861) and electrical stimulation of the cortex in animals (Ferrier, 1875) and then in humans during certain neurosurgical operations gave birth to establish the first functional maps. However, cerebral function that associates each cognitive process with neural activity allows localizing the functional regions (Van Essen & Deyoe, 1995).

It is worth noticing that the invasive observation techniques that have been applied on animals are not transferable to human beings only in exceptional neuro-surgical contexts. With the gradual advance in science, the neuroscientists have become able to conduct cognitive experiments on healthy subjects based on the functional imaging techniques and combine the various tools aiming to study the neuronal, hemodynamic and metabolic activity simultaneously, as will be closely illustrated. Such studies have opened unexpected horizons in the field of exploring the brain activities.

This chapter is designed to give a brief introduction to the structural anatomy of the brain aiming to provide a general knowledge about the brain and basically to introduce the unfamiliar reader of the thesis' subject to the most common terminology used in the field of neurology. Then, metrics of the cerebral activity are briefly introduced where the neural activity together with metabolic activity are illustrated. After that, metabolic activity and the cerebral blood flow are briefly discussed. This is followed by providing an overview about the several exploration techniques that have been developed so far in the literature to yield an insight to the brain structure and function. The most common characteristics of

each functional exploration technique will be introduced at the end of this chapter to provide a clear comparison.

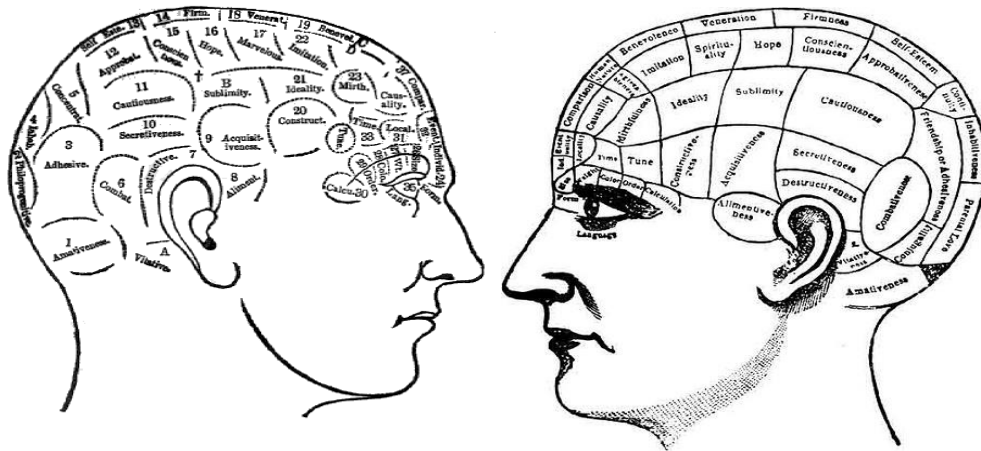


Figure I-1 Localization of human higher mental functions as phrenology  
( [http://www.bc.edu/bc\\_org/avp/cas/fnart/phrenology/](http://www.bc.edu/bc_org/avp/cas/fnart/phrenology/) )

## I.2 Brain structure

With its high complexity and its vital functions, a considerable analytical effort is required in order to exhibit the most important processes and their diverse interactions. In this scope, several works have been currently arranged seeking to shed the light on the different brain structures, either architecturally or cognitively.

The human brain is contained within the skull, which protects it. It contains as many as 100 billion nerve cells called neurons that are divided into 100 to 1000 types. Each neuron has the ability to establish to 10,000 connections and has a weight around 1300 to 1400 grams. The communication between these neurons forms the basis of all brain functions. The brain is composed of Glial cells with a number of 10 to 50 times greater than neurons. These Glial cells play a vital role in facilitating the exchanges between neuron by establishing connections, both among themselves and with neurons.

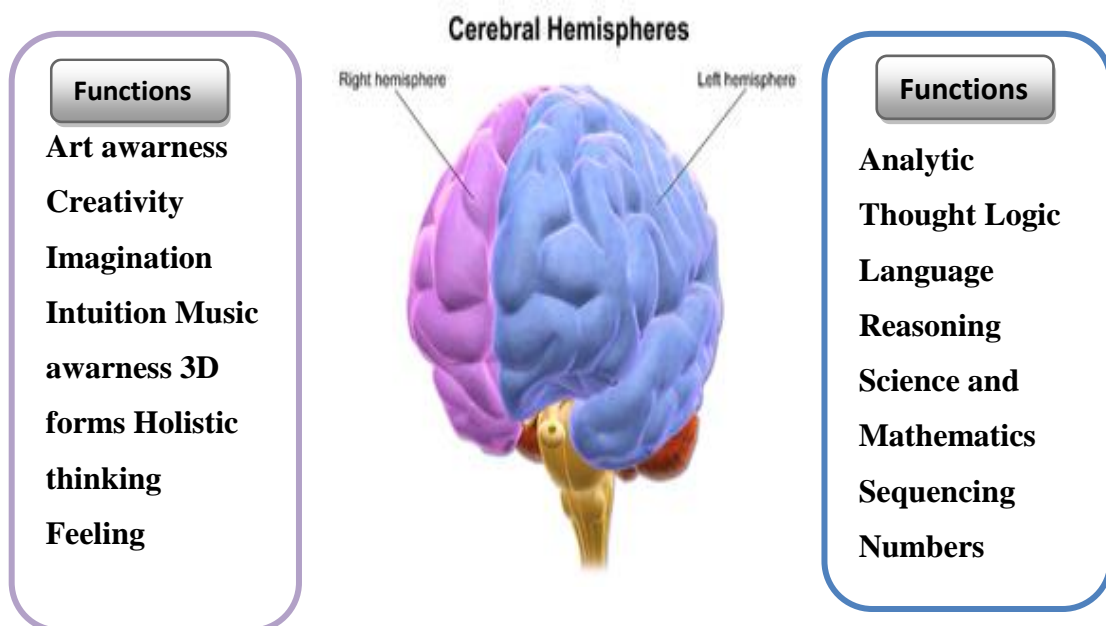
Given that, the brain is a highly complex system with two complete networks working in parallel and interaction (Khotanlou, 2008). Basically, the central nervous system, referred to as (CNS), is built up from the brain and the spinal cord which is protected by the vertebral column and communicates with muscles and the sense organs below the head. The central nervous system represents a very large interactive processor that is able to process a diverse body of sensory inputs and to save data either for short or long periods.



In this section, we will briefly describe the complex structure of the brain that consists mainly of three parts: the cerebrum, cerebellum and brainstem. Each part has different functions to perform and consists of different substructures.

### **I.2.1 The cerebrum**

As illustrated in figure I.2, the cerebrum forms the most dominant part of the brain. It is divided into two cerebral hemispheres, a right hemisphere and a left hemisphere (see figure I.2). Despite the split, the two hemispheres communicate with each other via the corpus callosum that is a large bundle of nerve fibers connecting them together. Below the corpus callosum lie the basal ganglia. One thing to note is that the right cerebral hemisphere controls the left side of the body. It has a perception of more spatial world, global and intuitive and permits recognizing shapes and faces. The right hemisphere is the one that enables us to understand and appreciate art, music, or the beauty of nature. Conversely, the left hemisphere participates in the operation of the right part of the human body. It controls speech, writing, calculating, and reasoning, etc. The most essential functions of the two cerebral hemispheres are illustrated in the figure which follows:

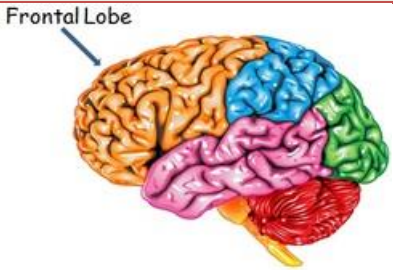
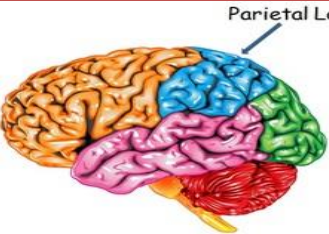
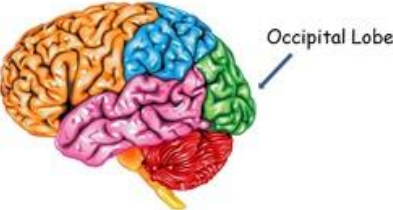
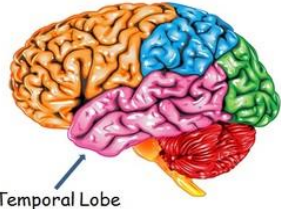


**Figure I-2 The two cerebral hemispheres and their functions**

Each hemisphere is organized into four distinct parts that are connected together in a specific and amazing way. Each part is called a lobe and has specific main functions to perform. These lobes are: Frontal lobe, parietal lobe, temporal lobe and occipital lobe. In

what follows, an illustrative table (table I.1) describes briefly the four lobes of each hemisphere with their essential functions.

**Table I-1: The principal functions of the four lobes**

Lobe	Function	Figure
Frontal Lobe	Speech and language, complex thoughts, reasoning, memory, making decision, problem solving, prediction, judgment, planning and organizing, associations and social thinking, personality and behavior, initiating and coordinating motor movements	
	<ul style="list-style-type: none"> <li>• Occupy the top part of the brain.</li> <li>• The right frontal lobe controls the movements of the left side of the body.</li> <li>• Conversely, the left frontal lobe controls the movements of the right side.</li> </ul>	
Parietal Lobe	Reading, helping us form words and thoughts, attention, perceptions, location in space, sensory processes (making senses of the world), arithmetic.	
	<ul style="list-style-type: none"> <li>• Located in the middle top of the brain</li> <li>• The right parietal lobe controls the sensibility of the left side of the body and vice versa</li> <li>• If the right side of the parietal lobe is damaged, a difficulty in exploring the familiar spaces will result.</li> <li>• A damage to the left side results in reducing the ability to understand spoken and/or written language.</li> </ul>	
Occipital Lobe	<b>Vision:</b> It processes all visual information (shapes and colors, images...)	
	<ul style="list-style-type: none"> <li>• Located in the extreme back of the brain</li> <li>• Damage to the occipital lobes can result in blindness</li> </ul>	
Temporal Lobe	Language, short-term memory, understanding and emotions, processing auditory information and integrating information from the other senses.	
	<ul style="list-style-type: none"> <li>• Located in front of the visual areas and lie under the parietal and the frontal lobes</li> </ul>	

In addition, we can distinguish three fissures (sulci) in the brain surface from these morphological structures. The first fissure is known as (Ronaldo fissure); it separates the two cerebral hemispheres. The second fissure is the one that vertically divides the two hemispheres. The third lateral fissure (Sylvian fissure) is a horizontal fissure passing through the centres of each hemisphere (see Figure I.3.) These three fissures are involved in the presentation and separation of the four anatomic lobes of the brain that have been discussed previously.

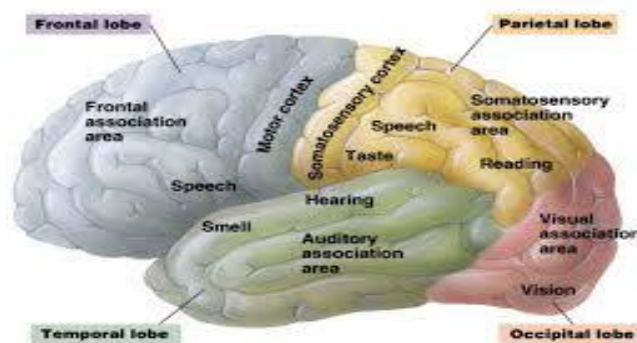


**Figure I-3 The subdivisions of the cortex**

## **I.2.2 Brainstem**

Beneath the cerebrum lays one of the most sensitive components of the brain the brainstem. The latter extends from the top of the spinal cord to the centre of the forebrain, i.e., it is situated between the deep structures of the cerebral hemispheres and the spinal cord. As clearly shown in figure 1.4, the brainstem is divided into different main sections: the diencephalon, the midbrain (mesencephalon), the pons (metencephalon), and the medulla oblongata (myelencephalon). An illustrative table of the brainstem structure with a brief description of the specific functions of each part is given below to facilitate to the unfamiliar reader. In fact, the brainstem controls vital body functions and any simple damage to that part will result in severe effects. It should be noted that all the pathways between the cerebrum and cerebellum stream through the brainstem. The most important neural structures that are involved in both motor and sensory functions are contained within this small section of the brain. Figure I-4 depicts the basic structure of the brainstem.

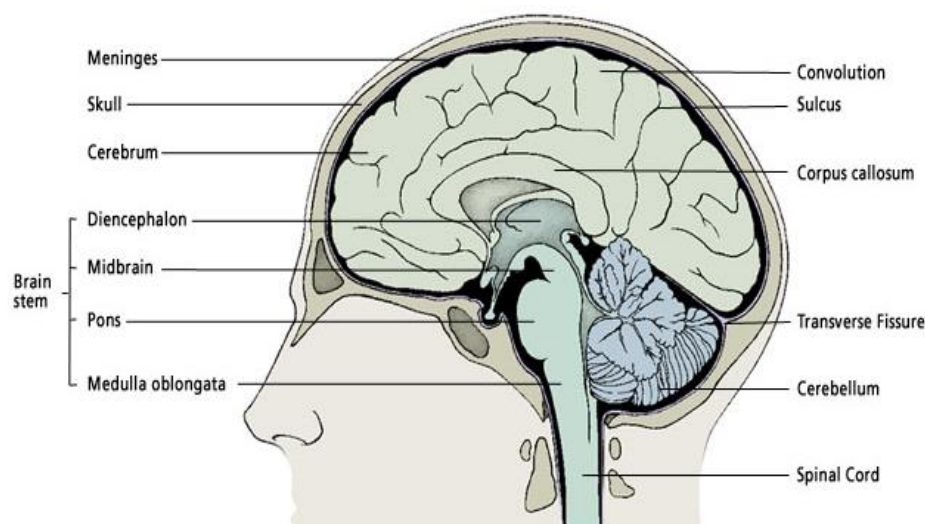


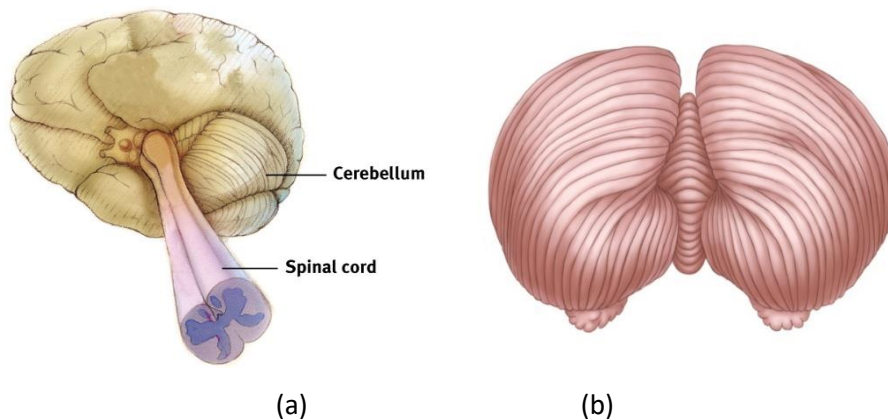
Figure I-4 : The brainstem structure(<http://www.princetonbrainandspine.com/brain/brain-anatomy/>)

Table I-2: The structure of the brainstem

The brainstem		
Component	Description	
Diencephalon	<b>Thalamus</b>	The main part of the brain; it contains the gray matter. Most sensory inputs pass on to the cerebral cortex through it after helping to prioritize it.
	<b>Hypothalamus</b>	A small region located in the heart of the brain. It is involved in body temperature regulation and balancing sleep, thirst and hunger functions. It is also in charge of the sexual behavior and emotions.
Midbrain	A short segment of the brain stem connected to the brain, located between the pons and the diencephalon. It integrates sensory information and transmits it.	
Pons	It is located in the central part, surrounded by the midbrain and the medulla oblongata. It is a major route made up of tracts that connect the spinal cord with higher brain levels, and it also contains cell groups that transfer information from the cerebrum to the cerebellum. It plays various roles in motility, facial sensitivity, autonomic functions (eye movement, chewing, facial expressions, urination, swallowing and secretion of saliva and tears, hearing, equilibrium, taste,), sleep, respiration, and posture.	
Medulla oblongata	The lowest portion of the brainstem and connected by the Pons to the midbrain. All nerve fibers that connect the brain to the spinal cord pass through the medulla. it controls the rate and depth of breathing, heart rhythm moderation, regulation of arterial smooth muscles , coughing, sneezing, swallowing, vomiting, salivation, sweating, movements of tongue and head.	

### **I.2.3 The cerebellum**

The cerebellum is an important section in the brain and plays a critical role in coordinating sensory input with muscular responses. Typically, it is situated just behind the brainstem, below the cerebral hemispheres and above the medulla oblongata. Similar to the cerebrum, the cerebellum is split into two lateral hemispheres that are joined by a medial part called the vermis (see figure I.5). Mainly, each of the hemispheres is made up of three lobes with different functions to accomplish. First, the flocculonodular lobe serves to receive sensory input from the vestibules of the ear. Second, the anterior lobe receives sensory input from the spinal cord. Third, the posterior lobe receives nerve impulses from the cerebrum. To illustrate more, a general view of the cerebellum is given in the following figure:



**Figure I-5 : (a) The cerebellum (b) Poster inferior view**

### **I.3 Basic Functions of the brain**

As previously mentioned, the brain is a vital organ that defines the centre of movement control and behaviors. Mainly, it has three basic functions. On the one hand, it acts a receptor where it receives signals through nerves from the different regions of the human organism. On the other hand, it is considered an interpreter that makes a response operation on the basis of integrating the received electrical signals. So, the brain serves as a centre of transmission of signals interpreted by creating responses or reactions to the environment. To sum it up, the major functions of the brain are reception, integration, and transmission of signal processes that involves sensations, movement, memory and consciousness at the same time, (Berthoz, 2002).

To better accomplish its complex task, the brain is organized into functional subsystems that use neurons to communicate. A very important information for the study of its activity is that the brain mainly uses glucose and oxygen as energetic substrates. However, the energy consumption of the brain is not particularly variable, however the active regions of the cortex consume more energy than the non-active areas.

To understand the activity or the brain connectivity, we should recognize the different measures of the brain functional activity. These measures are the subject of the following sections.

## **I.4 Metrics of the cerebral activity**

During the performance of certain tasks like movement, perception, cognition and emotion, a specific region in the brain that is made up of set of neurons, controls this kind of tasks. This fact refers to the process of the neural activity. Given that, three types of signals need to be measured as will be discussed below:

### **I.4.1 Electrical activity**

As regards the nervous system, the developed brain imaging techniques have permitted depicting the neuronal activity. Before we describe the process of the electrical activity, the basic morphological characteristics of a typical neuron need to be described. Neurons, also called nerve cells represent the primary functional unit of the nervous system; i.e. they are the basic information-processing unit of the brain. Various types of *Glial cells*, including *ependymal*, *astrocytes*, and *oligodendrocytes*, cells act as a support for the nerve cells. Neurons are connected to each other to establish different neural networks. They are characterized by their particular structure and chemical activities. In fact, neurons can't regenerate however they are very well preserved by Glial cells; and the older human beings are, the smaller number of neurons they have.

In the following, we describe the basic structure of a typical neuron to facilitate the understanding for the unfamiliar reader with neuroscience. This short description aims to introduce a basic comprehension of the neuronal information-processing on which brain mapping techniques rely.

Typically, each neuron is composed of three organs: a cell body, dendrites and an axon (see Figure I.6). The cell body (Soma) is the body of a neuron; it contains nucleus where most of the required molecules for a neuron to survive and function are



constructed. Similar to the branches of a tree, the dendrites extend out from the cell body and serve to transmit information received from other neurons to the cell body. The branching of dendrites can be extensive and adequate to receive as many as 100,000 inputs to a single neuron. The axon, also known as nerve fiber, is another expansion of the cell body, however it is longer than the dendrites. Typically, the function of an axon is to deliver the messages to different neurons, muscles and glands. Depending on where it connects to the central nervous system, the axon may be very short or very long reaching for instance from the spinal cord down to a toe. Some neurons have no axon and convey signals from their dendrites. However, no neuron has more than one axon.

In fact, the main role of the neuron is to receive, to process and to transmit the information (see Figure I.7). This process is performed via the synapses, the place where a signal passes from a neuron to another cell. Parts of the neuron situating before the synapse and convey the signal are known as presynaptic. Conversely, postsynaptic refers to the parts of the neuron receiving the signal. It should be noticed that presynaptic and postsynaptic parts are located on another/second neuron; either its dendrites or its soma. Signal transmission operation has a biochemical and electrical nature that is characterized by the transport of sodium ions between the intra and extracellular environment, creating an electrochemical impulse called the action potential or postsynaptic potential. This potential is transmitted from the dendrite to the soma. If the internal potential exceeds a threshold of activation, an electric shock will occur. (Berthoz, 2002)

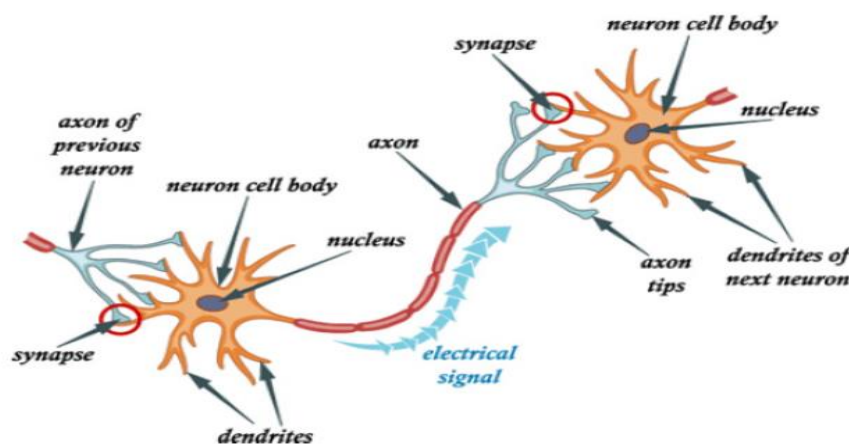


**Figure I-6 Basic structure of a typical neuron (Sanei & Chambers, 2013)**

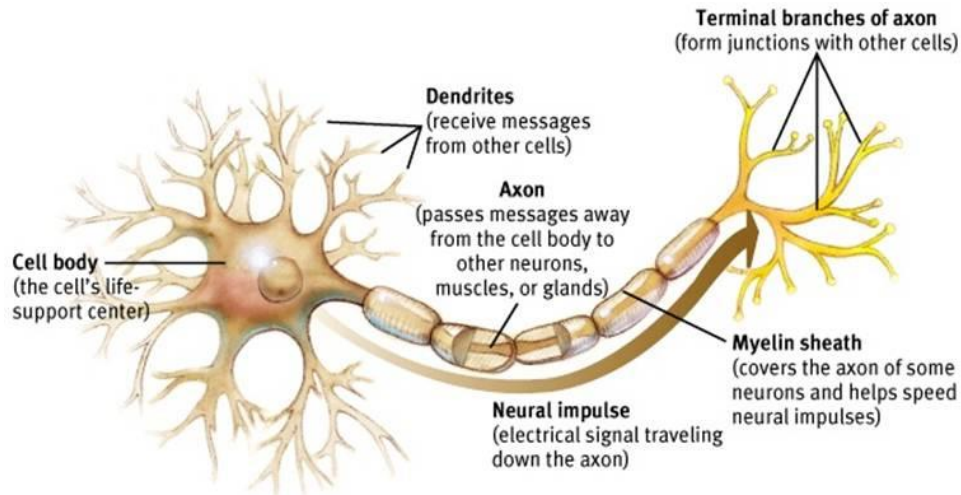


Figure I-7 : Function of neurons(F.wendling,2008)

According to Maxwell laws, all the currents that flow in the cerebral nervous tissues produce a potential distribution in the adjacent conductor volumes. This potential distribution can be measured on the scalp thanks to the different brain diagnostic techniques.

#### I.4.2 Metabolic activity

The chemical activities of neurons naturally depend on the use of energy. Basically, the main energy source is obtained from converting the Adenosine Triphosphate (ATP) molecules in nerve cells that have only small reserves. This results in glucose and oxygen metabolism. Thus, the electrochemical activity of the neurons corresponds to a metabolic activity. All these activities are linked with a hemodynamic activity.(Aubert, Costalat, & Valabrègue, 2001)

In fact, the supply of glucose and oxygen is carried by the blood, and moves in the capillary system within the tissues of the nervous system. Regulating the amount of blood flow to the brain allows increasing the amount of energy necessary to the activity of the nerve cells. The increase of Cerebral Blood Flow (CBF) that results in the increase in the amount of oxygen and glucose introduces the hemodynamic activity. In contrast, the decrease of (CBF) is called the des-activation. And more specifically, the hemodynamic activity goes through different stages that are illustrated as follows:(Buxton & Frank, 1997)



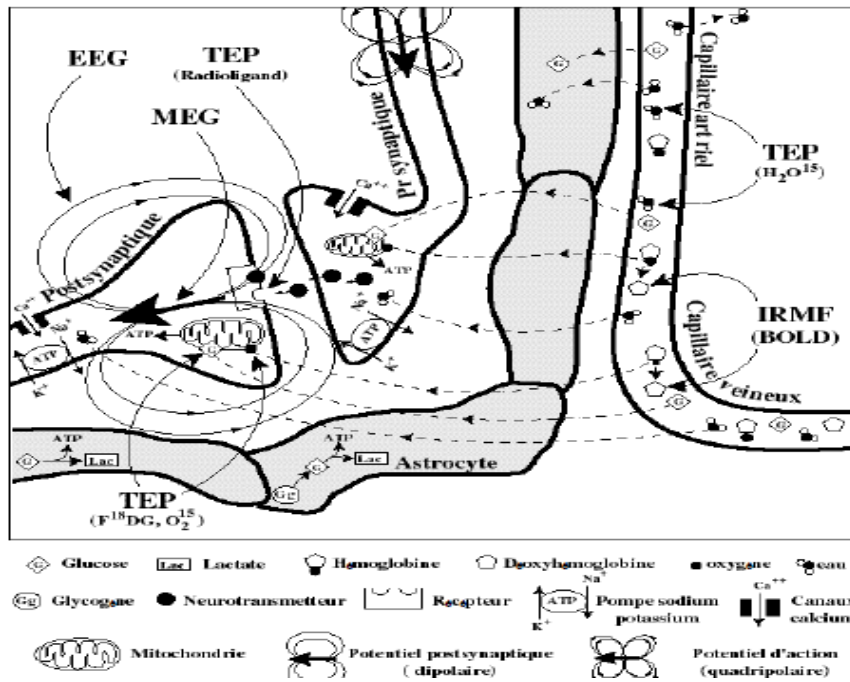


Figure I-8: the deferent measures of brain function

The oxygen is retrieved from the local system by the cells of blood vessels whose electrochemical activity consumes large quantities of (ATP).

- The (CBF) experience a strong increase in the region and the important contribution of the red blood cells containing the hemoglobin (Hb). This results in over-concentrating the oxygen of the region. The concentration of  $\frac{Hbo2}{dHb}$  is caused by strong fluctuations at the beginning. Because of the oxygen extraction, in the second phase it has been caused by the increase in blood flow and the set of the following operations called the hemodynamic response.

Note that the hemodynamic response depends highly on other factors than the local electrical activity. More particularly, its extent as its temporal reduction are dependent, among other things, on cell metabolism, control of blood flow, the local density of the capillary network, membrane permeabilities and possibly on the pathological character of the tissue (Heeger 2002). Therefore, it seems appropriate to explicitly recall that the hemodynamic activation is an indirect marker of the neuronal electrical activity, which itself is associated with the brain information processing.

### **I.4.3 Metabolic activity and the cerebral blood flow**

The metabolic activity is realized by a regional adjustment known as Regional Cerebral Blood Flow that characterizes the hemodynamic activity or the vascular in correlation with the considered cognitive activity. As previously mentioned, neurons have a high demand for ATP, and therefore, oxygen and glucose that is the only source of energy used by the brain to sustain its functions. So, a constant glucose supply through the blood is crucial to the nervous system. Thus, any interruption of this supply then would result in a failure of brain functions. In the case of hypoglycemia, interruption of blood flow may cause impaired consciousness or loss of consciousness when the brain is no longer irrigated. However, this condition is not sufficient to establish a correlation between blood flow and energy consumption at regional level.

This issue has been extensively studied using the autoradiography method developed by (Sokoloff, 1977). Based on this technique, several authors have established a strong correlation between the regional CBF (RCBF) and glucose consumption better in animals than in humans. Similar studies have shown the existence of a coupling between the blood flow and metabolism at the global level and then at the regional level.

### **I.4.4 Couplings between different activities**

The couplings between these different activities are applied at different levels. At a synaptic level, numerous data exist about the characteristics of the neuro-chemical transmission. On the contrary, couplings between the electrical, energetic, metabolic and hemodynamic activities are less well known in this level. The situation turns out to be complicated at the macroscopic level where the various activities can be regulated at different levels of integration. Much remains necessary to gain a better understanding of what exactly the synaptic signals (an Excitatory Postsynaptic Potential (EPSP), an Inhibitory Postsynaptic Potential (IPSP)) are significantly contributing to signals registered in MEG. The same question arises when it is about coupling between electrical activity and hemodynamic and metabolic response. At this stage, we are faced with a real inverse problem when the "indirect" modalities such as PET and fMRI are implemented; and that the electrical activity should be detected again from the measured signals.

In particular, there is a difference between the electrical activity areas and hemodynamic and metabolic response areas (Malonek & Grinvald, 1996) . On the one hand, it raises an important question about the mediators of this coupling. On the other

hand, it encourages to a certain caution on the resolution and interpretation of cognitive maps that technique such as fMRI that can achieves better results.

Yet, the coupling between the hemodynamic and metabolic activities is not fully clarified. It was previously reported that references in the literature have established a close relationship between the changes in the neural activity and the changes in blood flow and glucose consumption. However, a nonlinear relationship links these two quantities and the local oxygen consumption. The increases in blood flow exceed a lot of the oxygen requirements of the tissues of the neuronal activities and vice versa. This situation is called decoupling. It does not permit to plot because it is opposed to the principle of parsimony on one hand; and it suggests on the other hand that the replacement of the ATP would be carried out by anaerobic pathway of glycolysis that is almost 20 times less productive than the aerobic pathway. In this vision, the astrocytes, barriers between vessels and neurons, play a key role.

The energy input in glucose is carried through blood. The heart controls blood circulation and pumps it to the arteries and cerebral arteries. These arteries have nerve fibers that permit to control its relaxation and contraction. In the brain tissue, the arterioles join into pre-capillaries and then into capillaries. It is worth noticing that the number of capillaries in a region appears closely linked to the number of synapses in that region and not to the number of cell bodies (Brooks, 1992). Frequently, the capillaries dilate and constrict to ensure a reasonable distribution of oxygen and glucose to the brain tissues. In the case of a brain activity, the expansion of capillaries results in increasing the RCBF. This increase creates an opening of more capillaries and the volume of the transported blood increases.

## **I.5 Exploration techniques of the brain activity**

A clear understanding of the basic brain functions requires knowledge about the important information processes. Thus, extensive studies with different brain mapping techniques have been conducted to achieve better insight of the brain. The existing brain exploration methods are classified into structural and functional imaging techniques. Computerized Tomography (CT) is the earliest paradigm that has been developed for imaging the structure of the brain. Recently, Magnetic Resonance Imaging (MRI) has become a dominant technique for brain structure imaging. With the development of

functional techniques, neuroscientists are able to examine the function of the human brain while performing a particular cognitive task. Mainly, functional techniques are classified into two main types. The first class consists of methods that directly measure the electrical activity, such as electroencephalography (EEG) and magnetoencephalography (MEG). The second consists of methods that measure the neuronal activity indirectly given that neural activity is sustained by an increase in local blood flow which refers to the metabolic activity. Examples of these techniques include Positron Emission Tomography (PET) and functional Magnetic Resonance Imaging (fMRI). In these subsections, we briefly introduce the most common of the previously noted techniques employed in investigating the brain.

### **I.5.1 Magnetic Resonance Imaging (MRI)**

MRI is a very dominant medical imaging technique figure I.10. It is used to make an accurate diagnosis on the structural anatomical plan and allows obtaining a 2D view with possibly a 3D effect of a portion of the body, particularly the brain. MRI is based on the principles of the Nuclear Magnetic Resonance (NMR). In other words, it is to detect variations of the macroscopic magnetic moment in a material under the action of a static magnetic field and an electromagnetic wave of an appropriate frequency. This modality was an important revolution in medical imaging in view of its excellent spatial resolution that is of the order of a millimetre and an average time resolution of the order of seconds (Daunizeau et al., 2005).

The basic researches on the interactions between the nucleus of the atom and the magnetic fields have started between 1930 and 1940. The physical principles of the magnetic resonance imaging technique have been included since 1950. In addition, the researchers Lauterbourg, Damadian and Mansfield have shown that this idea is feasible using the physical theories of the nuclear magnetic resonance. However, the first reviews by this technique emerged in the early 1970. Regarding medical applications, they have been developed in laboratories and medical centres between 1983 and 1993. Figure I-09 presents the MRI apparatus and a sample of images obtained by the MRI scan.

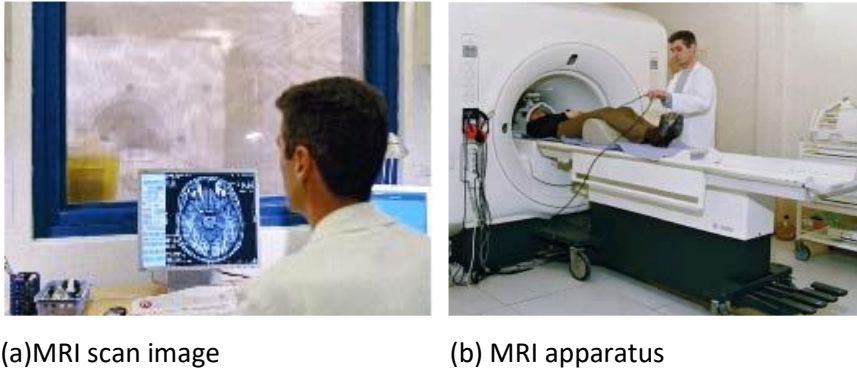


**Figure I-9 Magnetic Resonance Imaging**

### **I.5.2 EEG (Electroencephalography)**

The EEG is a non-invasive technique that has been widely used to capture different aspects of neuronal activity. It measures a difference of electric potentials generated by the bioelectric activity of neurons. This difference is of the order of micro volts; however the collected signals are amplified. The employed apparatus is called the electroencephalograph and consists of several electrodes placed on the scalp as the 10/20 electrode system as will be discussed in detail in the following chapter, building what is called the EEG headset. At the time, the detected waves are picked up by electrodes and transmitted to the device to translate them by tracing on graph paper. Today, the techniques have evolved and the tracings appear on a computer screen, and have to be saved on physical media (Figure I.10). The measurements obtained by EEG can be frequencies, amplitudes or specific waves. EEG modality will be extensively discussed in the second chapter.



**Figure I-10 : Electroencephalography**

### I.5.3 Magneto encephalography (MEG)

MEG is a new non-invasive examination technique that records the magnetic signals emitted from the nerve cells of the brain. Particularly, it helps scientists to measure brain activity in real time. More specifically, MEG allows the investigation of brain function in all that is related to taste, touch, speech and vision.

The magnetic fields measured on the scalp surface are in the order of 10 femto-tesla, (1ft = 10-15 Tesla). They are very small compared with the terrestrial magnetic field that is greater than 10 billion. For magnetic field measurement, the MEG uses an apparatus based on the **SQUID** magnetometers, "Superconducting Quantum Interference Devices", and placed in a room isolated magnetically by mu-metal that are cooled with helium.

Although the MEG technique is mainly used for functional mapping, it has also been employed in neurology for a patient passing a clinical examination; especially for the epilepsy disease; as well as in the cognitive neuroscience area of research. In addition, MEG has been used to the study of the developmental, psychiatric and neurodegenerative diseases such as schizophrenia, dyslexia, Parkinson and Alzheimer.

In MEG, we measure the variations in the magnetic fields that are produced by the ionic currents primarily generated by the postsynaptic potentials of pyramidal cells of the cerebral cortex where the magnetic fields inside the brain are very low, in a very important condition that must be isolated from external magnetic fields which are carried out at the sensor. The reel receiving the flow is usually a gradiometer that is formed by two or more reels assembled in phase opposition and permits to measure the gradient of the magnetic field in the tangential direction or the radial. This one acts as a filter that permits to eliminate the magnetic fields of small variations. That is useful in the case of external interference parasitic fields. These disturbances affect cerebral magnetic fields that decrease according to the distance from the source. This implies using supplementary correction systems during the measurement of the external field at sensors taken away from the head. The most effective solution is to place the entire measurement system in a shielded room formed of metal walls that strongly diminishes external magnetic fields (see figure I.11). Although MEG is similar to the EEG, it does not require any electrodes. Unlike the EEG, MEG can also record signals from deeper regions of the brain.

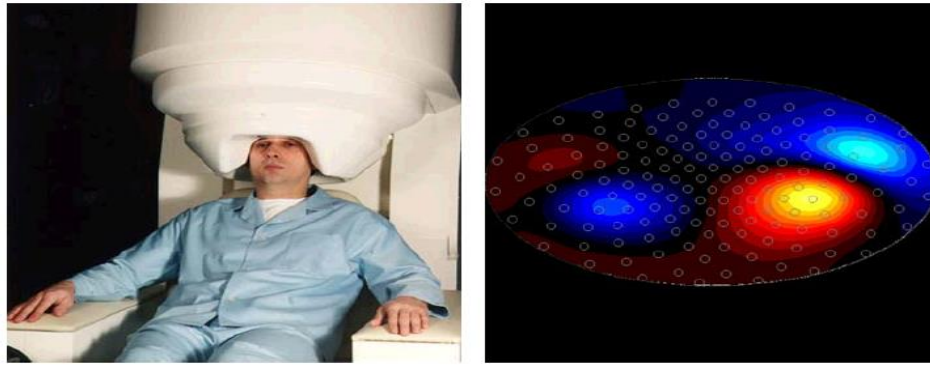


Figure I-11:MEG machine

#### I.5.4 Functional Magnetic Resonance Imaging (fMRI)

With the development of data acquisition and processing techniques in the MRI medical field, it has become possible to produce magnetic resonance images in a reasonable time. We can say that MRI has become "functional", i.e. exploring the functional activity of the brain in the course of time.

Functional MRI is a technique that permits detecting the functional activity of the brain when a human being performs certain defined tasks. For instance, it is employed during those exercises that require mental calculation, recall of a face, or the observation of a picture or making a movement ... etc. Some areas in the brain are activated in order to control the performed task. This activation causes an increase in local blood flow in the concerned brain regions which causes the magnetization of the haemoglobin contained in the red blood cells. In particular, this technique is a quantitative measure of the brain activity during the execution of behavioural tasks.

The blood flow is observed by functional MRI permitting to identify the brain areas that are involved in these exercises. In other words, fMRI consists in measuring Blood Level Dependent, referred to as BOLD signal. The latter reflects local and transitory variations in the amount of oxygen carried by the haemoglobin according to the need of the neuronal activity of the brain. In particular, it consists to record local hemodynamic changes of brain areas (i.e., changes of blood flow properties) when these regions are stimulated.

Although fMRI was introduced in 1990, it has become gradually a promising technique that permits detecting the functional areas of the brain in the course of time in a non-invasive way. fMRI has a spatial resolution of 3 to 4 mm and a temporal resolution of

the order of one second. A detailed description of fMRI modality will be the subject of chapter 3.

## **I.6 Characteristics of the different functional exploration techniques**

The different medical imaging techniques are differentiated from each other on the basis of three criteria: (i) their spatial resolution (ii) their temporal resolution and (iii) the degree of invasiveness.

### **I.6.1 Spatial resolution**

Regarding the criterion of spatial resolution, MRI has a high resolution of 3 to 5 mm that provides a good brain anatomical description. Also, its spatial resolution is in the order of a few mm<sup>3</sup> allowing yielding a good localization of functional brain areas. Both EEG and MEG techniques have low spatial resolution of about ~ 10mm; and it can be improved by increasing the number of the used electrodes if we get to 256 electrodes for EEG. However, in EEG and MEG, several difficulties are encountered to accurately locate the functional brain regions originally from the measured signals and such precision can only be achieved if a single small region contributes to the EEG or MEG data, which is rarely the case.

### **I.6.2 Temporal Resolution**

The different medical imaging techniques have a very long temporal resolution comparing to the duration of cognitive phenomena, although it is possible to obtain best temporal resolutions by selecting a limited region of interest (ROI). On the one hand, MRI and fMRI do not allow monitoring the precise changes in the brain activity. On the other hand, EEG and MEG which present the dynamic brain imaging techniques have a high temporal resolution in the order of a millisecond. This permits following the chronology of cognitive processes in a real time. However, MEG and EEG facilitate the dynamic study of brain function.

### **I.6.3 Invasiveness degree**

The degree of invasiveness corresponds to the negative consequences that the measuring method can have on the subject. Among the major advantages of the EEG and MEG, they are totally non-invasive techniques (Spinelli, 1999). In comparing those with other techniques such as PET (Positron Emission Tomography) or scanner, there is an



injection of radioactive tracers and contrast products. For the MRI and fMRI, they do not necessarily require the introduction of this product however the presence of a significant magnetic field that prohibits the use for subjects with a metal part in the body that can disrupt the magnetic or the electric signal. This implies that the use of MRI always remains limited. The level of invasiveness degree is illustrated in figure I.12 by the gray colour where more highly invasive techniques are shown in darker gray.

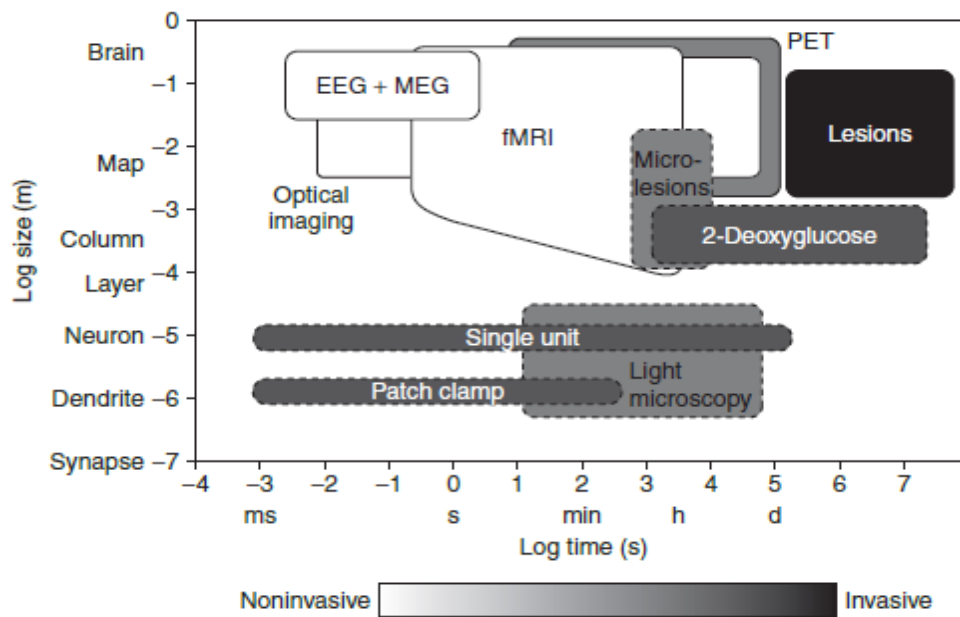


Figure I-12 A comparative diagram of the different functional brain imaging techniques. The level of invasiveness of each technique is indicated by a grayscale; more highly invasive techniques are shown in darker gray. Adapted from Cohen and Bookheimer (1994)

## I.7 Conclusion

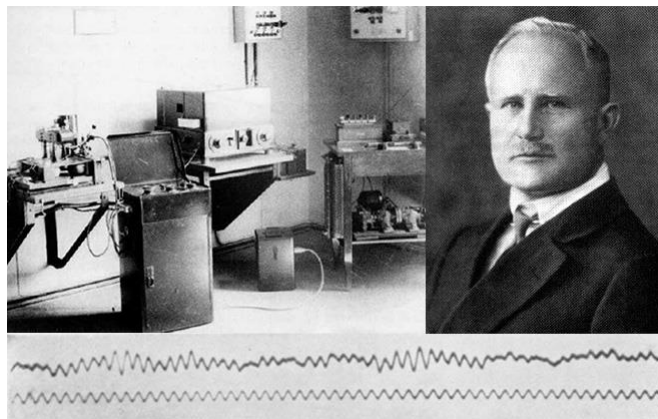
In this chapter, we briefly discussed the brain anatomy by giving a brief description of the main brain parts. We also provided a short introduction to the basic functions of brain. It is important to notice that studying the structure of the brain plays a vital role in deducing the electrical and hemodynamic changes and their relation to the brain activity. This chapter also gives a general view about the most common techniques that have been widely used in brain data acquisition.

Scientists sought to get an accurate brain activity mapping with different neuroimaging techniques. However, combining data obtained by these techniques such as the coupling between fMRI and EEG has gradually become an important task. It aims to take advantage from the several imaging modalities in order to better characterize

neuronal population networks involved in brain information processing. Therefore, the multimodal neuroimaging takes its place in the recent research of neuroscientists due to its ability to provide direct and precise information of neuronal activity. EEG/fMRI fusion technique will be the subject of the fourth chapters.

## Chapter II

# *EEG Electroencephalogram*



*Right: German psychiatrist Hans Berger*

*Left: EEG Recording Equipment, 1926*

*Bottom: First recorded EEG by Hans Berger*

## **II.1 Introduction**

One of the major issues in neuroscience is finding ways to accurately study the dynamic activity of the human brain or what is happening inside the brain; that is to examine the basic functions of the brain while people are thinking, acting, and feeling, etc. In this scope, several techniques have been developed seeking to see the brain at work. As previously mentioned in the first chapter, Electroencephalography (EEG) is used to measure the electrical activity of the brain. It is compatible with synaptic events that occur at the millisecond level. This temporal modality has gradually become an important tool in investigating how the brain functions. EEG has been widely used by neurophysiologists, cognitive scientists, cognitive psychologists, and other researchers interested in exploring the brain.

This chapter is intended to provide a comprehensive overview of EEG modality. At first, it describes a simplistic historical background of electroencephalography and targets the unfamiliar reader with neuroscience. Then, a clear illustration of how to conduct an EEG experiment is illustrated with the EEG recording technique that exists in the literature. The current chapter also describes rhythmic activity. Next, it depicts the evoked potentials where its main types, the Visual Evoked Potentials (VEP), the Auditory Evoked Potentials (AEP), Somatosensory evoked potentials (SEPs) and Cognitive Evoked Potentials, are separately discussed. The current chapter also reviews the different types of electrodes before it moves to introduce positioning of the several electrodes. Then, principles of EEG are the subject of this chapter as well. The last focus of this chapter concerns brain electrical activity and modelling.

## **II.2 Historical background**

Electrophysiology EEG is the oldest functional brain imaging technique. It has been introduced in 1786. Particularly, the researcher Galvani has observed a movement of a frog after a contact with two metal plates by the accidental experience. Additionally, he has found that the muscle was capable of generating an electric current in the absence of any metal (Goodwin & Hall, 1939). About a century after, no discovery has been witnessed in the field.

In fact till 1875, the biologist Richard Catton has detected the presence of electrical currents in mammals (monkeys and rabbits) through the use of electrodes placed on their

skulls confirmed by galvanometer oscillations (fluctuating electrical activity on the surface of the cerebral cortex).(Caton, 1875). Thus, the history of the EEG has started. After, Hans Berger has applied this technique to the human being when he first recorded the EEG signals in 1929 as a potential variation. He has published his discovery of two types of quasi-sinusoidal electrical brain activity that he called "alpha rhythm" and "beta wave" (Berger, 1929) Figure II.1. These works have been resumed and completed by Edger Douglas Adrian who has been awarded the Nobel Prize where it would be very easy to visualize these electrical activities on paper. The survey basics are still being applied today. It has become the common method applied in current medical practice and diagnostic tool especially in epileptology practice (Adrian, 1934),(PIDOUX, 2007).

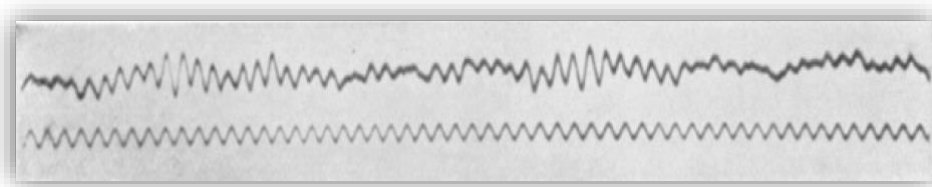


**Figure II-1: The first EEG recorded by Hens Berger and published in 1929(Berger, 1929)**

However, the first recorded seizures date back to 1938 by (Gibbs & Gibbs, 1946). The first intrusive methods using depth electrodes have been established after the Second World War, precisely in the late of 1940s. It took until the 1950s for the EEG to be commonly used in medical practice, especially in the diagnosis of epilepsy. A sample of recorded EEG signals is depicted above in Figure II.2.

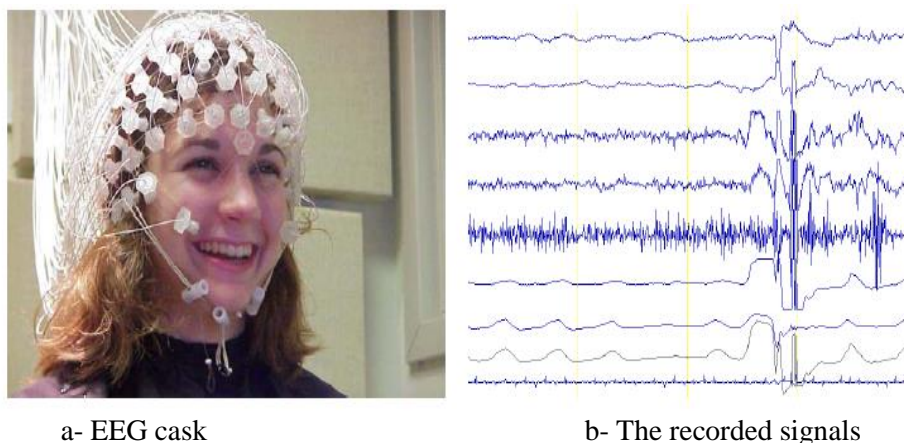


**Figure II-2 : EEG technique**

This pathology requiring exploration by the EEG is a consequence of an original synaptic or cellular imbalance that causes a sudden change in brain electrical activity. This activity arises when neurons sets synchronize abnormally. The result often corresponds to discharges, called critical discharges, of high frequency and variable amplitude. It is the centre of the discharge and its propagation depends on the clinical aspect of crises. There are two types of seizures (Caparos, Louis-Dorr, Wendling, Maillard, & Wolf, 2006).

1. Generalized seizures cause the appearance of unconsciousness or bilateral motor signs. During this crisis, electroencephalographic abnormalities are bilateral, symmetrical and diffused to the entire cerebral cortex.
2. Partial seizures result of clinical focal signs, and do not produce loss of consciousness as to the generalized epilepsies. In this type of epilepsy, electrical abnormalities are limited to a well defined area of the cerebral cortex.

The primary means for transmitting information along the nervous system is the movement of ions across the cell membranes of neurons. This would result in producing an electrical current which provokes voltage changes that extend over a large area of neural tissue. Measuring these potential changes is the basis of EEG. To simplify, EEG signals recordings are measures done on the scalp surface and arise from the large dendritic currents generated by a diverse body of neurons. To perform EEG measurements, it is necessary to model head as a conductive volume and apply the electromagnetism laws to estimate the volume distributions of current sources (Crouzeix-Cheylus, 2001).

### **II.3 Conducting and performing an experiment EEG**

The electroencephalogram (EEG) measures the electrical signals of brain activity. It is obtained by using a set of electrodes; usually silver coated with silver chloride, placed on the scalp surface. The contact of these electrodes with the skin is made by using a conductive paste and they are held in place by an elastic headset. The measured information corresponds to differences in electrical potential between two electrodes. In fact, the amplitude of the received signals is low. Thus, they must be amplified using differential amplifiers and care must be taken to reduce the interference from the external sources that might degrade the quality of the signals such as eye movement and muscle activity. EEG signals are alternative, more or less sinusoidal, entering the low frequency band: from 0.5 to 60 Hz. The signal recording stage takes some minutes (~ 10mn). This is

generally made in the following conditions: (i) the subject in a state of rest and (ii) the subject with eyes closed (iii) the subject with eyes opened followed by two stimulation tests: In the first test, the subject breathes for a period of 3 to 5 minutes with a highly accelerated rate of breathing. This deep breathing is repeated continuously in order to provoke discomfort sensation with nausea sometimes. This technique is used because it can increase the EEG abnormalities in several types of epilepsies and it can cause a complex partial seizure. However, the second test submits the subject to light flashes with a rotation frequency between 1 and 30 turns per second. In addition, it allows identifying photosensitivity that is the cause of some epilepsy forms. It is worth to note that this test can be performed sometimes with closed eyes.

The previously mentioned techniques have emerged due to the technological development. Several EEG recording techniques exist in the literature and have a noticeable impact in the field of electroencephalography. Among these several types, we state the following:

Table II-1: Types of EEG recordings

Type	Features
<i>Numerical EEG</i>	Once the EEG signals are amplified and filtered, they are converted to numerical signals which allow visualization on a screen in the form of drawing changes over time, and the possibility of recording these signals by the use of IT support. Other advantages come to a post-processing of signals, data storage and archiving, remote transmission in a real time by telecommunications.
<i>Polysomnography</i>	A medical exam performed during sleep. It involves recording physiological changes such as breathing rhythm and cardiac rhythm or electroencephalogram in order to determine certain problems related to sleep. The EEG recording in this case is carried out in a long period of time that permits better following the subject.
<i>Holter EEG</i>	EEG signal recording on mobile equipments allows recordings even at home especially for handicapped.
<i>EEG video</i>	Coupling EEG with monitoring systems, such as video recording, allows better interpreting the marked events.

## II.4 The rhythmic activity

The term rhythm refers to the activity or waves whose period and morphology are almost constant. Rhythms are obtained from the recording of an EEG. They allow defining frequency bands. Thus, it is possible to identify and differentiate rhythmic electrical brain activities and classified according to their frequency band. Figure II.3 shows the diagram of each of the existing types of brain waves. Two types of regularities can be described:

- Rhythms (called basic) which characterize the cerebral state on variable temporal periods varying from a few seconds to several minutes or even an hour.
- An approximately circadian cyclicity of behavioral and electrical events, grouped under the generic name of state of vigilance.



As previously noted, the brain is also defined by its rhythmic activity. In fact, several types of activity exist at the cerebral cortex level. For better illustration, we will introduce closely two illustrative tables to briefly summarize the main features and frequencies of each of these different types.

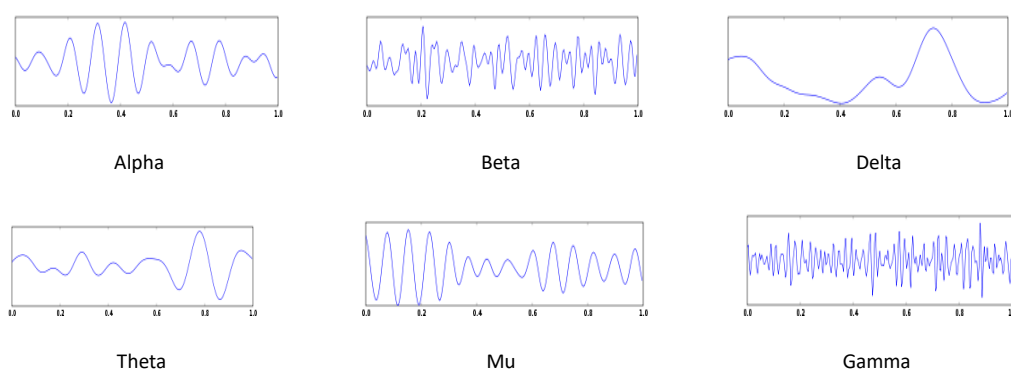


Figure II-3 : Types of Signals

Table II-2: Typical Frequencies and Amplitudes of Synchronized Brainwaves

Rhythm	Frequencies (Hz)	Amplitude (uV)
Alpha	8-13	20-200
Beta	13-30	5-10
Delta	1-5	20-200
Theta	4-8	10
Gamma	30-100	5-10
Mu	7 – 11	100

Table II-3: Types of Cerebral Rhythmic Activity

Type	Location	Normally	Pathologically
Delta	<ul style="list-style-type: none"> <li>frontally in adults,</li> <li>posteriorly in children;</li> <li>high-amplitude waves</li> </ul>	<ul style="list-style-type: none"> <li>adult slow-wave sleep</li> <li>in babies</li> <li>found during some continuous- attention tasks</li> </ul>	<ul style="list-style-type: none"> <li>subcortical lesions</li> <li>diffuse lesions</li> <li>metabolic encephalopathy hydrocephalus</li> <li>deep midline lesions</li> </ul>
Theta	Found in locations not related to task at hand	<ul style="list-style-type: none"> <li>higher in young children</li> <li>drowsiness in adults and</li> </ul>	<ul style="list-style-type: none"> <li>focal subcortical lesions</li> <li>metabolic encephalopathy</li> </ul>

		teens <ul style="list-style-type: none"> <li>• idling</li> <li>• Associated with inhibition of elicited responses (has been found to spike in situations where a person is actively trying to repress a response or action).</li> </ul>	<ul style="list-style-type: none"> <li>• deep midline disorders</li> <li>• some instances of hydrocephalus</li> </ul>
<b>Alpha</b>	posterior regions of head, both sides, higher in amplitude on dominant side. Central sites (c3-c4) at rest	<ul style="list-style-type: none"> <li>• relaxed/reflecting</li> <li>• closing the eyes</li> <li>• Also associated with inhibition control, seemingly with the purpose of timing inhibitory activity in different locations across the brain.</li> </ul>	<ul style="list-style-type: none"> <li>• Coma</li> </ul>
<b>Beta</b>	both sides, symmetrical distribution, most evident frontally; low-amplitude waves	<ul style="list-style-type: none"> <li>• range span: active calm -&gt; intense -&gt; stressed -&gt; mild obsessive</li> <li>• active thinking, focus, hi alert, anxious</li> </ul>	<ul style="list-style-type: none"> <li>• benzodiazepines</li> </ul>
<b>Gamma</b>	Somatosensory cortex	<ul style="list-style-type: none"> <li>• Displays during cross-modal sensory processing (perception that combines two different senses, such as sound and sight)</li> <li>• Also is shown during short-term memory matching of recognized objects, sounds, or tactile sensations</li> </ul>	<ul style="list-style-type: none"> <li>• A decrease in gamma-band activity may be associated with cognitive decline, especially when related to the theta band; however, this has not been proven for use as a clinical diagnostic measurement</li> </ul>
<b>Mu</b>	Sensorimotor cortex	<ul style="list-style-type: none"> <li>• Shows rest-state motor neurons.</li> </ul>	<ul style="list-style-type: none"> <li>• Mu suppression could indicate that motor mirror neurons are working. Deficits in Mu suppression, and thus in mirror neurons, might play a role in autism.</li> </ul>

## II.5 Evoked Potentials

An evoked potential refers to the brain activity generated by the stimulus. It is an electrical event collected at the surface of the scalp. In other word, it is a response of the brain to a specific stimulus which may be external such as sound and light or internal like

decision making and motor preparation. When stimulations occur, changes occurred in the captured signals. These changes, known as evoked potentials, summarize in a series or succession of waves with appearance latency, defined as the time it takes sensory stimulation to be received by a receiver and the time of its transmission to the brain. Evoked potentials test the integrity of visual, auditory systems and motors. They allow the detection of lesions in the spinal cord or the brain.

The evoked potential test has been widely used to evaluate the neurons functional state in the brain. Typically, evoked potentials have slight intensity stimulus. That is stimulus -evoked signals are in the range of a few micro-volts, which implies that the signal-to-noise ratio is much smaller than 1. Evoked signals are superimposed to spontaneous brain activity with much larger amplitude. This therefore requires the use of specialized equipment to bring out these repetitive responses (i.e. these evoked potentials) to the stimulus among the spontaneous electrical activities.

Two categories of evoked potentials can be distinguished. Particularly, the first type is exogenous evoked potentials, called "mandatory". There exist three types of exogenous evoked potentials: (i) Auditory Evoked Potentials (AEP), (ii) Visual Evoked Potentials (VEP) and (iii) Somatosensory Evoked Potentials (SEP). The second category is the endogenous evoked potentials considered as "cognitive" or eventual or ERP (event related potential) relatively to the active processing of information regardless of the type of stimulation. In the following, we describe each of the previously mentioned types of evoked potentials.

### **II.5.1 The visual evoked potentials (VEP)**

In this experiment, the subject undergoes visual stimuli. For instance, the subject is exposed to a sequence of images that periodically reverses and let him recall or remember. Usually, the image of a black-white checkerboard that periodically reverses. However, potentials are obtained as a result of these visual stimuli. These VEP are recorded using electrodes placed on the scalp surface at the occipital region as shown in Figure II.4.

Usually, this test is used to assess the integrity of the visual pathways from the eye to the corresponding brain areas. Also, VEP is a powerful tool used in the investigation of the following pathologies: atrophy and optic neuritis, tumors in the path of the visual pathways, plate sclerosis, etc.

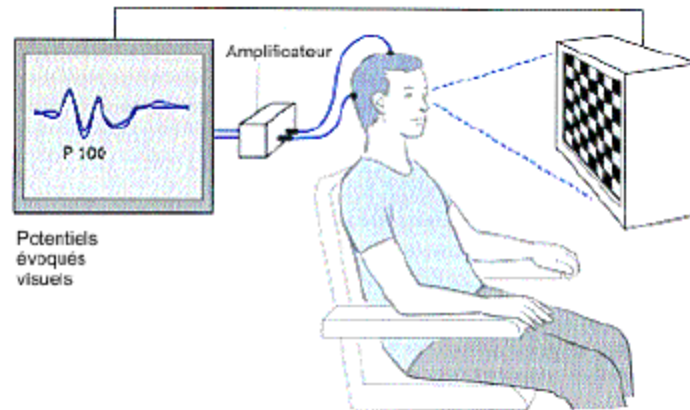


Figure II-4: Study of visual evoked potential

### II.5.2 The Auditory Evoked Potentials (AEP)

Auditory Evoked Potential of the brain is among the clinical analyzed evoked potentials. During these experiments, the subject puts a headphone on his ears. However, the AEP are caused by a loud click to stimulate the ear cochlea, the responsible area for receiving the sound message and transcoding into nerve signal. Also, they are the nervous endings of the inner ear (see Figure II.5). In this test, electrodes are placed on the surface at the top of the skull and on the lobes of the left and right ears.

The brain AEPs are used for diagnosing auditory and nerve problems. Also, they provide more information in cases of hearing loss or problems. Brain AEPs are applied as supplementary examination in the audiogram. Furthermore, they are very useful in nervous problems, the brain AEPs permit to assess the function of structures or profound auditory pathways in the brain that are difficult to record otherwise. However, it would be possible to detect via the signals picking up electrical potentials from the left and right auditory areas, and so get to discover some abnormalities and accordingly interpretations may be possible.

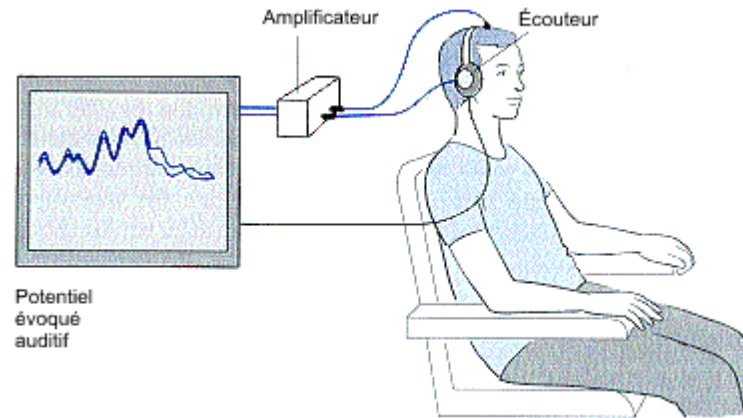


Figure II-5 Study of auditory evoked potential

### II.5.3 Somatosensory evoked potentials (SEPs)

Somatosensory is the system responsible for somatic and deep-rooted sensations from the skin. Diagnostic on this system is carried out using an electrical device placed on a point of the subject nerve. This device generates electrical impulses that cause the SEP. As illustrated in Figure II 6, for recording the reaction, response is presented by a valid signal for the study of nerve conduction. The SEPs are used in the exploration of sensory pathways lesion in the periphery (nerves) and also in the central level (spinal cord and brain). They are also used during certain surgical interventions.

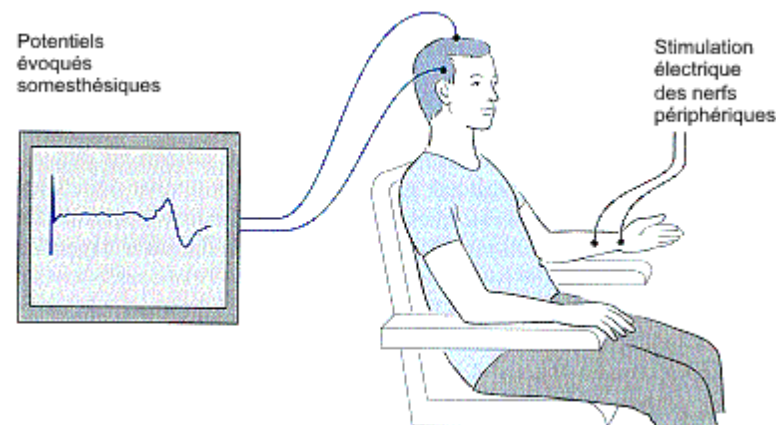


Figure II-6 Study Of Somatosensory Evoked Potential

Using the SEP, physiologists can acquire knowledge about the function of peripheral sensory nerve pathways in different areas: cervical, thoracic, lumbar or sacral and also the spinal sensory nerve pathways and intra-cerebrals.

The collected signals during the examination (figure II.6) depend on certain factors such as the age and size of the subject, for example. When variations are produced at latency and amplitude of the somatosensory evoked potentials, this indicates the existence of problems in the sensory pathways. Also, the SEP permits to measure the degree of such damage (lesion) according to the type of change. In addition, the use of SEP enables to acquire information on the cognitive function problems during the appearance of dementia. Besides, the electrophysiological explorations have as a goal being non-invasive; they are used in the diagnosis of Alzheimer's disease.

#### **II.5.4 Cognitive Evoked Potentials:**

The Cognitive Evoked Potentials are known as "Events Related Potentials", denoted as (ERP). It consists in the difference of exogenous evoked potentials caused by external stimuli. They are interpreted as being a reflection of the information processing related to the psychological reaction of the subject in relation to the stimulation. ERPs are successions of waves; their appearance latency measures the time it takes for the brain to carry out the recognition work based on the stimulation (words, geometric shapes, sounds ...). It allows a chronometer of some cognitive functions.

ERPs play a significant role in understanding the cognitive functioning system of the subject in close interaction with its physiological state. Indeed, they have been the interest of several researches for over half a century. They are recognized as physiological signs of a particular psychological activity and specific to each individual. Mainly, two types of ERP can be distinguished:

- The so-called ERP (early): They indicate the perceptual processing of physical characteristics of the stimulus. They occur from approximately 100ms after the simulation.
- The so-called ERP (late): they are recognized as an indicator of a deeper processing of information involving a level of sustained attention and often taking decision. They occur beyond 150ms

However, from these two types of ERP and according to their polarity (positive or negative), we can distinguish different ERPs considered waves as N100, N170, N200, N400, N600, P100, P200, P300, P600, P800. Variation Factors, in these waves, are numerous: age, degree of deterioration, the level of vigilance.

## II.6 Types of electrodes

The electrodes are of 3 types:

- **Conventional electrodes or pad electrodes:** (Grey Walter-type electrodes): They have the form of a small dome of 2 cm<sup>2</sup> at the base, chlorinated silver covered with a soaked material pad of a saline solution. They are placed directly on the scalp after degreasing the scalp and applying a conductive paste. They are maintained by a helmet made of crossed rubber straps that married the skull of the subject.
- **Needle electrodes or subcutaneous:** They have the form of a silver hypodermic needle or stainless steel. Their end is stuck into the thickness of the scalp. Thus, they provide an electrical contact of good quality and a skin resistance / electrode substantially constant, without increasing the risk of infection. Their use is essential when it is imperative to collect an EEG signal in optimal technical conditions.
- **Cups electrodes:** They have the form of a silver disc with a diameter of 5 mm , the cup is filled with conductive paste and stuck directly on the scalp. These electrodes are connected to a recording apparatus using simple isolated wires. To ensure electrical continuity and good quality of the electrochemical interface (electrolyte-electrode-skin), the electrode resistance has to be measured. This measurement is made, according to the apparatus, relative to a reference electrode (so-called ground electrode) or with respect to all other electrodes placed on the scalp surface. These electrodes are used for extended recordings.

## II.7 Position of electrodes

The number of electrodes used for recording brain activity can be very variable. The most famous assembly, defined in 1958, is the 10/20 system as it is shown in figure II.7. With the improvement of electrodes and recording technologies, the number of electrodes has increased significantly to reach sometimes 64, 128 or 256. More recent standards exist, such as that of Gilmore in 1994 (Gilmore, 1994) however all arise from the 10/20 system. The 10/20 system meets strict rules:

- The depart line is that brings together nasion and the union in passing through the vertex
- This line is divided into 6 parts: 10% of the length is carried above the nasion to form the frontal plane and 10% above the union for the occipital plane, the rest is divided in equal four parts representing 20% of the total length.
- The symmetry must be perfect

The 10/20 system is altered in children; the number of electrodes depends on the head circumference. In premature infants and newborn, the device includes four electrodes that are arranged on each hemisphere in the frontal regions, parietal, occipital and temporal (Fp1, Fp2, C3, C4, O1, O2, T5, T6) and an earth electrode, and optionally two vertex electrodes: Cz, Pz. The number of electrodes increases with the age of the child up to 21 electrodes in young adults (Gilmore, 1994).

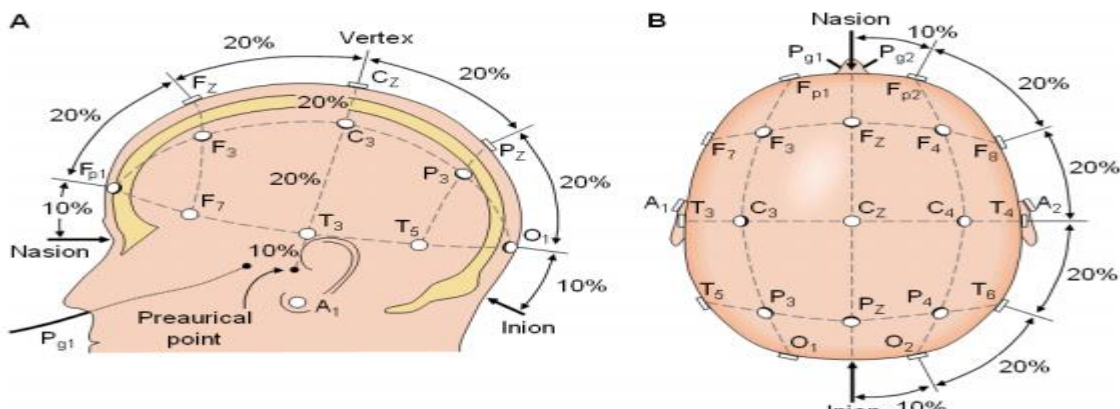


Figure II-7 position of electrodes in 10/20 system (<http://www.bem.fi/book/13/13.htm>)

As mentioned earlier, EEG measures the potential differences between electrode positions on the scalp. The EEG can be observed and detected by the following montages (Ernst Niedermeyer & da Silva, 2005),(Fisch & Spehlmann, 1999):

- Bipolar montage: A channel is usually made up by one pair of electrodes where each channel (waveform) represents the difference between two adjacent electrodes. The whole montage comprises of a series of these several channels. For instance, the channel "Fp1-F3" depicts the difference in the voltage between the Fp1 electrode and the F3 electrode. The next channel in the montage, "F3-C3," stands for the voltage difference between F3 and C3, and so on, through the entire array of electrodes.



- **Referential montage:** In this montage, each channel reveals the difference between a certain electrode and a designated reference electrode. It is worth noticing that there is no standard position for this reference. Thus, it is at a different position than the "recording" electrodes. Given that midline positions do not amplify the signal in one hemisphere versus the other, they are widely used. Also, "linked ears" is another common reference. Basically, it is a physical or mathematical average of electrodes attached to both earlobes and mastoids.
- **Average reference montage:** The outputs of all of the amplifiers are summed and averaged. Then, the obtained averaged signal is employed as the common reference for each channel. Average reference montage is ideal for focal activity, particularly from the temporal lobe and it can be improved by excluding affected electrodes.
- **Laplacian montage:** It is an example of a local average reference where each channel is referenced to an average of the electrodes surrounding it. To simplify, each channel represents the difference between an electrodes and a weighted average of the surrounding electrodes.

Basically, all signals are usually digitized and stored in a particular (generally referential) montage with digital EEG. Given that any montage can be constructed mathematically from any others, the EEGs can be seen by an EEG machine in any wanted display montage

## **II.8 EEG principales**

Continuous recording of brain activity is of recent appearance monitoring method. It has numerous indications in the field of resuscitation and anaesthesia.

The number and positioning of the electrodes depend on the purpose of monitoring. Abnormal electrical phenomena may be present on some derivations, reflecting focal dysfunction of the central nervous system, or across the scalp in the case of generalized dysfunction or drug impregnation. A compromise must be found between the initiation of simplicity and sensitivity of the system. The purpose of monitoring in the resuscitation is not to locate a source with precision, and the establishment of a complete 10-20 system consuming. Most often, monitoring of an assembly of seven or eight scalp electrodes is enough in intensive care.

The monitoring of only 2 channels by 5 electrodes can detect only 12 from 38% of "electrical seizures" identified by a 10-20 conventional system. In contrast, using a monitoring of 7 electrodes (frontal, temporal, vertex, inion) allows detection of 93% of "electrical seizures" (Shellhaas, Soaita, & Clancy, 2007).

The type of electrodes is also variable. In most cases, it is about cup electrodes. In this case, before being put in place, the stratum cornea must be greased even abraded to optimize the electric conduction. It is then highly recommended to check the electrode resistance. It must be low to ensure sufficient quality for interpretation. Thus, the resistance must be performed several times a day, usually twice, to ensure the quality of the plot and its interpretation.

## **II.9 Conclusion**

EEG technique has gradually become one of the most prominent tools for revealing the secret of the brain functionality due to the fact that EEG has a high temporal resolution.

The current chapter provided a detailed description of EEG technique. It introduced the historical background of the EEG modality. Then, it depicted the way an EEG experiment is performed. This chapter also introduced the several EEG recording techniques that exist so far in the literature and described the rhythmic activity. The evoked potentials were discussed with referring to its main types. Then, the different types of electrodes and their positioning were presented as well as the principles of EEG technique.

## Chapter III

# *Functional Magnetic Resonance Imaging*



Blood Oxygen Level Dependence (BOLD)  
contrast published in 1990 by Seiji Ogawa of Bell  
Laboratories and colleagues at the University of Minnesota

### III.1 Introduction

The brain, similar to any other body organ, involves a constant amount of oxygen to sustain its activity. The oxygen serves to provide energy after metabolizing glucose. It is worth noticing that hemoglobin is the component of blood that is in charge of supplying oxygen. Mainly, the magnetic properties of hemoglobin are related to the amount of oxygen it carries. Given this, an exciting technique evolved in the twentieth century for measuring brain activation. This method is known as functional Magnetic Resonance Imaging (fMRI).

With the advance in fMRI, the study of the human brain has entered a new era with new insights into neurology, psychiatry, psychology. As previously mentioned in chapter one, fMRI has gradually established its place as one of the most successful techniques in studying brain function. Basically, fMRI provides brain mapping in vivo in a non-invasive way by measuring the changes in oxygen level in the brain. In fMRI, data acquisition is commonly achieved by measuring Blood Oxygen Level Dependent (BOLD) signal changes.

The development of the BOLD contrast fMRI tools has yielded a considerable advancement in detecting the brain activity and connectivity. However, it is still far from giving accurate responses about the mechanisms involved in the functionality of the brain. Based on these tools several investigations, experiments and studies have been conducted on brain exploration. In fact, they have become one of the main knowledge sources about brain function that we have today and considered as an important means of knowing even more.

An fMRI experiment depends on various factors. Basically, fMRI experiments are composed of three main steps: (i) data acquisition in scans (ii) Experimental tasks defined by the paradigm design and finally (iii) data analysis. All these steps involve the use of different tools and methods. Mainly, the apparatus of data acquisition, fMRI data preprocessing methods, analysis and theories of the brain function are important for understanding all these concepts in order to extract valid knowledge from the information obtained in fMRI studies.

In this chapter, an overview of the principles of functional Magnetic Resonance Imaging (fMRI) signal is given. And, Blood Oxygen Level Dependent (BOLD effect) is introduced. The chapter starts by giving a brief history of fMRI technique. Then, it illustrates in details the BOLD signal on which fMRI is based. After this, the basic model to generate fMRI signal is described. Finally, the chapter ends with a discussion of the components of an fMRI experiment where the focus –in particular- has been placed on data analysis. This chapter serves only as an outline of the basic principles of fMRI. For more detail, we encourage the reader to refer to other references for a broader view of fMRI in general.

### **III.2 History of fMRI**

Functional Brain Imaging signals measured from brain activity, specifically those obtained with fMRI and PET (Positron Emission Tomography), are imaging technologies based on local changes of blood flow (Raichle & Mintun, 2006) and metabolism (glucose utilization and oxygen consumption) (Buzsáki, Kaila, & Raichle, 2007). It is known that these changes result from cellular activity in the brain, at astrocytes and neurons level.

Relating blood flow and brain activity is not a so recent idea. In the 19th century, it was first introduced by Angelo Mosso, an Italian physiologist. Recording the pulsations of the human cortex in patients with skull defects, during mental activity, Mosso observed that these pulsations increased locally (de Oliveira Jordao, 2010). It was in 1890 when the physiological relation between blood flow and neural activity has been explored by Charles Roy and Charles Sherrington (Roy & Sherrington, 1890) setting the base theories behind fMRI. During the 20th century, many contributions have been done in this area. Due the lack of tools, it was very difficult in the beginning to develop these ideas. For a more detailed review of the history of brain mapping, the reader is invited to see (Raichle, 2009).

In the two past decades, the development of fMRI has been the fruit of many discoveries and researches. Thus, fMRI has increasingly become a popular imaging tool in neuroimaging experiments for the investigation of brain functional areas that are responsible on specific tasks such as mental processes, including memory formation, language, pain, learning and emotion (Cabeza & Nyberg, 2000). fMRI has received this

considerable attention due to its various advantages. fMRI is a non-invasive technique that can provide a high spatial resolution. Also, it is relatively easy to use in neuroscience.

Two main events have paved the way for the development of fMRI: (i) the emergence of the MRI (Magnetic Resonance Imaging) technology, followed by (ii) the establishment of the basis of fMRI blood oxygen level dependent (BOLD) by Sieji Ogawa and colleagues in 1990 (Ogawa, Lee, Kay, & Tank, 1990). Since then, fMRI has been developed into the most prominent method used in functional brain imaging (Horwitz, Friston, & Taylor, 2000).

### **III.3 Magnetic resonance imaging (MRI)**

Magnetic Resonance Imaging (MRI) is a widely used technique to probe the anatomical and functional localization tool in neuroscience. MRI has been traditionally employed for structural analysis found in medicine seeking to enable the visualization and analysis of detailed internal structure of the body by producing pictures of soft tissues, organs and other internal structures.

Mainly, this technology is based on the fact that magnetic resonance signals are created by atomic nuclei from certain atoms (such as hydrogen, sodium, and phosphorous) when excited by radiofrequency (RF) (van Geuns et al., 1999). MRI provides a large number of flexible contrast parameters. This provides an excellent soft tissue contrast.

MRI brain imaging technique was first implemented by (Lauterbur, 1973). Several more years later, an imaging hardware has been developed for producing high-quality diagnostic images of the human body. After this, MRI has become a vital tool to use in diagnostics and facilitated the work of neuroscientists. Since the early 1980s, MRI has revolutionized diagnostic imaging in medicine because it provides unique contrast between soft tissues and high spatial resolution. Also, MRI has increasingly become indispensable technique in several research fields such as biology, engineering, as well as materials science.

The physical principles behind MRI rely on the phenomenon of Nuclear Magnetic Resonance (NMR). They were discovered independently in 1946 by two different groups of investigators. The first was in (Harvard) and the second was in (Stanford). In their work, they have developed methods for determining with precision magnetic nuclear

measurements (Bloch, 1946)(Purcell, Torrey, & Pound, 1946). More recently, NMR has been employed in exploring more complex structures such as living tissues. Thus, numerous applications have been applied nowadays in the clinic thanks to its potential to yield images of the body (through MR imaging) due to the spatial resolution at a millimetric scale.

MRI technology uses hydrogen proton nuclei, by far the most abundant in the human body where present in great concentration in water and macromolecules, to generate the images (Sands & Levitin, 2004). The hydrogen atoms absorb energy by the form of RF pulses and re-emit it as magnetic resonance which is perceived as a small voltage in a receive coil. Two mechanisms, known as T1 and T2 relaxation, bring the hydrogen nuclei back to a relaxed state. The relaxation time depends on molecule size and binding to other molecules (McKie & Brittenden, 2005). It should be noted that all tissues (e.g. muscle, bone, ligaments and tendons) have different T1 and T2 relaxation times. Based on this principle, it is possible to represent the tissues with different intensities in the scan images, measuring the energy emitted by the hydrogen atoms and applying different times of detection (TE, time to echo) and repetition of the RF pulse (TR, time to repetition). The obtained images have a good spatial resolution (in the millimetre scale) with a good contrast resolution (i.e. the ability to distinguish between two different tissues).

For more detail about the history and physical principles of the MRI technique, we invite the reader to see (Lauterbur, 1973). The interest of this chapter is to give a much more simplistic perspective of MRI in order to give just an overall understanding of its mechanisms. This is essential and necessary in view of the fact that MRI is the base of fMRI. A relatively new imaging technique (fMRI) , relying on sensitivity of the NMR signal from brain tissue to the different magnetic properties of oxygenated and deoxygenated blood, has revolutionized research in functional brain mapping. To simply explain this relation, we say that fMRI functionality maps into the brain structure obtained by MRI uses the same principles of magnetic resonance. The fundamental principles of Blood Oxygenation Level Dependent (BOLD), on which fMRI rely, are described in detail in the following section.

### **III.4 Blood oxygen level dependent (BOLD)**

The most common approaches towards fMRI use the Blood Oxygenation Level Dependent (BOLD) contrast. In 1990, Seiji Ogawa first demonstrated that by measuring the blood-oxygenation-level-dependent (BOLD) signal in rats. He observed that the intensity of the vascular signal in gradient-echo (GE) images decreased when blood was deoxygenated, and increased when the flow of freshly oxygenated blood increased. It was hypothesized that this effect, which later was termed as Blood Oxygenation Level Dependent (BOLD) contrast, would be used to visualize brain function (Ogawa et al., 1990).

In addition, several works have been developed in this context such as the work of (Kwong et al., 1992) that made functional mapping using the BOLD contrast. Furthermore, they have used long blocks of sustained visual stimulation followed by rest. The authors reported a sharp increase of the fMRI signal in relevant brain areas that remained for the whole stimulation period. The result was also demonstrated by (Ogawa et al., 1992). In this case, (Bandettini, Wong, Hinks, Tikofsky, & Hyde, 1992) made an experiment using a motor task to reveal brain activation and obtained similar results. Later, Blamire and colleagues performed a visual experiment cortex reported that even short duration stimuli gave rise to the same kind of MR signal increase (Blamire et al., 1992). However, they reported that there was a small delay, of approximately 3.5 seconds, between stimulus onset and the observable signal increase. To sum it up, we can say that the BOLD of fMRI was introduced by (Bandettini et al., 1992; Blamire et al., 1992; Kwong et al., 1992; Ogawa et al., 1992).

The BOLD fMRI technique is designed to measure primarily, changes in the inhomogeneity of the magnetic field that result from changes in blood oxygenation. It allows measuring the ratio of oxygenated (HbO<sub>2</sub>) to deoxygenated hemoglobin (dHb) in the blood. In other words, it doesn't measure neuronal activity directly. Instead, it measures the metabolic demands (oxygen consumption) of active neurons, figure III-1 illustrates the BOLD mechanism of fMRI figure III.1.

fMRI measures changes in cerebral hemodynamic which provide an indirect measure of neuronal activity. The dynamical properties of fMRI signals highly depend on



the neurovascular coupling that relates vascular changes to neural activity (K. J. Friston, Mechelli, Turner, & Price, 2000).

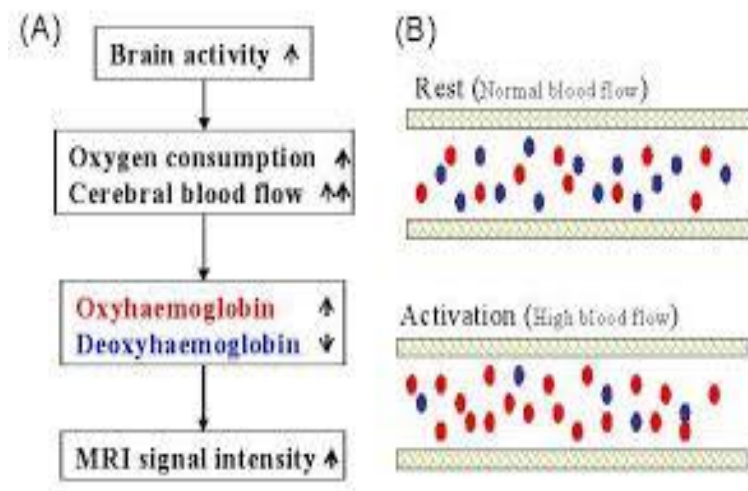


**Figure III-1 BOLD mechanism of functional MRI**

Blood-oxygen level-dependent signal mechanism (see figure III-1 (B)) oxyhaemoglobin and deoxyhaemoglobin blood flow during rest and activation.

Several research groups have repeated and extended their experiments. These experiments have been used to answer research question about brain activity and they helped them in investigating human brain function. Nowadays, fMRI is the standard tool for functional neuroimaging and it is capable of performing functional imaging due to the high availability of MR scanners. This has resulted in an explosion of fMRI studies and it has implied increase in the number of publication about fMRI field as illustrated in Figure III.2. The most common clinical application of fMRI is perhaps pre-surgical mapping of eloquent areas and evaluation of hemispheric language dominance prior to temporal lobectomy of certain epilepsy patients.

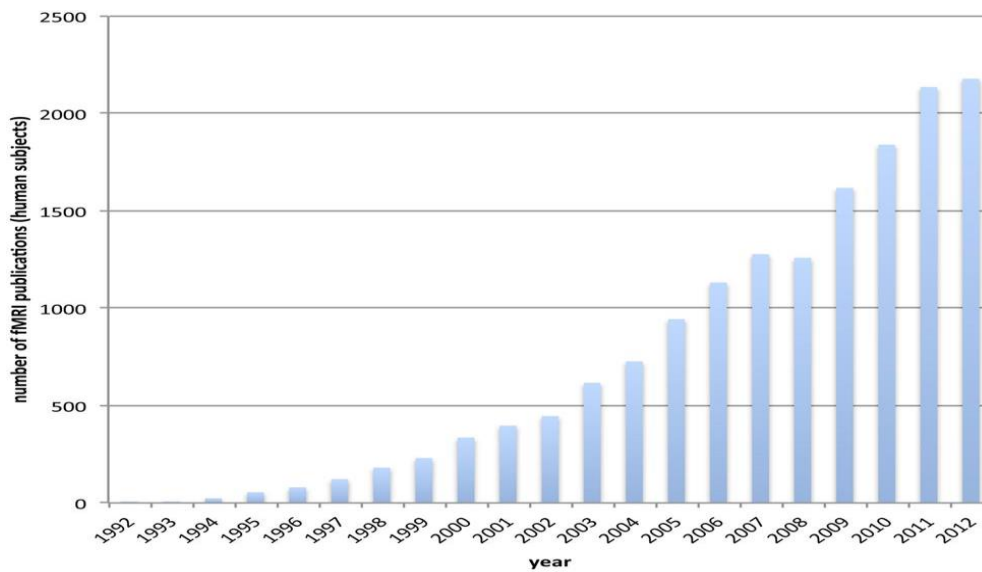


**Figure III-2** the number of fMRI publications by year (Stelzer, Lohmann, Mueller, Buschmann, & Turner, 2014)

### III.5 Hemodynamic Response Function

The major aim for all fMRI conducted experiments is to gain a better understanding to neural activity. As previously mentioned, neurons require energy, which is supplied by blood flow, in order to function. However, BOLD fMRI does not measure the activity of neurons directly. Instead, it measures the metabolic demands of active neurons. Giving this, reaching the above fMRI objective is waiting for further study.

To address this gap, the fMRI evoked response needs to be modelled using the so-called Hemodynamic Response Function which is a nonlinear function. In other words, we have to model the BOLD response into an impulse input. The box-car standard, the Gaussians and the canonical model proposed in (K. J. Friston, Jezzard, & Turner, 1994), (Aguirre, Zarahn, & D'esposito, 1998) are some of the several HRF models that have been developed. They have an essential role to play in characterizing the onset of the stimulus.

The hemodynamic response is the basis for the BOLD (Blood Oxygen Level Dependent) contrast in fMRI. Mainly, the hemodynamic response occurs within seconds of the presented stimuli. In the current section, we focus on the study of the canonical HRF model. As presented figure III-3, this model is divided into two parts; the first part describes the peak whereas the second one is employed to model the undershoot. A good model for the canonical HRF is obtained by the function whose peak is situated between

4-6 seconds (Gjedde, 2001). The relationship between the stimulus and BOLD response, denoted by  $y(t)$ , is typically modelled as the convolution of the stimulus function with an impulse response ( HRF) as presented in the following equation:

$$y(t) = s(t) \otimes h(\tau) = \int_0^T s(t - \tau)h(\tau)d\tau \quad (\text{III.1})$$

where  $h(t)$ ,  $y(t)$  and  $s(t)$  denote HRF , the result and the unprocessed fMRI signal respectively.

The convolution result is known as epochs in SPM (Statistical Parametric Mapping) (K. J. Friston, Holmes, et al., 1994). The canonical HRF performs well in many experiments. However, some activated voxels are ignored due to the fact that the real HRF varies in different people and in different brain regions of the same person as well (Penny, Holmes, & Friston, 2003) .

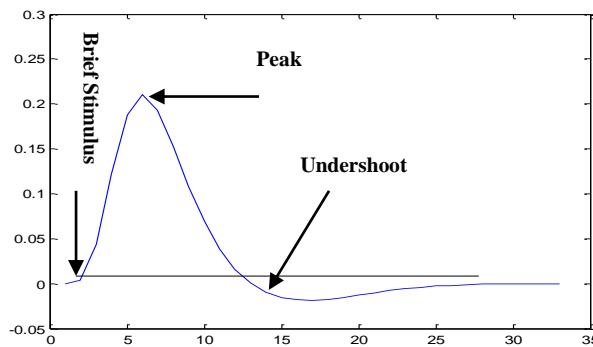


Figure III-3 Model of Canonical hemodynamic response

### III.6 Guidelines and Design for fMRI experimental studies

Generally, the study of fMRI time series is related to the activity of neurons in response to an input stimulus during the course of an experiment. Various fMRI analysis methods derived from methods of processing and statistical analysis have been used. They can be classified into two main groups: (i) the hypothesis-based methods, such as the general linear model (GLM), and (ii) the data-driven methods including clustering methods, Principal Component Analysis (PCA) and Independent Component Analysis (ICA). In fact, ICA has proven to provide a powerful method for the exploratory analysis of temporal and spatial fMRI data. All methods have, as common factor, the ability to identify more meaningful areas of brain activation in a patient (Bogorodzki, Rogowska, & Yurgelun-Todd, 2005).

Developing successful fMRI experiments requires careful attention to experimental design, data acquisition techniques, and data analysis. The fMRI data analysis greatly depends on cerebral hemodynamic changes, known as Hemodynamic Response Function. Thus, it is necessary to take into account the spatial and temporal resolutions of these hemodynamic effects. The spatial characteristics resulting from cerebral vasculature and the temporal characteristics relate to the inherent delay of signal changes in response to neural activity and the hemodynamic changes resulting dispersion over time.

Within fMRI methodology, there are three different ways typically used to present the stimulus based on the temporal characteristics of the hemodynamic phenomena. As illustrated in figure III-4, the three kinds of design are blocked, event-related or mixed (Petersen & Dubis, 2012) .

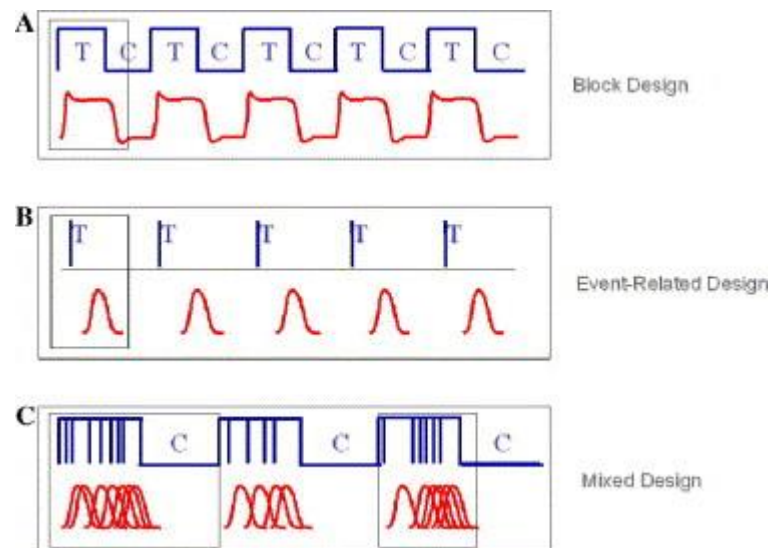


**Figure III-4 (a) blocked design (b) Event-Related design (c) Mixed design fMRI experiments**  
(<http://thoughtsfromanislnd.tumblr.com/post/61730578866/fmri-experimental-designs>).

### **III.6.1 Blocked design:**

This category of paradigm is based on segregating different cognitive processes by presenting stimuli sequentially within a condition into distinct time periods. In other words, the experience is performed in continuous mode in blocks of time (typically lasting 20-30 sec). The measurements are done following injection of radioactive bolus. Alternating these with other moments (epochs) is when a different condition is presented. The alternation of two conditions is known as an ‘AB block’ design. In this case, a boxcar designs with alternating activation and rest have been used in which a ‘cycle’ corresponds

to two epochs of each condition whose purpose is to create a "steady state" of neuronal and hemodynamic changes. This is an excellent way for determining small changes in brain activity.

At the beginning, blocked design (see figure III.4 (a)) has gained a considerable attention in the fMRI experimentation. According to Matthews and Jezzard (Matthews & Jezzard, 2004), the most efficient design for the BOLD fMRI data analysis is the block design. The later uses long alternating periods, during each of them a discrete cognitive state is performed. Furthermore, these two different states alternating during the experiment serve to prevent that patient, related artifacts or scanner sensitivity result in different impacts on the signal responses from both states. Block designs are well suited to localize functional areas and study steady state processes (e.g. attention). They are powerful in terms of detection and determination of which voxels are activated. (Chee, Venkatraman, Westphal, & Siong, 2003) On the other hand, block designs have a poor estimation power because of summation of the hemodynamic responses in time, i.e. a weak ability to determine the time course of the response.

#### **III.6.2 Event-related design**

Event-related designs are based on the assumption that neural activity will occur for short and discrete intervals. Experimentation based on Event-related designs have become increasingly very popular in fMRI research (Dale, 1999)(K. J. Friston, Zarahn, Josephs, Henson, & Dale, 1999) (Buračas & Boynton, 2002). Basically, Event-related designs (figure III.4 (b)) allow different trials or stimuli to be presented in arbitrary sequences, thus eliminating potential confounds, such as habituation, anticipation, set, or other strategy effects. Data may be recorded to monitor the BOLD response following a marked (pre-determined) event such as a single stimulus or task. In this type, each event is separated in time by an Inter-Stimulus Interval (ISI) ranging from few second to 20s. Temporal response patterns and the hemodynamic response characteristics associated with the linear application of multiple stimuli are used. Event related designs are based on the assumption that neural activity will occur for short and discrete intervals. These last are applied individually and in random order and measure the hemodynamic response to each of them. This method may be further divided into:

- Design of spaced single study with long intervals between stimuli and used in order to allow that in the end of each stimulus the hemodynamic response returns to its resting state);
- Design of fast single study takes advantage of the property of linearity and superposition of the hemodynamic response.

One of the major important points for these studies is to know how to recognize the key variables to consider such as spatial resolution, temporal resolution, and cerebral coverage and signal to noise ratio (SNR). Thus, they can be conveniently manipulated to obtain the desired results. To obtain a very high spatial resolution, it is essential to reduce the temporal resolution, limit the coverage and reduce cerebral SNR.

Concerning the event-related designs, the estimation power (how does its activity change over time) is often good. They permit inquiring the hemodynamic shape for each condition and comparing parameters such as the amplitude or the timing between conditions. Event-related designs are able to randomize and mix different types of events. This ensures that one event is not influenced by others and not affected by the cognitive state of an individual. So, there is no predictability of events.

However, the detection power is relatively weak when compared with blocked design. This is due to the fact that experimental power depends on the number of events that are averaged. Furthermore, other important aspects associated with these techniques must be considered, such as the extremely high financial costs and restrictions on patient safety (Cox & Savoy, 2003).

#### **III.6.3 Mixed designs**

Several researchers have recognized the need to take into account two distinct types of neural processes during fMRI tasks that use a combination of block and event-related designs which will be able to provide information relating to ‘sustained activity’ versus ‘transient activity’ during paradigm performance. This technique is an interesting mixture of the characteristic block design measurement of repetitive sets of stimuli and the transient responses detected by event-related designs. It allows extracting brain regions exhibiting an item-related pattern of information processing (transient), or a task-related information processing (sustained). In doing so, mixed designs (figure III-4 (c)) have

added a new perspective to psychologists to explore fMRI in understanding ‘what’ is the role of certain node of a network subsiding a task.

The mixed design has been used in a large number of studies over the intervening years since its inception. Although it has been applied successfully in memory studies, it involves more assumptions than other designs, and the researcher will have to tackle issues associated with poorer HRF shape estimation, and post hoc analysis of behavior correlated activation.

To sum it up, the following table highlights the main limitations and strengths of the three types of fMRI experimental designs

**Table III-1: Comparison of fMRI designs**

	<b>Blocked Design</b>	<b>Event- related design</b>	<b>Mixed design</b>
<b>Advantages</b>	<ul style="list-style-type: none"> <li>• Powerful for detecting activation</li> <li>• Useful for examining state changes</li> </ul>	<ul style="list-style-type: none"> <li>• Powerful for estimating time course of activity</li> <li>• Allows determination of baseline activity</li> <li>• Best for post hoc trial sorting</li> </ul>	<ul style="list-style-type: none"> <li>• Best combination of detection and estimation</li> <li>• Much more complicated analyses.</li> </ul>
<b>limitations</b>	<ul style="list-style-type: none"> <li>• Sensitive to head motion, especially when only a few blocks are used.</li> <li>• Many tasks cannot be conducted repeatedly</li> <li>• Poor choice of baseline may preclude meaningful conclusions</li> <li>• Very sensitive to signal drift</li> <li>• Difficult to estimate the HDR</li> </ul>	<ul style="list-style-type: none"> <li>• Long intervals do not optimally increase stimulus variance</li> <li>• Short intervals may result in refractory effects</li> <li>• Length of “event” may not be known</li> <li>• Detection ability dependent on form of HDR</li> </ul>	<ul style="list-style-type: none"> <li>• requires power considerations different from both block designs and event-related designs</li> <li>• Consideration of the number of subjects is necessary when designing mixed design experiments.</li> </ul>

### III.7 The Principle of The General Linear Model

The general linear model (GLM) has the following form:

$$y_i = \beta_0 + x_{i1}\beta_1 + \dots + x_{ik}\beta_{1k} + \dots + x_{ip}\beta_p + \varepsilon_i \quad i = 1, 2, 3, \dots, n \quad (\text{III.2})$$

where  $y_i$  stands for activate value of voxel in the  $i$ th scan, i.e, the measure in time  $t_i$ . Our interest focuses on the temporary evolution of a voxel which is represented by a column vector with a length  $n$  corresponding to  $n$  instants of images’ acquisition. Let  $m$  be

the total number of voxels in a cerebral volume. Column ( $y_i$ ) vectors are collected in a matrix denoted by  $Y$  with a size ( $n \times m$ ) in order to present the evolution of times series. The matrix becomes as follows:

$$Y = X\beta + \varepsilon \quad (\text{III.3})$$

where  $X$  denotes the design matrix which contains prior information on the protocol including a set of tasks carried out by the subject, or a set of stimulus to which the subject is submitted. Assuming that  $p$  is in general very inferior to ( $n$  and  $m$ ), The design matrix has a size of ( $n \times p$ ). It is important to note that the dimension is proportional to the factors' number (types of stimulus, of tasks) considered in the study. As aforementioned above, our work aims to generate this design matrix from the already known information about the experiment. Let  $B$  be the vector that contains parameters  $\beta_i$  which we seek to estimate and let  $\varepsilon$  be the vector which contains the residues (errors)  $\varepsilon_i$  that we suppose to be independent and identically distributed according to a normal law:  $N(0, \sigma^2)$ .

Once the model is constructed, we seek to find for each voxel of cerebral volume the linear combination of the model functions which better describes the temporal signal corresponding to a voxel i.e. it adjusts data to model. Given this, we search to reach the exact following linear decomposition:

$$Y = X\beta \quad (\text{III.4})$$

Therefore, the sum of errors will be minimized as  $(\sum \varepsilon^2)$

The estimation of  $\beta$  obtained by the method of least squares is given as follows:

$$\hat{\beta} = (X^T X)^{-1} X^T \quad (\text{III.5})$$

It is worth to note that computing of  $\beta$  parameters requires the calculation of the inverse matrix  $(X^T X)^{-1}$ . However, this one is badly scaled, in the sense that its determinant value is close to zeros ( $\det(X^T X)^{-1} \approx 0$ ) and yet can result in producing errors in calculation. To overcome this problem, we will resort to the use of Pseudo-inverse  $(X)^+$  de Moore-Penrose [5] for the estimation of  $\beta$ .

$$\hat{\beta} = (X)^+ Y \quad (\text{III.6})$$



While certain parameters will be important such as the effect of a particular sensory motor, cognitive state or the coefficient of regression of hemodynamic responses on the time of reaction, other parameters will be with no significance and they are connected with corresponding effects.

Inference on the estimation of parameters is realized by using its estimated variance i.e. we estimate the residual variance,  $\hat{\sigma}^2$ , for each voxel  $j$ . For better clarification,  $\hat{\sigma}^2$  refers to the variance of errors and it is calculated by:

$$\hat{\sigma}^2 = \frac{1}{N-p} (y - X\hat{\beta})^T (y - X\hat{\beta}) \quad (\text{III.7})$$

where  $N$  and  $p$  are the dimensions of the design matrix ( $X$ ).

In order to detect the functional activity, a t-test  $T$  (t-test student)[6] has been employed to make a test of the null hypothesis ( $H_0$ ). In this test, we intend to introduce line vector  $C$  called contrast.  $C=[1 \ 0 \ 0 \ ..00]$  is an example of such contrast.

By the  $t$  of t-test, we mean the contrast of parameters estimated on the root of the estimated variance. This one denotes a distribution of student in  $(N-P)$  degree of freedom whose statistic value is calculated by:

$$t = \frac{C^T \hat{\beta}}{\sqrt{\sigma^2 C^T (X^T X)^{-1} C}} \quad (\text{III.8})$$

As a final point, a Comparison of ( $t$ ) calculated with a distribution ( $t_\alpha$ ) of Student to  $(N-P)$  degrees of freedom is performed to turn the hypothesis ( $H_0$ ) out to be true.

Supposing that  $t_\alpha = 1.96$ , we get  $\alpha = 0.05$  if  $|t| > t_\alpha$ , then we say that the voxel is significantly active. We trace the absolute value of  $t$  in the site of the treated voxel. The performed process is repeated in the same way for each voxel.

### **III.8 Conclusion**

In recent years, functional Magnetic Resonance Imaging has become the most dominant technique to reveal better insights of the brain function due to its high spatial resolution. The focus of the current chapter was placed on introducing fMRI basics to the widest possible audience.

At first, the chapter briefly provided a brief history about fMRI. And then, it presented the BOLD effect in details. The latter is an essential element in the next chapter. After this, the basic model to generate fMRI signal was described. Also, the components of an fMRI experiment were discussed. At last, we highlighted the principles of the General Linear model.

## Chapter IV

# State of the art of EEG/ fMRI information fusion



*The figure shows the EEG electrode placement on the scalp when the subject is placed in the MRI head coil. From Bergen fMRI Group, GE 3.T Signa MR scanner with NNL Inc. LED goggles, and BrainProducts EEG amplifiers.*

## IV.1 Introduction

Brain imaging techniques such as Functional Magnetic Resonance Imaging and (fMRI) and electroencephalography (EEG) provide complementary spatio-temporal information about the brain function. Each modality has its own advantages. For example, EEG reflects the brain changes on timescale of millisecond (Eichele et al., 2008), which means that it can capture the brain dynamic changes very well. However, it has poor in spatial resolution due to being recorded from a limited number of electrodes. On the other hand, fMRI is powerful in investigating the brain function however it is slow in following the brain activities because it relies on the brain blood flow response rather than electrical activities(Steinberg, Bowman, & White, 1999). Given this, the integration of information obtained from these two modalities promises to provide a better understanding of brain function(Calhoun & Adali, 2009). Various methods have been developed to combine high spatial resolution data provided by fMRI with high temporal resolution generated by EEG (Bonmassar et al., 2001) (Calhoun, Adali, Pearlson, & Kiehl, 2006). The volume of papers and number of applications are steadily increasing (see Figure IV-1).

This chapter is devoted to shed the light on EEG/fMRI integration. At first, we begin with a description of state of the art of EEG-fMRI fusion techniques by providing the contribution about EEG and fMRI fusion data and especially their complementary natures based on a systematic technique.

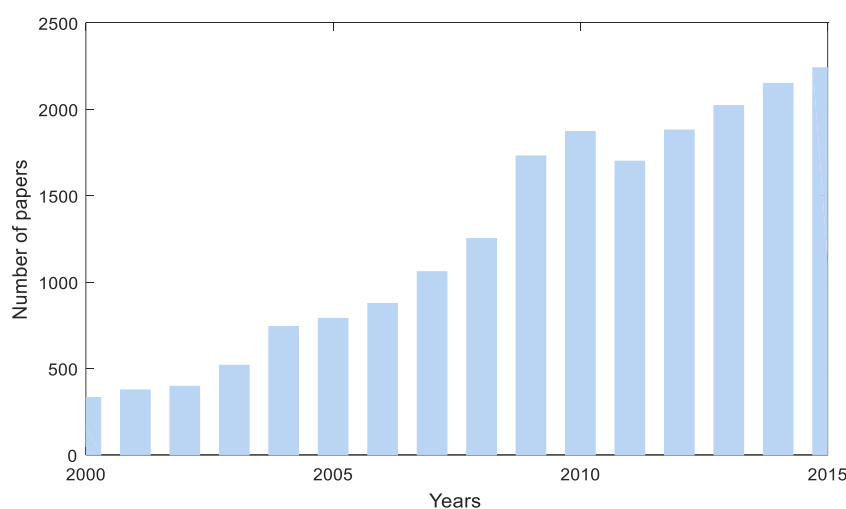


**Figure 0-1: Number of papers per year for EEG, fMRI, and their fusion (<https://scholar.google.fr>)**

## **IV.2 State of the art of fMRI-EEG fusion methods**

In the investigation of brain processes, both EEG and fMRI techniques have clearly shown their ability as non-invasive techniques to measure different attributes of brain activity. Therefore, the high temporal resolution and spatial resolution that can be separately acquired by EEG and fMRI respectively have received considerable attention during the past decade.

However, it is difficult to estimate the neural activity from hemodynamic response since fMRI data analysis relies on slow mechanisms such as blood flow, oxygen consumption and metabolism which yield only an indirect measure of the evoked BOLD signals. Likewise, it has been clearly observed that fMRI suffers from an ill-posed temporal inverse problem. On the other hand, the EEG modality suffers from spatial inverse problem beside noise raised due to the unavoidable artifacts during the course of the experiment which can strongly degrade the EEG signals quality.

Based on the fact that strengths and weaknesses of fMRI and EEG complete each other, simultaneous EEG-fMRI acquisition applications are fast becoming a key technique to provide a more comprehensive understanding of the nature of the cerebral activity with its enhanced spatiotemporal resolution. More specifically, the aim of this technique is to pinpoint the neural sources of epileptogenic EEG activity for both diagnosis and presurgical planning (Ives, Warach, Schmitt, Edelman, & Schomer, 1993). Primarily, both EEG and fMRI data measures the activity of neurons where the EEG, revealing the Event-Related Potentials (ERP) for investigating the psychophysiological states and information processing, is typical for the electrical activity and fMRI data are concerned with the hemodynamic signal. It is worth to note that the evoked electromagnetic and metabolic responses which are detected by both EEG and fMRI are not essentially the result of the same primary neuronal processes (Pflieger & Greenblatt, 2001). This will be the focus of this chapter. As will closely follow, this approach is categorized into symmetrical fusion (model or data) driven (Lei, Valdes-Sosa, & Yao, 2012). In figure IV-1, a brief summary to the EEG-fMRI fusion approaches is given.

During the past decade, a great effort has been devoted to develop EEG-fMRI integration procedures to take full advantage of the complementary data available from both modalities. Mainly, the existing potential approaches can be divided into two

categories. First, the asymmetric methods are divided into two influential approaches, fMRI informed EEG and EEG-informed fMRI analysis. The second category is the EEG-fMRI symmetric method. In the asymmetric approaches for EEG- fMRI analysis, prior information of one modality is considered as a cause or a predictor of the other. That is, it serves as a guide for the analysis of the other modality.

Assuming that “Neuronal activity” , denoted as  $\zeta$ , can be divided into two related sub-spaces, EEG  $\zeta$  and fMRI  $\zeta$  that correspond to the parts of  $\zeta$  that contribute to EEG and fMRI signals, respectively (Daunizeau et al., 2007). As will be illustrated in figure IV.2, the intersection 1  $\zeta$  describes a “common substrate” of neuronal activity. In contrast, 2  $\zeta$  (respectively 3  $\zeta$ ) stands for the subspace of neuronal activity detected by EEG (respectively fMRI) that does not contribute to fMRI (respectively EEG) measurements.

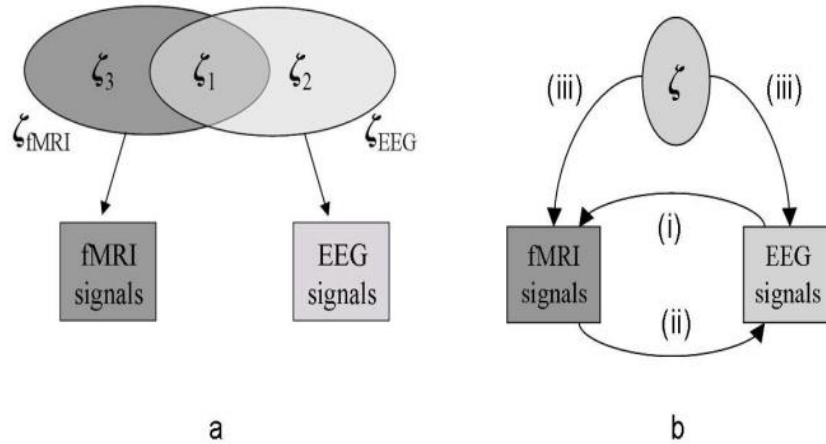


Figure 0-2: Formalization of the EEG/fMRI coupling-uncoupling (Daunizeau, Laufs, & Friston, 2009)

### IV.2.1 Asymmetric approaches

fMRI informed EEG, known as fMRI-constrained EEG imaging, employs spatial information from fMRI signal for reconstructing the source of the EEG signal (Dale et al., 2000) (Trujillo-Barreto, Martinez-Montes, Melie-Garcia, & Valdes-Sosa, 2001) (Lei, Qiu, Xu, & Yao, 2010). This approach has proven to be of high utility by providing a high and clear spatiotemporal resolution particularly in the neural generators of scalp EEG phenomenon. Nevertheless, it does not consider the variability in neural events which occur during the course of the experiment. However, EEG-informed fMRI technique is concerned with modelling the fMRI signal with features from EEG convolved with the hemodynamic response function (HRF) (Martinez-Montes, Valdés-Sosa, Miwakeichi,

Goldman, & Cohen, 2004) (Eichele et al., 2008). Using this technique, analysts are able not only to establish a link between the physiological measures of several modalities, also to reveal the relationship linking physiology and differences in perception, behavior and cognition. However, the symmetric approach implies the use of a common forward or generative model to explore and to explain EEG and fMRI data jointly. (Daunizeau, Laufs, & Friston, 2009)(Deco, Jirsa, Robinson, Breakspear, & Friston, 2008), (Valdes-Sosa et al., 2009).

In the context of asymmetrical approach, several methods have been proposed to fuse EEG and fMRI. In this technique, one modality is based on the assumption of another modality to detect neuronal activity (Pflieger & Greenblatt, 2001). As mentioned in (Baillet, Mosher, & Leahy, 2001) there are two models for source structure: The first is equivalent current dipole and the second is distributed source.

The Equivalent Current Dipole (ECD) method (Scherg & Von Cramon, 1986) is employed to limit the location of the dipoles in order to be within fMRI active region (George et al., 1995) . Likewise, the ECD method is also used by employing Markov Chain Monte Carlo sampling and a Bayesian formulation for fMRI mappings (Jun et al., 2008). Despite the popularity of ECD methods in practice, they suffer from major drawbacks. The number of dipoles is specified by the user. In addition, the optimization algorithm is not capable of finding the optimal dipole due to a local minimum, (Yao & Dewald, 2005).

Distributed Source Model (DSM) allocates a large number of dipoles with fixed locations which are dispersed over the cortex (Hämäläinen et al., 1993). Using dipoles with fixed locations implies that the forward problem is linear and the source localization can be regarded as solving an underdetermined linear system of equations.

Recently a Gaussian Source Model, referred to as GSM, has been introduced to integrate both ECD and Distributed Source Model (Lei et al., 2010). According to (Lei et al., 2012), GSM is mainly based on the parallel array of pyramidal neuron and the propagate property of cortical activity. In contrast, an alternative technique depends on the data in order to automatically extract sparse or distributed model (K. Friston et al., 2008). It is worth to note that both models are integrations of previous extreme source models

and are physiologically reasonable for EEG source reconstruction. The method relies on an adaptive Wiener filter and it is supposed that the energy of the electrical activity at every location on the cortex is proportional to the magnitude of the BOLD response at the same location (Liu & He, 2008). Phillips et al. introduced an approach based on a Bayesian EEG source localization method which can automatically choose priors from a set of candidate priors (Phillips, Mattout, Rugg, Maquet, & Friston, 2005), (Mattout, Phillips, Penny, Rugg, & Friston, 2006). Location priors can be derived from fMRI activation maps when using such a method for EEG/fMRI fusion (Mattout et al., 2006).

The prominent methods that have shown their ability in the analysis of combining EEG and fMRI data such As Principal Component Analysis (PCA) and Independent Component Analysis (ICA) can be used to explain the information observed from both modalities EEG and fMRI (Brookings, Ortigue, Grafton, & Carlson, 2009). Other methods based on multiple regressions of the BOLD on all EEG frequency bands or entire decomposed features (Laufs et al., 2003), (Eichele et al., 2008) have emerged from studies of EEG rhythm and have also shown that the relationship between EEG and fMRI is accordingly misled by high correlation between different frequency-band EEG signals (De Munck et al., 2007).

In this context, numerous studies based on convolution of both EEG features with a standard HRF (Lange & Zeger, 1997) have been conducted. In this case, hemodynamic response correlates with EEG rhythms (Goldman, Stern, Engel Jr, & Cohen, 2002), (Laufs et al., 2003) and adaptive modulations of event related responses (Debener, Ullsperger, Siegel, & Engel, 2006). However, several reports have shown the variability in the shape of the HRF as a function dependent on regions, subjects, age, task, sex, and sessions (LeVan, Tyvaert, Moeller, & Gotman, 2010), (Masterton et al., 2010). Other reports have interested in an intricate EEG phenomenon in epilepsy (Salek-Haddadi et al., 2003). HRF is stochastic model. Then this model is dependent on a specific shape of BOLD response may be an attractive alternative (Sturzbecher et al., 2008) (Sato, Rondinoni, Sturzbecher, de Araujo, & Amaro, 2010). However, these approaches have common problems which are the large number of parameters and lack in statistical inference.



## **IV.2.2 EEG/fMRI SYMMETRICAL FUSION**

As noted above, the main focus of this work lies on symmetrical approach wherein we introduce a new method based on Dempster-Shafer theory in order to fuse EEG and fMRI analysis. Explaining and analyzing both modalities (EEG/fMRI) simultaneously in symmetrical fusion approach entails using a so-called forward model (or generative model) that specifies the relationships between data and its sources. In contrast, the asymmetrical approaches refer to one modality (EEG / fMRI) privileged status as a prior knowledge for the other modality (Martínez-Montes et al., 2004). Including model-driven and data-driven fusion (Lei et al., 2012), as will be closely described with more details, symmetrical fusion techniques do not necessitate prior understanding. Regardless of the fact that each of data and model is individual, it seems obvious that the combination and interaction of data and model would be promising in the future for the simultaneous EEG/fMRI techniques figure IV.3.

### **IV.2.2.1 SYMMETRICAL MODEL-DRIVEN**

Model-driven symmetric fusions, such as GLM, require a precise biophysical model that shows post-synaptic potentials to EEG on one hand and BOLD signals on the other hand (Valdes-Sosa et al., 2009), this means that, Model-driven symmetric fusion is predicated on basis of the activity of an ensemble of postsynaptic potentials. This has two effects that translates into net primary current densities and then to EEG; and alternatively translates into vasomotor feed forward signal and then to BOLD. However, simultaneous EEG and FMRI recordings engages multivariate spaces and several essential specific actions, which in its turn gives raise to several problems for the model driven fusions. As a consequence, further investigation on model driven is required.

### **IV.2.2.2 SYMMETRICAL DATA-DRIVEN**

Data-driven fusions are well-known for neuroimaging data study and most work conducted on them has measured the relationship or difference between the EEG and evoked BOLD signal. In brief, these techniques employ a symmetric method to mutually assess information provided by both modalities and allow the user to ignore the exact form of the response depending on an assumption of independence or orthogonality. Using the advantages of each modality, the ultimate objective of symmetric data fusion approaches is to reveal the common neuronal sources producing both EEG and fMRI signals with high accuracy. Taken joint ICA as an example (Lei et al., 2012), data-driven

fusion is typical for specific hypotheses on spatial and temporal relationships are lacking, or ill-specified. A fine example for such hypothesis is the traditional inference tests (K. J. Friston, Jezzard, et al., 1994) when they are neither demonstrated nor sensitive due to conservative significance thresholds. Data-driven fusion proves its ability to eliminate noise from the data, localize the generators of EEG phenomena and provide empirical constraints for model-driven methods. Also, Aspects of brain function that are previously unrevealed or seems difficult to model can be detected via data driven techniques. Examples of such aspects are those faced by neurovascular transformation function estimation (Deco, Jirsa, McIntosh, Sporns, & Kötter, 2009).

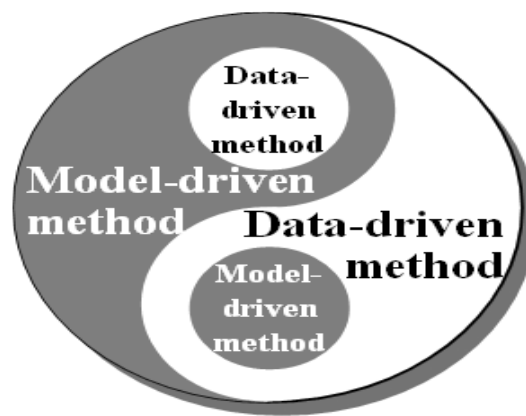


**Figure 0-3: Integration of data- and model-driven fusions. Despite the individuality between them, the integration and interaction of data and model might be promising for EEG/fMRI fusion.**

### **IV.3 EEG FMRI INFORMATION FUSION APPLICATIONS**

Since the first simultaneous acquisition of fMRI-EEG in humans (Ives et al., 1993), this non-invasive method is gaining a considerable attention in several research areas.

#### **IV.3.1 fMRI-EEG in epilepsy**

The initial motivation for EEG-fMRI was in the field of epilepsy research (Bonmassar et al., 2001), and in particular the study of interictal epileptic discharges (IED or interictal spikes), and their generators, and seizures. The Freedom from Distractibility Index FDI are random events and subclinical patients with epilepsy that cannot be observed using the EEG (or MEG). Therefore EEG recording during fMRI acquisition allows us to study hemodynamic changes correlated in the brain during seizures. (Gotman & Pittau, 2011) The method can reveal hemodynamic changes associated with IED attacks, and it has proved to be a powerful scientific tool.

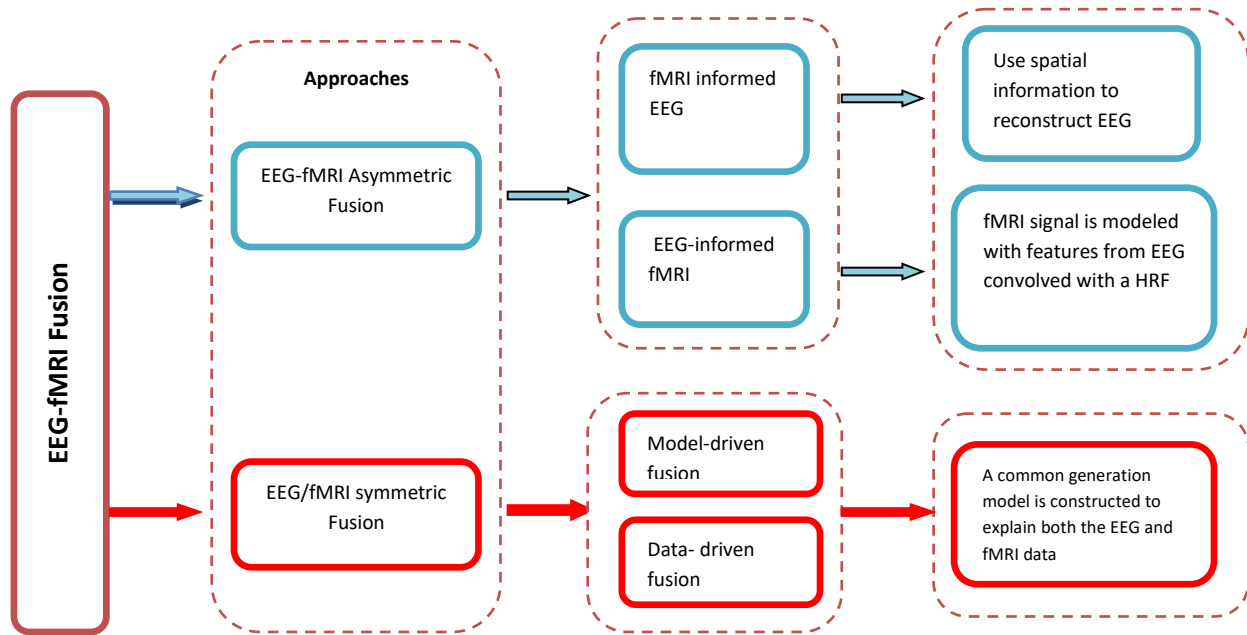


Figure 0-4: the approaches of EEG-fMRI techniques fusion

### IV.3.2 fMRI- EEG for sleep study

Several studies have used fMRI- EEG during sleep. Activation of the occipital lobe and deactivation of frontal lobe could be detected during paradoxical sleep (Lövlblad et al., 1999). fMRI / EEG has also been used to characterize different types of areas during sleep and compare their location (Schabus et al., 2007) . Other studies have been conducted regarding the auditory stimulation (Czisch et al., 2004), (Portas et al., 2000) and visual stimulation (Born et al., 2002) during sleep. However, this type of study is faced to the noise generated by the acquisition that can disturb sleep despite the use of quieter sequences (Lövlblad et al., 1999). The second difficulty is the length of acquisitions that can reach 5-7 hours to make recordings during paradoxical sleep.

### IV.3.3 fMRI-EEG and evoked potentials

Because of their low amplitude which requires excellent quality of the EEG signal, the study of evoked potentials (EP) in fMRI-EEG is quite delicate. EP obtained in MRI appear similar to those obtained outside of the MRI (Kruggel, Wiggins, Herrmann, & von Cramon, 2000). Most dedicated Evoked Potentials fMRI / EEG studies have investigated a spatial location thereof. The first study of PE performed simultaneously with fMRI

concerned visual evoked potentials (Bonmassar, Anami, Ives, & Belliveau, 1999). It showed that the electrical sources of evoked potentials corresponded to the fMRI hemodynamic activations. However, the various components of evoked potentials may be associated with either activation or deactivation of a hemodynamic point of view. (Kevin, Doug, Matthias, & Gerhard, 2008).

#### **IV.3.4 fMRI-EEG and spontaneous rhythmic activity**

some studies have examined the localization of alpha rhythm using fMRI- EEG (Goldman et al., 2002), (Moosmann et al., 2003). This rate appears on the EEG, especially in the posterior regions, when the subject closes his eyes.(E Niedermeyer, 1997) Those studies have demonstrated the activation of the thalamus and sometimes the occipital lobe accompanied by deactivation of the parietal and frontal regions corresponding the active regions during the conscious resting state, called "default mode". (Raichle & Snyder, 2007) This state corresponds to the periods during which the brain works without specific instruction.

#### **IV.4 CONCLUSION**

We presented a state of the art of information fusion. It is remarkable that a variety of different methods have already proposed the concurrent analysis of EEG and fMRI data. The chosen methods will strongly depend on the research question addressed interested (applications) in the neural generators of scalp EEG phenomena; fMRI informed EEG is the method of choice. Analysis based on EEG informed fMRI has already shown the ability not only to link physiological measures of different modalities with each other but also to expose associations between physiology and variations in cognition, perception and behavior. It is also clearly observed that the EEG-fMRI data fusion in human systems, cognitive and clinical neuroscience is rapidly evolving and has received substantial attention.

## Chapter V

# **Contribution: Dempster Shafer theory in EEG/ fMRI information fusion**

“Andrea : La science ne connaît qu'une loi : la contribution scientifique.”

— Bertolt Brecht

Source: La Vie de Galilée, Bertolt Brecht (trad. Éloi Recoing), éd. L'Arche, 1990 (ISBN 2-85181-248-3), scène 14, p. 129 - Scène 14

## **V.1 Introduction**

This chapter is concerned primarily with the works realized in studying brain activity by both EEG and fMRI modalities signals. First, two contributions on fMRI data are presented.

Basically, an accurate decision that a voxel is activated depends on the choice of both the metric and the clustering algorithm. Given this, a new framework for investigating the brain activity has been introduced in the first work. Dynamic Time Warping (DTW) has been used as a metric whereas the Potential-Based Hierarchical Agglomerative (PHA) has been employed as a clustering method. Firstly, DTW between all voxels have been computed to get the square matrix of DTW distance, denoted as DTWD. Then, PHA method uses the DTWD matrix for building clusters. Experiments with both real auditory and artificial simulation data have been conducted to evaluate the performance of the proposed approach. Then, false and positive activation rate (FAR, TAR) and false discovery rate (FDR) have been employed to establish a comparison between the new paradigm and both General linear method (GLM) and t-test method.

Although an extensive research has been carried out on EEG-fMRI fusion, there has been no reliable technique until recently able to deduce exactly what is meant by neural activity. However, EEG-fMRI fusion needs a common theoretical framework to analyze and combine information sources which have different nature. Seeking to enhance the accuracy of the combined EEG-fMRI activation detection, the second contribution introduces a new approach based on symmetric fusion using Dempster Shafer theory (DS) to explore fMRI data. In this work, Basic Belief function and combination rule have been employed. More precisely, our approach aims to capture the activity of neurons which process and convey information through peak detected by HRF (K. J. Friston, Holmes, et al., 1994). However, the main hypothesis of this study is that (DS) theory can be used in the fusion of spatiotemporal information and can detect activate areas in the brain.

The overall structure of the study takes the form of six sections, including this introductory section. In section 2 we describe the first method based on DTW and PHA method. Then section 3, we describe the basics of Dempster Shafer theory. Besides the brief review of the hemodynamic response model, the proposed model by using Dempster Shafer is introduced in section three. Then, we put the proposed approach for fMRI data

analysis in details in section four. Together with the findings of the research, the conducted experiments on real and simulation data are discussed in section five. Section six describes the contribution of EEG-fMRI fusion with experiments and result. At last, a conclusion is given.

## **V.2 An Efficient fMRI Data Clustering Method using PHA Algorithm and Dynamic Time Warping**

Recently, functional Magnetic Resonance Imaging has established its position as a prominent and significant subject of research. However, an accurate decision that a voxel is activated is a challenge that relies on the choice of both the metric and the clustering algorithm. Given that, this paper proposes a new framework for investigating brain activity where Dynamic Time Warping (DTW) has been used as a metric and the Potential-Based Hierarchical Agglomerative (PHA) has been employed as clustering method. Mainly, this technique seeks to detect activated areas by using a hybrid approach that implies to take into consideration the power or the advantage of these two methods that are described in details in what follows closely. Thus, an extensive study of the method has been conducted to evaluate the influence of the parameters of the method on the overall performance.

### **V.2.1 Dynamic time warping**

This section is designed to give a brief introduction about Dynamic Time Warping (DTW) that has been used for comparing and computing the distance and aligning the time series data as well. DTW was originally developed for speech recognition (Sakoe & Chiba, 1978). Furthermore, it has been widely applied in different fields such as econometrics, bioinformatics, data mining, signal processing, handwriting recognition and time series (Niennattrakul & Ratanamahatana, 2007),(Gu & Jin, 2006),(Bahlmann & Burkhardt, 2004). In the current study, time series represent fMRI signals (voxels). Given two sequences of voxels  $v_i$  and  $v_j$  represented by the values  $(x_1, x_2, \dots, x_m)$  and  $y_1, y_2, \dots, y_m$  respectively, two principal steps are necessary in this technique. The first is time warping whereas the second step is to determine the best path. After performing these steps, the DTW distance (DTWD) is obtained.

In this case,  $(m \times m)$  distance matrix ( $M$ ) is constructed where each cell  $M[i, j]$  of this matrix represents the distance between the  $(x_i, y_j)$  elements of both sequences  $v_i$  and

$v_j$  denoted by  $d(x_i, y_j) = (x_i - y_j)^2$ . The best path built by DTW that conducts to the DTWD metric is a sequence of points  $P = (p_1, p_2, \dots, p_k)$  called the warping function with  $p_l = (p_i, p_j) \in [1..m] \times [1..m]$  for  $l$  in  $[1..k]$  which must satisfy the following constraints:

**1. Boundary condition:**

The alignment begins at  $p_1(1,1)$  i.e. it is situated in the bottom at left and ends at  $p_k(m,m)$  in the top at right.

**2. Monotonicity condition:**

It consists to preserve the time ordering of elements so that  $x_i$  is after  $x_{i-1}$  and so on. In other word, we can note this by  $x_1 < x_2 < x_3 \dots < x_m$  for sequence  $v_i$  and  $y_1 < y_2 < y_3 \dots < y_m$  for  $v_j$

**3. Continuity:**

This constraint is to ensure that important features are not omitted; so does not jump the alignment in time index whereas aligning sequences. In other word, the warping path is composed by adjacent cells.

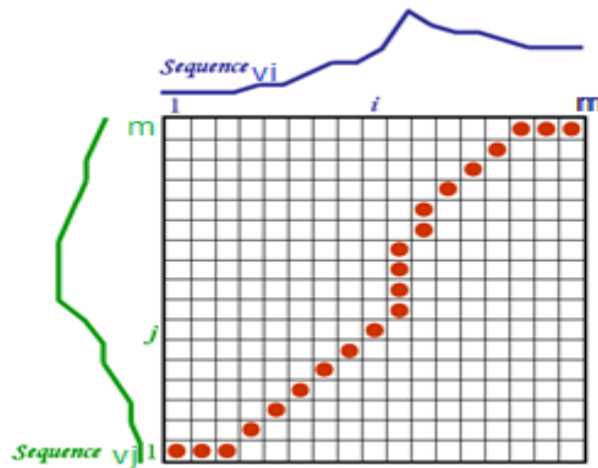


Figure V-1: The optimal warping path aligning time series

The dynamic programming is an optimal solution for finding the warping path where the cumulative distance  $dtw[i,j]$  used is defined as:

$$dtw[i,j] = d[i,j] + \min \{ dtw[i-1,j-1], dtw[i-1,j], dtw[i,j-1] \}$$

$DTW(v_i, v_j, D)$  //  $v_i$  and  $v_j$  are the two sequences .

$D$  refers to the distance matrix, each  $d[i,j]$  in  $D$  is the distance between  $x_i$  and  $y_j$ . The algorithm of DTW can be summarized as follows:



```

dtw[ ]= new double [n,m];      // initialize matrix dtw
dtw[0,0]= 0;
  for i = 1: n;
    dtw[i,1]= dtw[i-1,1] + d[i,1];
  for j= 1:m;
    dtw[1,j]= dtw[1,j-1] + d[1,j];
  for i = 1: n;
    for j= 1: m;
      dtw[i,j]= d[i,j]+min{dtw[i-1,j-1], dtw[i-1,j], dtw[i,j-1]}
return dtw distance;

```

### V.2.2 PHA algorithms

Clustering methods are one of the important steps used to separate activated voxels from non-activated voxels in fMRI data analysis. Seeking to find an efficient clustering algorithm with a high performance, the potential-based hierarchical agglomerative (PHA) clustering method has been used (Lu & Wan, 2013). This method can separate data into groups based on certain similarities. There are two kinds of clustering methods; partitional and hierarchical. However, PHA method is classified into hierarchical types that give a nested clustering result in the form of dendrogram. So that, several levels of partitions can be obtained. PHA method produces the potential field. For two points  $i$  and  $j$ , if  $r_{i,j}$  is the distance between them, the potential at point  $i$  from point  $j$  is given by the formula:

$$\phi_{i,j}(r_{i,j}) = \begin{cases} -\frac{1}{r_{i,j}} & \text{if } r_{i,j} \geq \delta \\ -\frac{1}{\delta} & \text{if } r_{i,j} < \delta \end{cases} \quad (\text{V.22})$$

Where  $\delta$  is used to avoid the problem of singularity when  $r_{i,j}$  becomes zero

The total potential at point  $i$  is the sum of potentials from all the data points and described as follows:

$$\phi_i = \sum_{j=1..N} \phi_{i,j}(r_{i,j}) \quad (\text{V.23})$$

where  $N$  stands for the total data points.

In the PHA method, both the potential field produced by all the data points and the distance matrix are used to define a new similarity metric. In potential field model, different distances have being used such as Euclidian distance and Euclidian squared distance which are not useful to find distance between time series. For that reason, we use

in this work dynamic time warping as a distance between two voxels because it is an efficient technique in aligning and analyzing time series.

Once the potential field model is constructed, PHA proceed to build edge weighted tree by using function to compute for each point the weighted and parent node. Finally, these metrics are used to build dendrogram. For more details about PHA method, we invite the reader to see (Lu & Wan, 2013). The PHA clustering algorithm is as follows:

```

PHA_Clustering(Dist[1..N,1..N] {
     $\delta \leftarrow$  the value computed from Dist[1..N,1..N]
    (parent[1..N], weight[1..N])  $\leftarrow$  Build_Edge_Weighted_Tree(Dist[1..N,1..N],  $\delta$ )
    (dendrogramRoot, dendrogramParent[1..2 $\times$ N-2])  $\leftarrow$  Build_Dendrogram(parent[1..N],
weight[1..N])
    Rturn(dendrogramRoot, dendrogramParent[1..2 $\times$ N-2])
}
    
```

The algorithm described above has time complexity  $O(N^2)$  and allows to choose a max number of clusters , denoted as (k). However, generating automatically a number of clusters that is less than or equal to the selected max number (k) is done by using CLUSTER function provided by Matlab. The CLUSTER function constructs clusters from a hierarchical cluster tree. Among these clusters, we show the target cluster and more information like the number of voxels by cluster and the centroid of cluster denoted by (c) as well.

### V.2.3 Proposed approach

This section provides details about the introduced framework to explore and analyze fMRI time series by using DTW and PHA clustering methods to accurately mapping brain activated areas. The approach consists of three principal steps. We consider a group of voxels and corresponding time series. First, we compute the DTW distance between all times series and we get a matrix n-by-n of DTW distance denoted as vdDTW (voxels distances DTW). Second, we use the vdDTW as an input to PHA algorithm in order to obtain a hierarchical clustering. Third, as mentioned above, PHA calls for a function CLUSTER which has parameters in input which is max number of cluster K. So that, to determine the target cluster, we perform to vary this parameters K at each experiment and

we observe the generated clusters. We repeat this till no new cluster is generated and at the end we show the target clusters. Figure V.2 shows a block diagram that illustrates the principle of our approach.

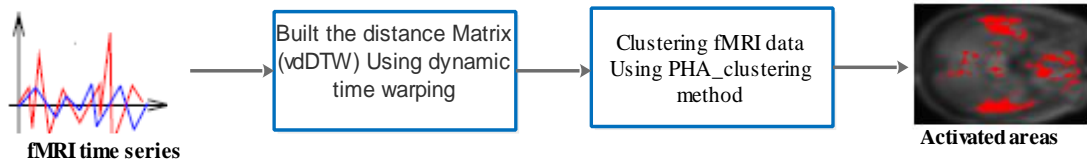


Figure V-2: flowchart of the proposed approach

## V.2.4 Experiment and result

This section examines the accuracy and effectiveness of the proposed method. It also aims to validate and compare the introduced approach that relies on DTW and PHA algorithm with both GLM and t-test methods. Thus, synthetic and real data have been used.

The new framework and t-test method are implemented in Matlab code. The code of GLM method used in this study is available in(<http://www.lion.ucl.ac.uk/spm>) . The conducted experiments are run on a laptop with an Intel 2.16 GHz Dual-Core CPU and 2 GB of RAM.

To analyze the performance of the proposed approach, two metrics need to be defined herein: (i) True activation rate (TAR) stands for the ratio between the number of time series correctly identified as activated and the total of truly activated time series. (ii) False activation rate (FAR) refers to the ratio between the numbers of time series incorrectly identified as activated and the total number of truly non-activated time series. Also, these two ratios serve to establish a comparison between the previous conducted studies like the GLM and t-test. To study the influence parameters K of PHA clustering method, the TAR and FAR have been computed at different K values. For the GLM and t-test methods, the false activation rate provided by p-value is the probability used to identifying the TAR and FAR.

### V.2.4.1 Artificial dataset:

The introduced method has been first tested on the artificial dataset constructed by simulating the same process with real data. fMRI data have been simulated as described in([http://mlsp.umbc.edu/simulated\\_fmri\\_data.html](http://mlsp.umbc.edu/simulated_fmri_data.html)). This dataset contains eight sources denoted as  $(S_i, i=1 \text{ to } 8)$  where each simulated source is of  $60 \times 60$  image with 100

point courses. However, some modifications have been made in the current experiment where the virtual source for fMRI was created into a two dimensional spatial map of  $53 \times 63$  voxels for each source, as depicted in figure V.3, as the same size of the real fMRI data.

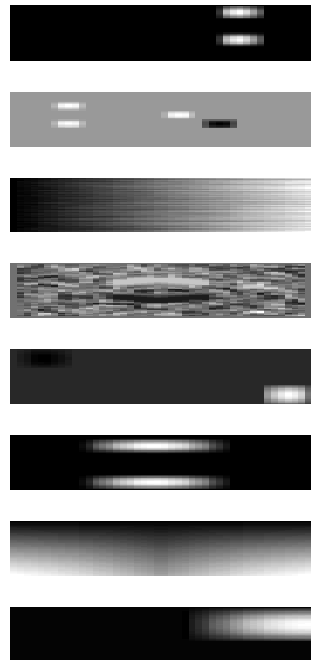


**Figure V-3 simulated fMRI data**

The introduced method has been applied on synthetic data that are described above. First, the vdDTW distance has been computed. After, the PHA clustering method has been applied to get a hierarchical clustering. Since we perform in input the  $k$  parameter of PHA method by using the values between [3..10] three and ten and at each value of  $k$ , the metric FAR has been computed and TAR and so on. Figure V.4 presents the plots of TAR and FAR obtained by the proposed method. It is clearly noticed that there is a loss of some activated voxels whereas the number of non activated voxels increases when  $k$  is small. In contrast, the number of activated voxels increases with a decrease in the number of non-activated voxels in the case where  $k$  is great.

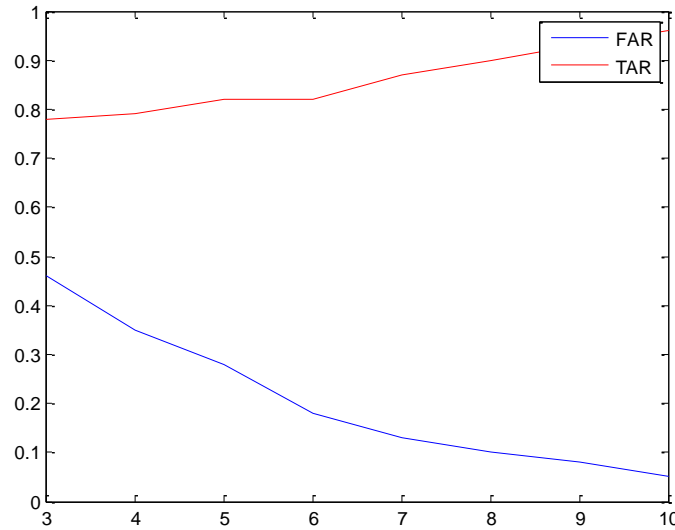


Figure V-4:FAR and TAR on regions started by K= 3 regions to K= 10

To evaluate the achieved results, t-test method has been used. In this method, time series have been divided in two groups: the series called on activation and the series called off activation, denoted as (XON) (XOFF) respectively. To determine these both groups for all time series, hemodynamic response function (HRF), introduced in (K. J. Friston, Jezzard, et al., 1994) as kernel, has been employed. Then, t-test statistic has been applied between XON and XOFF. Detecting activated voxel depends on using a p-value. Finally, TAR and FAR metrics have been computed at each p-value between 0.001 and 0.05. The plot in figure V.5 depicts the TAR and FAR obtained results by t-test. Table1 presents the mean of TAR and FAR for the proposed method and t-test method

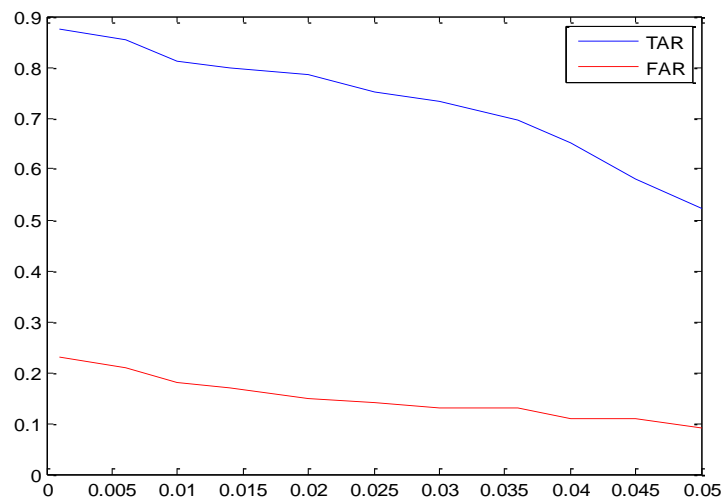


Figure V-5: true and false activation rates by t-test method

The obtained results have clearly shown that when the more the p-value is smaller, the more we get nearer to the activated areas and the number of false activation rate increases.

Where p-value is nearer to 0.05, more precision is obtained in activation rate with low false activation rate

**Table V-1: Average of true activation rate and false activation rate obtained by applying the proposed method and t-test method to the artificial data set**

	AVG of TAR	AVG of FAR
<b>Our method</b>	0.796	0.160
<b>t-test</b>	0.733	0.150

Accordingly, these results have obviously shown the ability of the presented approach to detect true activation rate better than t-test method. However, the t-test performs better than the new approach in terms of false activation rate.

Figure (V.6a) presents the mixed active areas detected by the proposed method. As clear in slice one and three, in the left, the active regions are clearly shown in source (S1, S5 and part of S4). Slices in the right show the activated areas in (S6 and S8).

In figure (V.6.b), the active regions are depicted in slices one and three on the left of the sources (S1, S3 and S6) whereas the active areas of sources (S6 and s8) are shown in slice seven and eight on the right slices

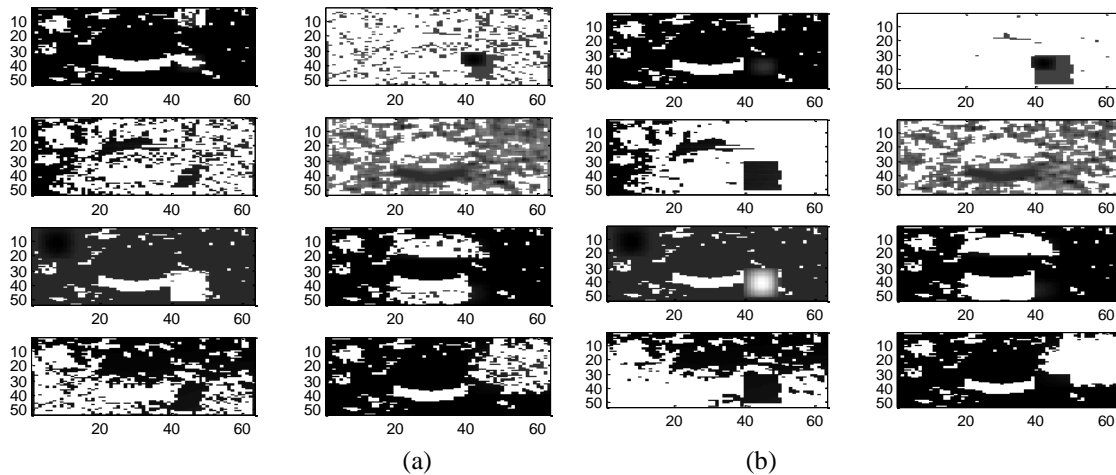


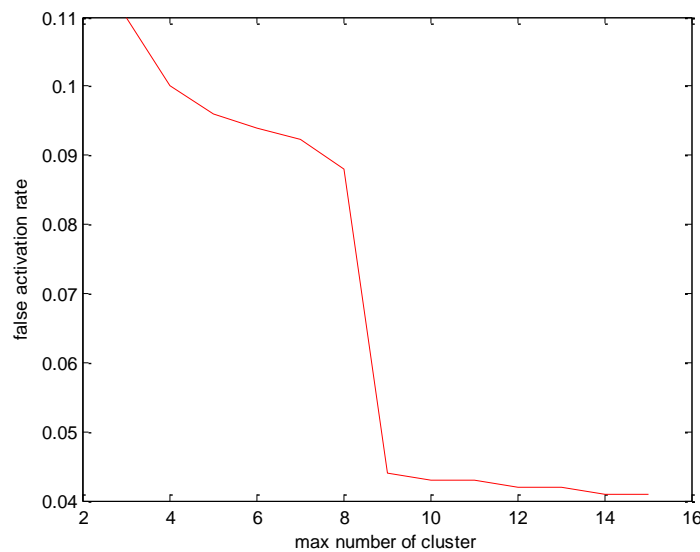
**Figure V-6: (a) activated areas of simulated data by proposed approach. (b) Activated areas of simulated data by t-test**

To sum it up, the TAR used in the presented method is very motivating to identifying more activated regions. In other word, it performs better than the t-test in detecting more accurate activation however the t-test outperforms regarding identifying FAR.

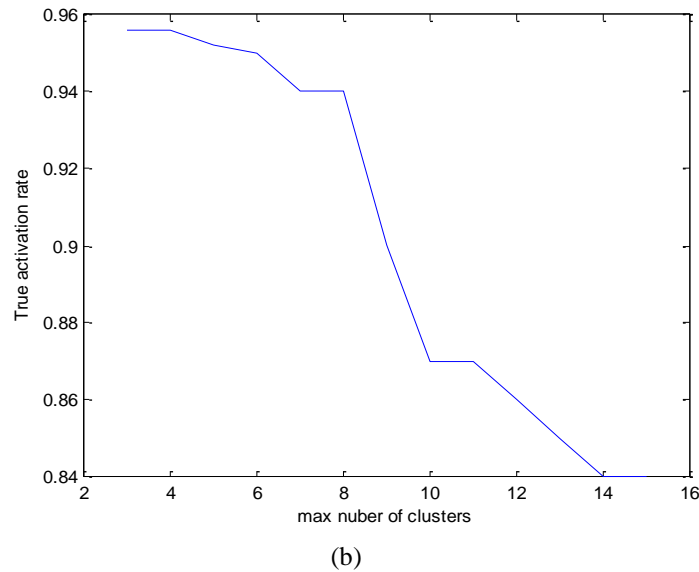
#### V.2.4.2 Real fMRI Dataset

The current section reports the obtained results of the new paradigm that has been tested on a real fMRI dataset related to an auditory stimulus. This dataset was collected by Geriant Rees et al. (<http://www.lion.ucl.ac.uk/spm/> ). The whole brain BOLD/EPI images were acquired on a modified 2T SIEMENS MAGNETOM Vision system. Each acquisition is composed of 64 contiguous slices (64x64x64 3mm x 3mm x 3mm voxels) where any acquisition occurs in 6.05s, with the scan to scan repetition time (TR) set arbitrarily to 7s. So that, 96 acquisitions were made (TR=7s), in blocks of 6, giving 42s blocks. Starting with rest, the condition for successive blocks alternated between rest and auditory stimulation which was bi-syllabic words presented binaurally at a rate of 60 per minute. In this experiment, the authors mentioned that the functional data start at acquisition 4.

To apply the proposed approach, the vdDTW distance has been computed and then the PHA method has been applied. PHA method consists of two components: build\_Edge\_Weighted\_tree and Build\_Dendrogram. By using PHA clustering method, a change in the max number of cluster (k) has been done by increment. Then, FAR and TAR measures have been calculated in each k. This process has been repeated till no new cluster will be generated. The first step in this experiment is fixing K at (k=3) and then computing both FAR and TAR metrics. It has been obviously observed that the process is becoming at stationary state when (k = 15) that is presented by the plots in figure V.7.



(a)



(b)  
Figure V-7: (a) the various false activation rate. – (b) The true activation rate

It is clearly noticed in these plots that the proposed method detects a high accurate activation map when  $k$  is smaller than eight. However, false activation rate decreases with the increment in the number of max cluster  $k$

#### V.2.4.3 Comparison with GLM method and t-test

The following section provides a comparison between the obtained results by GLM and t-test method and the results of the presented method. Firstly, the GLM results realized by SPM tools assumes that the fMRI time series correspond to the realization of an identically independent stochastic process and divides data into two groups, obtained during on (activation) and off (no activation) periods. This separation is done by p-value (0.05) and (0.001). This is for computing the TAR but for the FAR; False Discovery Rate (FDR)(Chumbley & Friston, 2009) has been used. FDR plays an important role as well as FAR. It is a proportion of activated voxels that are false positives. Then, p-value between 0.001 and 0.05 has been employed by using SPM tools that provides the results of FDR and the number of voxels detected as activated in the regions used to compute the TAR measures. Figure V. 8 presents the result of this experiment.

Figure V. 9 presents the TAR and FAR provided by p-value of t-test. After, changing the p-value at each experiment starting by 0.001 to 0.05, the TAR and FAR measures has been computed. These plots show that t-test method detects true activation with high false activation however the false activation are decreasing were p-value goes nearer to 0.05



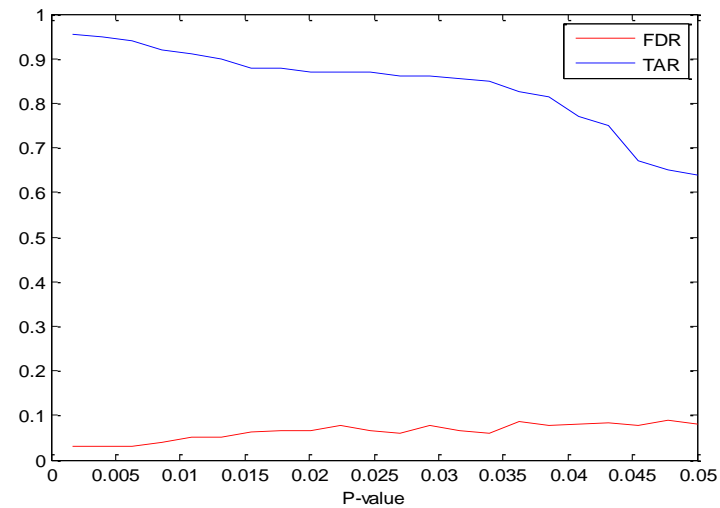


Figure V-8: false discovery rate and true activation rate obtained by GLM method

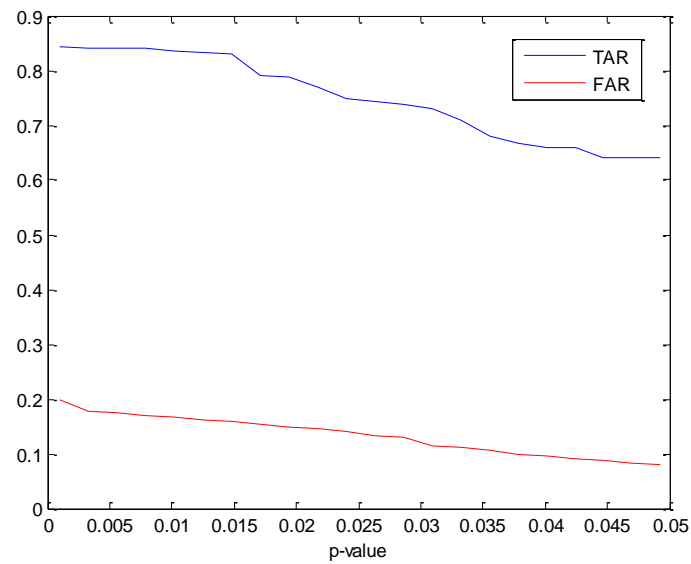


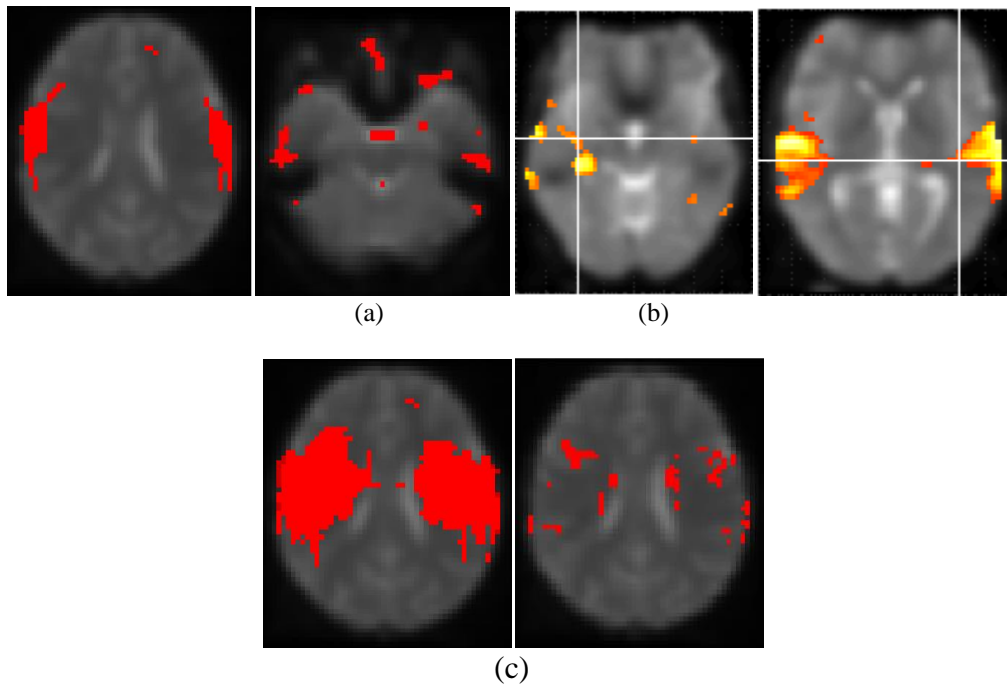
Figure V-9: true and false activation rate obtained by t-test method

Table V-2 :Average of true activation rate and false activation rate obtained by applying the proposed method and t-test and GLM to the real data set.

	AVG( TAR)	AVG( FAR)
Our method	0.902	0.068
GLM	0.887	0.071
t-test	0.848	0.114

Table V.2 depicts the average of FAR, TAR measures provided by the presented method, GLM and t-test method

As illustrated in figure V.10, some slices that show the activated areas by GLM, t-test and proposed method are presented.



**Figure V-10: Some slices illustrate the activated regions: a) activated areas by t-test method b) the result is generated by GLM method; c) the result obtained by proposed method**

Finally, this approach addresses a new paradigm to detect activation areas in fMRI time series. In addition, the suggested method is registered within the context of unsupervised classification (clustering) methods.

Mainly, this approach is divided into two principal steps. To compare all voxels to each other, DTW has been used as a metric to measure the similarities between them. The PHA algorithm has been employed to portion the fMRI data. The performance of the proposed approach has been evaluated on both real and synthetic data sets related to an auditory stimulus. A detailed comparison has been provided between the proposed method, GLM and t-test using the metrics (TAR FAR and FDR) to make performance analysis with artificial and real data sets. The findings have clearly shown that the proposed method is promising and can usually produce more satisfying results.

### V.3 Approaches based on Dempster-Shafer Theory of Evidence

In this part, a new approach based on Dempster Shafer theory of evidence is suggested to improve extracting brain activity. Particularly, the emphasis of this work has been placed on developing a method that is able to provide an analytical framework for

detecting the brain active regions. These subsections describe in details the proposed method including a brief simplified description of the hemodynamic response model and the basics of Dempster-Shafer theory. Experiments and results on both simulation and real data are also discussed.

### **V.3.1 The Dempster-Shafer Theory of Evidence**

In the following, we introduce the fundamentals of the Dempster-Shafer (DS) theory of belief function that has been proven to be an efficient tool in representing uncertain knowledge. This theory has paved the way for many researchers to study various aspects related to uncertainty and lack of knowledge and has shown its ability to solve real problems (Dempster, 1967). In fact, Dempster-Shafer theory can be considered as a generalization of the probability theory (Cuzzolin, 2008). The references (Shafer & others, 1976) (Schocken & Hummel, 1993),(Smets & Kennes, 1994),(Yager, 2001) provide further information about this theory. In what follows closely, a brief introduction to the basic notions of the theory of evidence is given.

Let  $\Theta = \{\theta_1, \theta_2, \dots, \theta_k\}$  be a finite set of possible hypotheses. This set is referred to as the frame of discernment, and its power set is denoted by  $2^\Theta$  where:

$$2^\Theta = \{\emptyset, \{\theta_1\}, \{\theta_2\}, \dots, \{\theta_k\}, \{\theta_1 \cup \theta_2\}, \{\theta_1 \cup \theta_3\}, \dots, \Theta\} \quad (V.1)$$

A key point of the evidence theory is known as Basic Belief Assignment (BBA). It is defined as:

A basic belief assignment  $m$  is a function that assigns a value in  $[0, 1]$  to every subset  $A_i$  of  $\Theta$  and satisfies the following:

$$m(\emptyset) = 0, \text{ and } \sum_{A_i \subseteq \Theta} m(A_i) = 1 \quad (V.2)$$

The BBA ( $m$ ) is associated with the belief function, denoted by  $\text{bel}()$ . The definition of belief function is given. A belief function assigns a value in  $[0, 1]$  to every nonempty subset  $D$  of  $\Theta$ . It is called degree of belief in  $D$  and is defined by

$$\text{bel}(A_i) = \sum_{A_j \subseteq A_i} m(A_j) \quad (V.3)$$

The function,  $pl(.)$ , associated with the BBA  $m(.)$  is a function that assigns a value in  $[0, 1]$  to every nonempty subset  $D$  of  $\Theta$ . It is called “degree of plausibility in  $D$ ” and is defined by

$$pl(A_i) = \sum_{A_i \cap D \neq \emptyset} m(A_i) \quad (V.4)$$

Furthermore, a BBA can also be viewed as determining a set of probability distributions over  $\Theta$  so that  $bel(A) \leq P(A) \leq pl(A)$ . It can be easily seen that these two measures are related to each other as follows:

$$pl(A) = 1 - bel(\bar{A}) \quad (V.5)$$

Therefore, one needs to know only one of the three values of  $m$ ,  $bel$ , or  $pl$  to derive the two other ones, where  $\bar{A}$  stands for the negation of a hypothesis  $A$  shown in Figure V.11

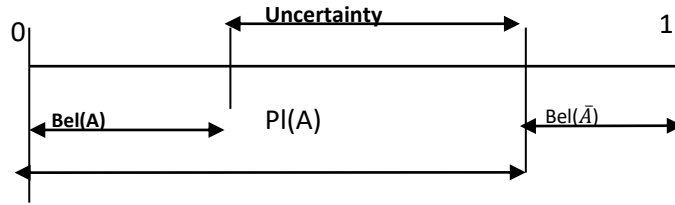


Figure V-11: Basics measures of Dempster-Shafer Theory of Evidence

The interest of this work has been also placed on employing the combined rule for pooling of evidence from two belief functions,  $Bel_1$  and  $Bel_2$ , over the same frame of discernment, however it induced by different independent sources of information. The Dempster’s rule of combination for combining two sets of masses,  $m_1$  and  $m_2$  is defined as:  $m_{12}(\emptyset) = 0$

$$m_{12}(A) = \frac{1}{1-k} \sum_{B \cap C = A \neq \emptyset} m_1(B) m_2(C) \quad (V.6)$$

where  $k$  denotes a measure of the amount of conflict between two evidences. If  $k = 1$  the two evidences cannot be combined because their cores are disjoint. This rule is commutative, associative, but not idempotent or continuous.  $k$  is calculated as follows:

$$k = \sum_{B \cap C = \emptyset} m_1(B) m_2(C) \quad (V.7)$$

In what follows, the notations  $m_{fMRI}(.)$ ,  $m_{EEG}(.)$  and  $m_{EEG,fMRI}(.)$  have been used to refer to BBA (fMRI), BBA (EEG) and the rule of combination respectively.

### V.3.2 Proposed Method

#### V.3.2.1 Overview :

Figure V.12 illustrates the proposed scheme for fMRI data analysis and detection of activated area that is composed of five stages: i) data preprocessing and dimensionality reduction ii) HRF modeling iii) convolution with fMRI signal, iv) computation of the  $m()$ , the belief function  $bel()$  for each voxel and v) separation of the activated voxels from non-activated ones using threshold by using OTSU thresholding method because it permits to get a threshold automatically .

#### V.3.2.2 Data preprocessing

Prior to analysis, fMRI data goes through a series of preprocessing steps to identify and remove the artifacts and to validate model assumptions as well. First, the fMRI slices have been spatially realigned. However, spatial smoothing may cause unforeseen changes to occur into the data. Thus, spatial smoothing has been avoided to ensure better performance. Then, the mean value has been subtracted from each of the time series and the variance has been normalized to a unit. The previous steps were realized via SPM tools (K. J. Friston, Holmes, et al., 1994).

#### V.3.2.3 Modeling HRF by Dempster-Shafer method

We model a peak and a subsequent undershoot of canonical hemodynamic response function by DS method using the sum of two gamma functions known by the density of probability function, as described above.

The modeling process of the HRF function has been performed as follows: HRF function has been partitioned into two hypotheses( $\theta_i, \theta_j$ ). The hypothesis  $\theta_i$  corresponds to both detecting neural activation and determining a peak (on activation) while  $\theta_j$  is assigned for modeling undershoots (off activation). Each hypothesis is a sum of degrees of beliefs. In particular, the focus of this work lies on the first hypothesis. This latter is divided into two parts A and D, where A stands for degrees of belief included in D. (D-A) denotes the uncertainty part. Figure V.13 illustrates the proposed model.

At first, we localize the interval of stimulus. In the example where the repetition Time (TR=4), the peak is in the first interval [4..8] seconds (Chumbley & Friston, 2009). To find a second stimulus in this example, 16sc have been added. In the second step, we determine the next interval and so on. The same process has been repeated till the end of

fMRI signals. Finding these intervals is the focal aim of this conception. Figure V.14 illustrates the projection of the proposed model with fMRI signal to extract all intervals.

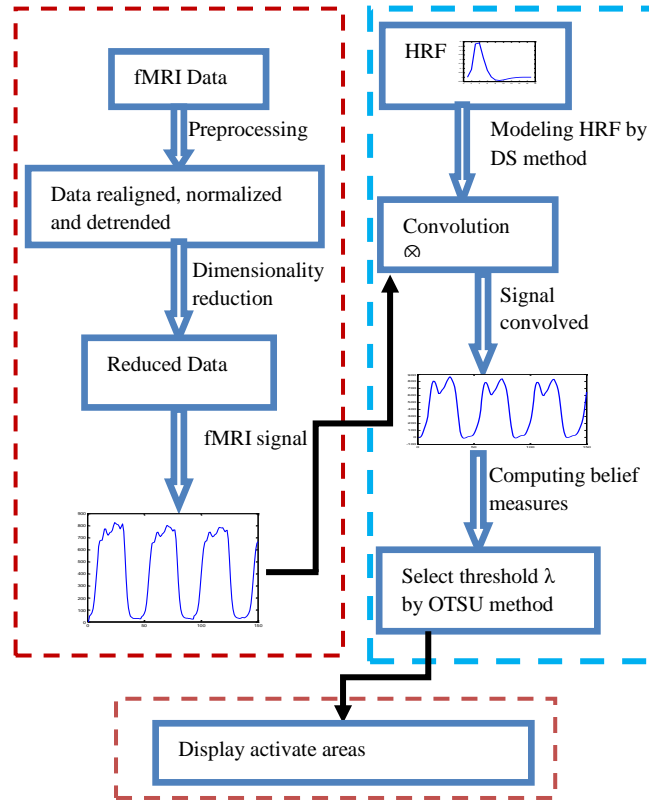


Figure V-12: Flowchart of the proposed model fMRI analysis with DS

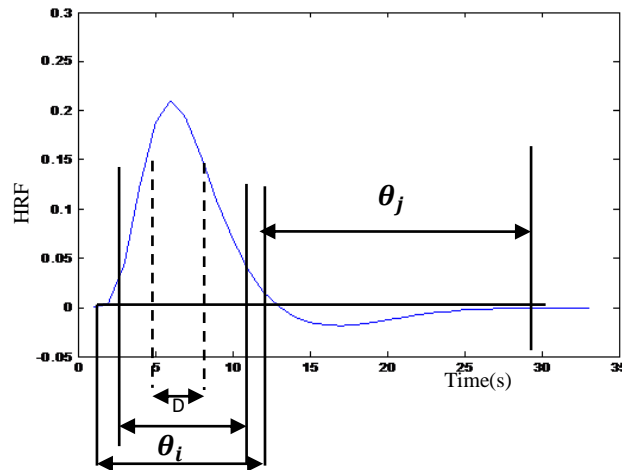


Figure V-13: Flowchart of the proposed model of HRF

### V.3.3 Computing the basic belief assignments and the belief measure

After the convolution process, the  $m()$  of each time (second) in fMRI times series must be first computed in order to compute the belief and the plausibility measures. Thus,

the formula that consists in a transformation of each fMRI signal into a density probability function is described below. The used integral has the form:

$$\alpha = \int_0^{tn} |y(t)| dt \quad (V.8)$$

In the above equation, the global surface is denoted as  $\alpha$ . So,  $m()$  is calculated as follows :  $m(t_i) = \frac{1}{\alpha} \int_{t_{i-1}}^{t_i} |y(t)| dt$  for  $i = 1$  to  $n$

$$m(t_i)=0, i=0 \quad (V.9)$$

A vector of probability have been obtained where the sum of mass briability function ( $m()$ ) is 1 as mentioned above in section 3. To compute the belief and plausibility measures, the formulation described in (3) and (4) has been employed.

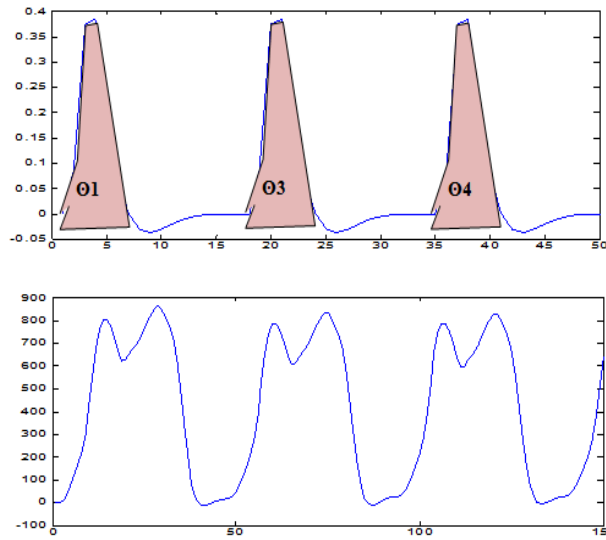


Figure V-14: the projection of the introduced model with fMRI data

(where  $\theta$  corresponds to a finite set of possible hypotheses)

### V.3.4 Separating the activated voxels from the non-activated ones

To extract activated voxels, the belief measures have been employed in this stage. Each voxel of fMRI time series is presented by  $bel()$  value. At first, the histogram of belief measures has been used and an appropriate threshold denoted as  $\lambda$  has been chosen. The OTSU method (Otsu, 1975) was employed to choose ( $\lambda$ ) threshold. It permits extracting an automatic threshold that minimizes the weighted within-class

variance  $\sigma_w^2(t)$ . This turns out to be the same as maximizing the between-class variance  $\sigma_B^2(t)$ . The algorithm is as follows:

**Step 1** compute the histogram of bel() measure and the probability at each i level of histogram

**Step 2** initialize the  $\mu_i(0)$  and  $q_i(0)$

**Step 3** Browse all possible thresholds  $t=1$  to  $n$

Update  $\mu_i(t)$  and  $q_i(t)$  Compute  $\sigma_B^2(t)$

**Step 4**  $\lambda = \max ( \sigma_B^2(t)$

where the weighted within-class variance is:

$$\sigma_w^2(t) = q_1(t)\sigma_1^2(t) + q_2(t)\sigma_2^2(t) \quad (V.10)$$

And the between-class variance is:

$$\sigma_B^2(t) = q_1(t)[1 - q_1(t)][\mu_1(t) - \mu_2(t)]^2 \quad (V.11)$$

The total variance is:

$$\sigma^2 = \sigma_w^2(t) + \sigma_B^2(t) \quad (V.12)$$

where the class probabilities are estimated as:

$$q_1(t) = \sum_{i=1}^t p(i) \quad (V.13)$$

$$q_2(t) = \sum_{i=t+1}^n p(i) \quad (V.14)$$

And the class means are given by:

$$\mu_1(t) = \sum_{i=1}^t \frac{ip(i)}{q_1(t)} \quad (V.15)$$

$$\mu_2(t) = \sum_{i=t+1}^n \frac{ip(i)}{q_2(t)} \quad (V.16)$$

The individual class variances are:

$$\sigma_1^2(t) = \sum_{i=1}^t [i - \mu_1(t)]^2 \frac{p(i)}{q_1(t)} \quad (V.17)$$

$$\sigma_2^2(t) = \sum_{i=t+1}^n [i - \mu_2(t)]^2 \frac{p(i)}{q_2(t)} \quad (V.18)$$

And  $[0, n-1]$  is the range of intensity levels of the histogram.

#### V.4 Evaluation metrics and proposed algorithm

The following subsections describe the metrics of evaluating the proposed approach and the proposed algorithm based on DS theory.

##### V.4.1 Evaluation metrics

The threshold  $\lambda$  has been used to compute two metrics, the true and false activation rate. These two terms need to be defined herein: True activation rate (TAR) stands for the ratio between the number of time series correctly identified as activated and the total of truly activated time series. And the other one is false activation rate (FAR) referring to the ratio between the number of time series incorrectly identified as activated and the total number of truly non-activated time series. Also, these two ratios serve to analyze the performance of the proposed approach and to establish a comparison with the previous conducted studies like the GLM. It has been noticed in the presented work that the voxels



with belief measure more than or equal to  $\lambda$  have been considered to be true active voxels. And the voxels that are less than the selected threshold have been considered as false active voxels. This process leads to obtain the activated regions.

#### **V.4.2 Algorithm DS-fMRI analysis**

To sum it up the proposed algorithm is illustrated as follows:

```
INPUT: Tr : repetition time, h(t) : hemodynamic response function,
s(t): fmri signal with nb : size of signal
[a,b] : First_intrval and T : period
OUTPUT:
Y(t) : fMRI signal convolved with HRF
m(t) : Basic Belief Assignment
bel(n) : belief measures
 $\lambda$  : belief threshold for extracting activated voxels
Description:
For each signal fMRI s(t) do
{
  y(t) = conv(s(t), h(t))
  (*convolution fMRI signal with HRF*)
}
For every y(t) do
{Compute m(t) by using equations (V.8) and (V.9)
  (*compute belief measures*)
  s = 0
  For k=0 to nb do
  {
    s = s + m((a + k  $\times$  T): (b + k  $\times$  T))
    (*from (a+k $\times$ T) to (b+k $\times$ T)*)
  }
  bel(t) = s (*extract activated voxels *)
}
{
  Show histogram of belief measure
  Choose  $\lambda$  OTSU method
  show the activated region
}
```

#### **V.5 Results and Discussion**

This section describes fMRI data that have been used in the conducted experiments. Both artificial and real fMRI data have been employed to determine the identically activated areas. To test the performance of the presented approach, a comparison of the obtained results with the GLM and t-test results has been performed. It is worth

mentioning that the tests have been conducted on the same benchmark. This comparison has been done by using the true activation rate and false activation rate as defined above. However, we illustrate plots of true and false activation rates at different belief thresholds.

### V.5.1 Artificial data

This section describes a form of artificial data used by Francois et al. (Meyer & Chinrungrueng, 2005). In general, fMRI signal is a stochastic process. So, a synthetic three-dimensional fMRI dataset (64, 64, 64) has been generated. The number of slices is 64 and each signal is generated by the following formula:

$$A(t) \times e^{i\Theta(t)} + n_c(t) \quad (V.19)$$

The above function is a complex signal where  $A(t)$  stands for the amplitude. Let  $M$  be the levels of activation and let  $\phi$  be the Gaussian random delay distributed with zero mean and unit variance. Let  $\omega$  be the frequency of the signal and selected to be  $\pi/10$  because the fMRI signal is relatively weak. The amplitude on such a basis is defined by a sinusoidal function as follows:

$$A(t) = M \times \sin(\omega t + \phi) \quad (V.20)$$

We consider  $\Theta(t) = \pi/4$  where the real and imaginary channels play a symmetric role and  $n_c(t)$  are the complex Gaussian white noise centered with unit variance. The phase of this signal is not used, and we only consider the magnitude:

$$s(t) = |A(t) \times e^{i\Theta(t)} + n_c(t)| \quad (V.21)$$

We generate a set of signals in order to build sequences of fMRI time series as shown in Figure V.15

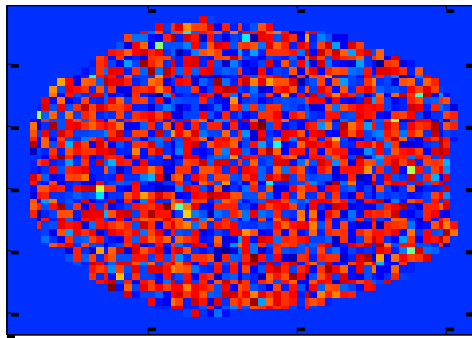
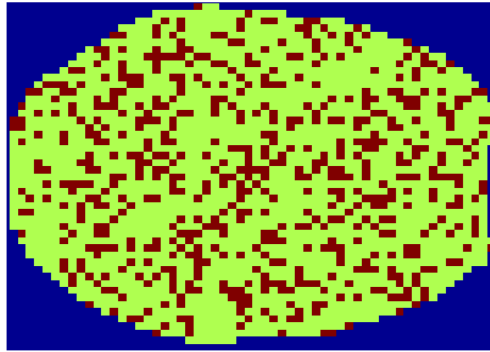


Figure V-15: The fMRI artificial data

After applying the proposed approach on this artificial data, the obtained results are presented in figure V.16 where brown areas stand for the activated voxels.



**Figure V-16: The activate voxels with fMRI artificial data by the proposed approach**

Figure V.17 presents some results using the simulated data described above. These results contain the TAR and FAR measures that have been obtained with  $bel()$  threshold. The t-test statistic method has been used in order to compare the introduced method. Basically, t-test statistic method has been used to compute the TAR and FAR metrics at each p-value between 0.001 and 0.05. At first, the fMRI time series are divided in two groups i.e. determine the fMRI time series called on activation denoted as (XON) and the fMRI time series called off activation denoted as (XOFF). To determine these both groups for all fMRI signals the box-car hemodynamic response function have been employed as kernel. The plots in Figure V.18 present the TAR and FAR obtained results with t-test method

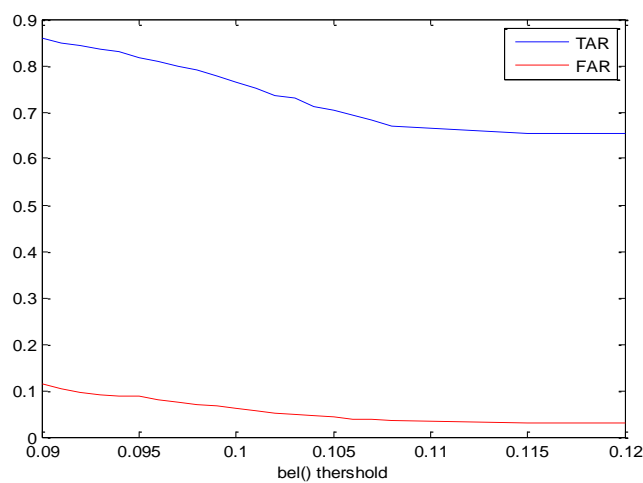


**Figure V-17: The plots show the false activation rate and the positive activation rate using belief threshold.**

These results show that when the p-value is smaller, we get nearer to the activated areas and the number of false activation rate increases. Where p-value is near to 0.05, more precision is obtained in activation rate with less false activation rate. Table V.3 presents the mean of TAR and FAR for the proposed method and t-test method.

Accordingly, these results have obviously shown the ability of the presented approach to detect true and false activation rate better than t-test method.

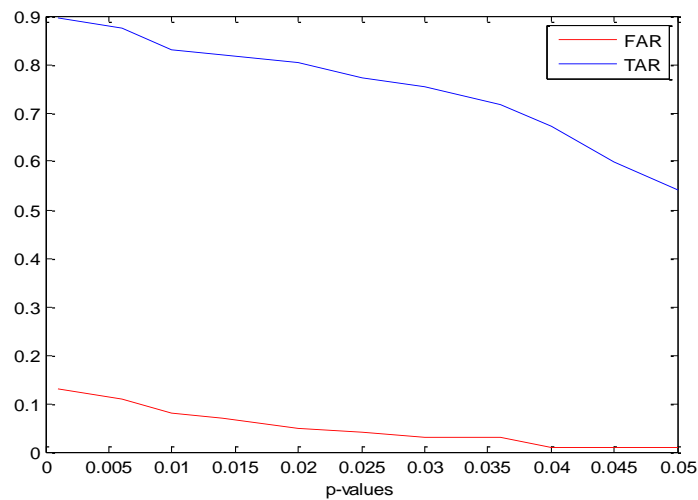


Figure V-18: True and false activation rates by t-test method

Table V-3: Average of true activation rate and false activation rate of the DS method and t-test method to the artificial data set

	AVG of TAR	AVG of FAR
DS method	0.766	0.063
t-test	0.753	0.082

### V.5.2 Real fMRI Dataset

This section reports the result of proposed method tested on a real fMRI dataset that concern an auditory stimulus. These data were collected by Geriant Rees et al. and are available in <http://www.fil.ion.ucl.ac.uk/spm/data>. These whole brain BOLD/EPI images were acquired on a modified 2T SIEMENS MAGNETOM Vision system. Each acquisition is composed of 64 contiguous slices (64x64x64 3mm x 3mm x 3mm voxels) where any acquisition occurs in 6.05s, with the scan to scan. However the TR have been approximated to 7s. So that, 96 acquisitions were made (TR=7s), in blocks of 6, giving

42s blocks. Starting with rest, the condition for successive blocks alternated between rest and auditory stimulation that was bi-syllabic words presented binaurally at a rate of 60 per minute. In this experiment, the authors mentioned that the functional data starts at acquisition 4.

After modelling the HRF by Dempster-Shafer method (DS), a basic belief assignment, denoted as  $m(v_i)$ , has been calculated for all subset  $A_i$  of  $\theta$  (where  $v_i$  stands for  $i$ th voxel). We have noticed that all fMRI signals have a similar pace with a difference in values of  $m()$  which plays a primordial role in computing belief measures. This latter has been used to characterize the voxel activity. Then, computing the belief measures enables to obtain the results at  $(TR = 7)$  which is in  $[0.2702, 0.3338]$ .

To separate the activated voxels from non-activated voxels, the histogram described in Figure V.19 has been used and the threshold of belief measures ( $\lambda$ ) by OTSU method has been selected automatically.

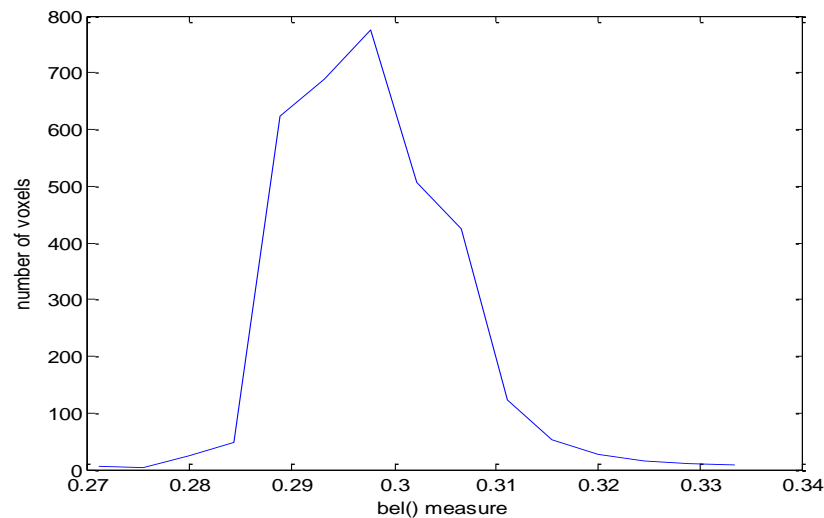


Figure V-19: The histogram of belief measures

To study the influence of the belief measure that presents the key parameters of proposed method, on the whole performance, we have generated and plotted activation regions (number of voxels ) at different values of belief thresholds more than  $\lambda$  obtained by OTSU method. In addition, we have measured TAR and FAR values given by belief threshold. Figure V.20 shows the number of true and false activation rate as a belief threshold. This experiment shows that the proposed method can identify more TAR with

less FAR when  $\text{bel}()$  near to  $\lambda$ . And the number of true and false activation rate tends be lower when  $\text{bel}()$  threshold between 0.292 and 0.3

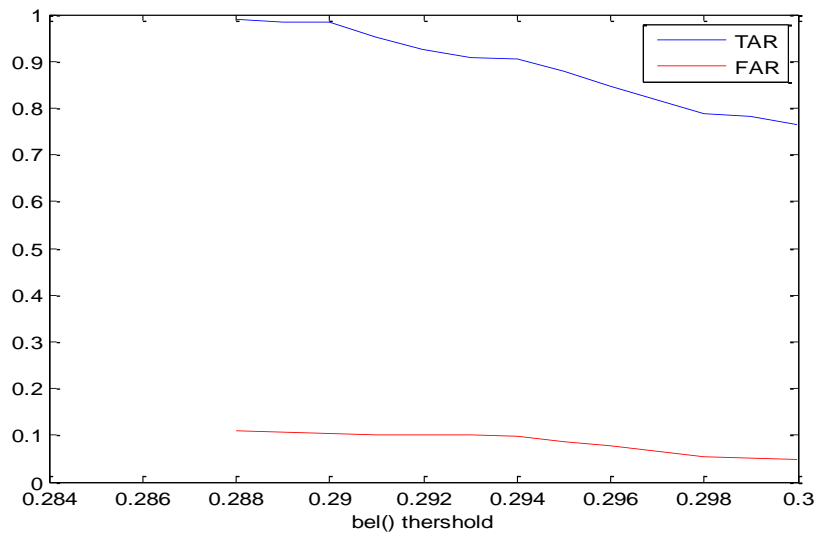
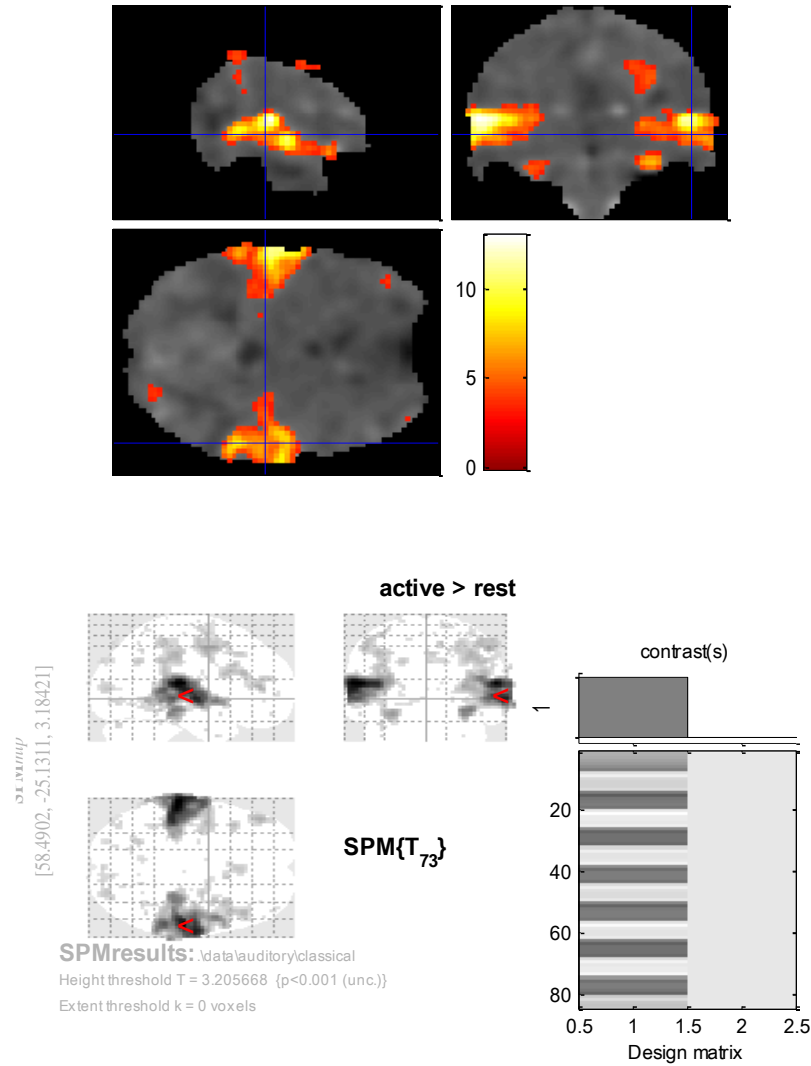


Figure V-20: False and true activation rate obtained by DS method

### V.5.3 Comparaison with GLM method

This section provides a comparison of the GLM results with the obtained results of the introduced framework. Firstly, the GLM results realized by SPM tools assumes that the fMRI time series correspond to the realization of an identically independent stochastic process and divides data into two groups, obtained during on (activation) and off (no activation) periods. This separation is done by p-value (0.05) and (0.001). The GLM results have shown the different projection (axial, coronal and saggittal) as well as the design matrix Figure V.21. Another important feature that distinguishes the GLM method is the long time needed for completing the job. In contrast to GLM, the method based on Dempster-Shafer theory is not difficult to understand and it is easy to implement however it needs to have prior knowledge about the experiment conditions.



**Figure V-21: The obtained result with GLM method**

However SPM tools provide the metrics true activation rate and False Discovery Rate (FDR) that play an important role as well as false activation rate. In other words, it is a proportion of activated voxels that are false positives (Chumbley & Friston, 2009).

However, we proceed to use p-value between 0.001 and 0.05 by using SPM tools that provides the results of FDR and the number of voxels detected activated in the regions used to compute the true activation rate measures. Figure V.22, shows the result of this experiment.

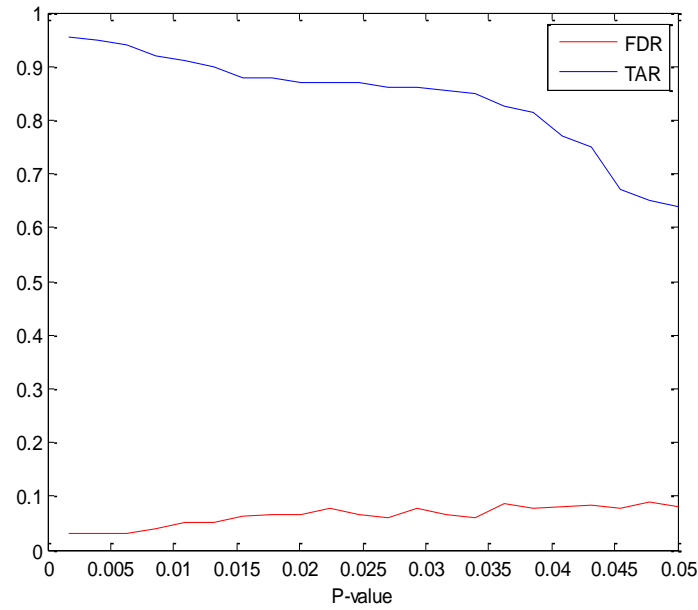


**Figure V-22: False discovery rate and true activation rate obtained by GLM method**

To sum it up, Table V.4 presents the average of TAR and FAR measures by the presented method and GLM method

**Table V-4: Average of true activation rate and false activation rate obtained by applying the DS method and GLM to the real data set**

	AVG( TAR)	AVG( FAR)
<b>DS method</b>	0.896	0.056
<b>GLM</b>	0.887	0.071

This experiment shows that the proposed method based on DS theory outperforms the GLM method in identifying more true activation rate with low false activation rate. Figure V.23 presents some slices that show the activated areas by both method GLM and the proposed method

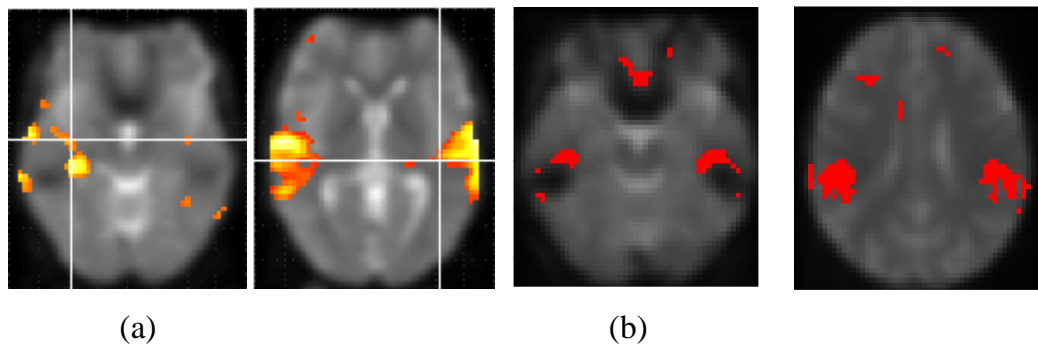


**Figure V-23: Some slices illustrate the activated regions: a) the result is generated by GLM method; b) the result is generated DS method**



## V.6 EEG fMRI fusion using Dempster shafer theory

Since BOLD signal is usually considered to have the same time evolution as the EEG (Lei et al., 2012), this approach uses the HRF model as a key element for modelling both EEG and fMRI modalities by DS method to fuse spatio-temporal information and detect activated areas in the brain

At first in the proposed approach, we compute the vectors of probability of  $m(t_i)$  for each modality that are employed. For computing combination rule measures via the equations (3) and (4) that need to determine the intersection intervals  $A = B \cap C$  which are different of empty set  $\emptyset$  which are illustrated in figure V.24.

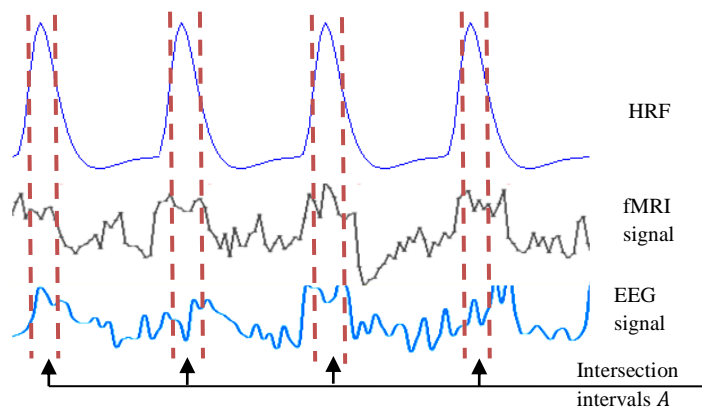


Figure V-24: Figure shows how to detect the interval A

### V.6.1 JointICA method

JointICA has been introduced by (Calhoun et al., 2006). It is implemented in the Fusion ICA Toolbox(FIT), available at <http://icatb.sourceforge.net>. Joint ICA enables us to jointly analyze multiple modalities which have all been collected in the same set of subjects. In this work, we assume that the electrical activity (ERP) and the hemodynamic response to brain activity (BOLD signal) are generated by the same population of neurons. Hence, the amplitudes of the ERP wave (peak) and of the BOLD response invoked by an activated area will increase and decrease synchronously: a stronger ERP peak activation will yield a stronger BOLD response in this particular brain region, and vice versa.

The basic steps of the Joint ICA are depicted in Figure V.25, and summarized as follows, (<http://mialab.mrn.org/software/fit/>):

- Step 1:** The features of each imaging modality are computed and collected.
- Step 2:** For each task a normalization process is done on the collected features.
- Step 3:** Principal Component Analysis (PCA) is used in reducing the dimensions of the normalized features.
- Step 4:** The spatially independent Components are extracted from the reduced data obtained by PCA, and as noted each component will share a common loading or mixing parameter between the tasks.

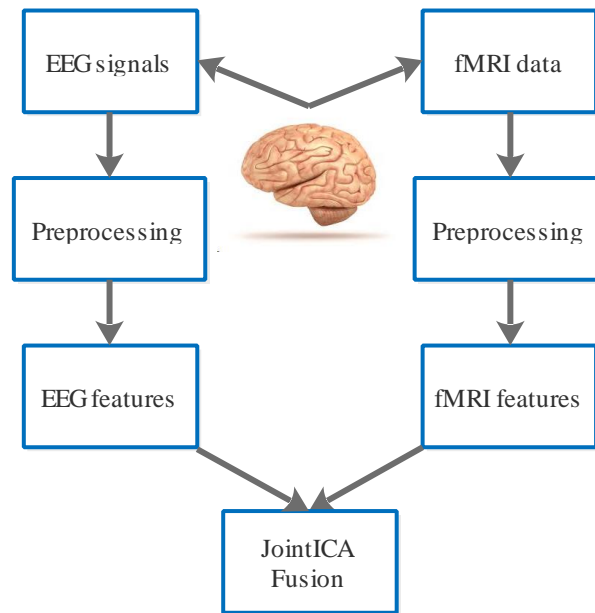


**Figure V-25: fMRI-EEG fusion using Joint ICA.**

Joint ICA fusion method offers several advantages in the context of brain exploration. Thus, it has received an increasing interest in recent years. Joint ICA fusion method serves to identify certain diseases such as Schizophrenia (SZ), a mysterious disease that requires further investigation, because it can provide similar activation patterns in multiple tasks from different brains images of patients suffering from Schizophrenia. Given that fMRI has a good spatial resolution and EEG has a good temporal resolution, Joint ICA enables to obtain a good spatial and temporal resolution when fusing fMRI and EEG modalities together (Mohammed, Taha, & Faragallah, 2014).

### V.6.2 The Proposed Method

As will be illustrated in Figure V-26, the proposed scheme for EEG-fMRI symmetrical fusion is as follows: (i) pre-processing both fMRI and EEG data, (ii) generating HRF model by DS method, (iii) Calculating the  $m_{fMRI}()$  for each voxel, (iv) computing  $m_{EEG}()$  after extracting ERP from EEG signals and then, (v)  $m_{fMRI}()$  and  $m_{EEG}()$

metrics have been used to compute  $m_{fMRI,EEG}()$  measure. This combination rule measure ( $m_{fMRI,EEG}()$ ) has been used to extract activated voxels via clustering. To separate the activated voxels from non-activated voxels, the clustering methods have been used because they can separate data into groups based on certain similarities. In this step, the PHA has been employed. As mentioned above, PHA generates automatically a number of clusters which is less than or equal to the selected max number (K). Furthermore, among these clusters, we show the target cluster and more information like the number of voxels by cluster and the centroid of cluster denoted by (c) as well. The process is described in Dempster Shafer algorithm (algorithm DS) and consists of six steps as follows:

**Algorithm DS:****INPUT:** fMRI data, EEG signals, HRF**OUTPUT:**  $m_{fMRI}()$  ,  $m_{EEG}()$  ,  $m_{EEG,fMRI}()$  , activated areas**step 1:** first model HRF by using DS method, described in section 2**step 2:** project HRF model with fMRI signal and compute  $m_{fMRI}()$  vector for each voxels using equations (5) and (6).**step 3:** from EEG to ERP**step 4:** the same process applied in step 2 has been repeated on ERP to compute vector of  $m_{EEG}()$ **step 5:** compute the combination rule measure using the equations aforementioned in (3) and (4)**step 6:** use PHA method to cluster vector of  $m_{EEG,fMRI}()$  combination measure in order to identify active areas .

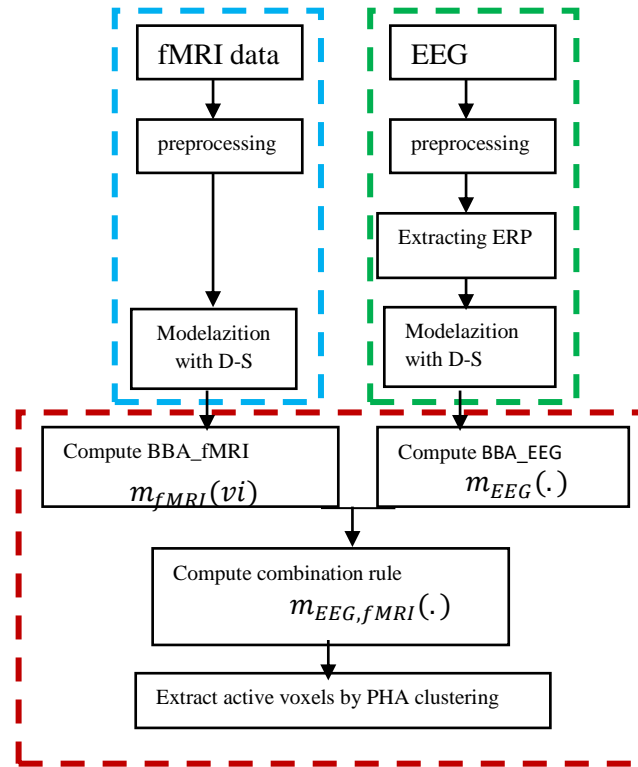


**Figure V-26: flowchart of the EEG-fMRI data fusion based on DS method**The chart is divided into three main parts. The blue part concerns preprocess and modelisation of fMRI data. The green part is about EEG data and contains three steps; preprocessing, extracting ERP and modelisation by DS. The red part denotes clustering extract activated voxels

### V.6.3 Experiments and results

The proposed method that relies on Dempster Shafer theory has been evaluated on both synthetic and real data. The performance of the introduced method has been based on statistical measurements. The MATLAB has been used for all implementations. At last, a comparison with jointICA has been provided to evaluate the efficiency of the proposed method. The evaluation metrics and experimental results are discussed below.

#### V.6.3.1 Evaluation metrics

This subsection describes the evaluating metrics serving to analyze the performance of the introduced approach and to establish a comparison with the jointICA method. Basically, two main metrics have been given in (Meyer & Chinrungrueng, 2005): (i) True activation rate (TAR) presents the ratio between the number of voxels correctly identified as activated and the total number of truly activated voxels and (ii) false activation rate (FAR) is known as the ratio between the number of voxels incorrectly identified as activated and the total number of truly non-activated voxels. A more comprehensive

description of these two metrics allows to correctly plotting the Receiver Operating Characteristics Curve ( ROC) (Sorenson & Wang, 1996)for comparing between methods.

To compute these measures, it should be noted that jointICA has been performed on the basis of the t-test that uses a p-value or Z-threshold to map the activated voxels. The introduced method relies on the combination rule  $m_{EEG,fMRI}$  ( ) to separate between activated and non-activated voxels.

#### ***V.6.3.2 Artificial dataset***

First, the proposed method has been tested on artificial dataset basically developed with their simulation algorithm by Correa et al. (Correa, Adali, Li, & Calhoun, 2005) and it is available at ([http://mlsp.umbc.edu/simulated\\_fmri\\_data.html](http://mlsp.umbc.edu/simulated_fmri_data.html)) .This dataset contains eight sources where each simulated source is of  $60 \times 60$  image with 100 point courses. However, in the current experiment, the virtual source for fMRI has been created into a two dimensional spatial map, as depicted in Figure V.27(a), as the same size of the real fMRI data. Given that the information obtained from the brain is a stochastic process, a collection of sinusoid signals of the ERP data has been considered.

Let  $\phi$  be the Gaussian random delay distributed with zero mean and unit variance and let  $d$  be the amplitude. Accordingly, ERP sources have been simulated by using the formula:

$$x(n) = 100 \times d^n \sin(2\pi fn + \phi), n = 1 \dots 200 \quad (v.24)$$

This sinusoid signal is with a mixture of very low frequencies from [0.014- 0.811 Hz]

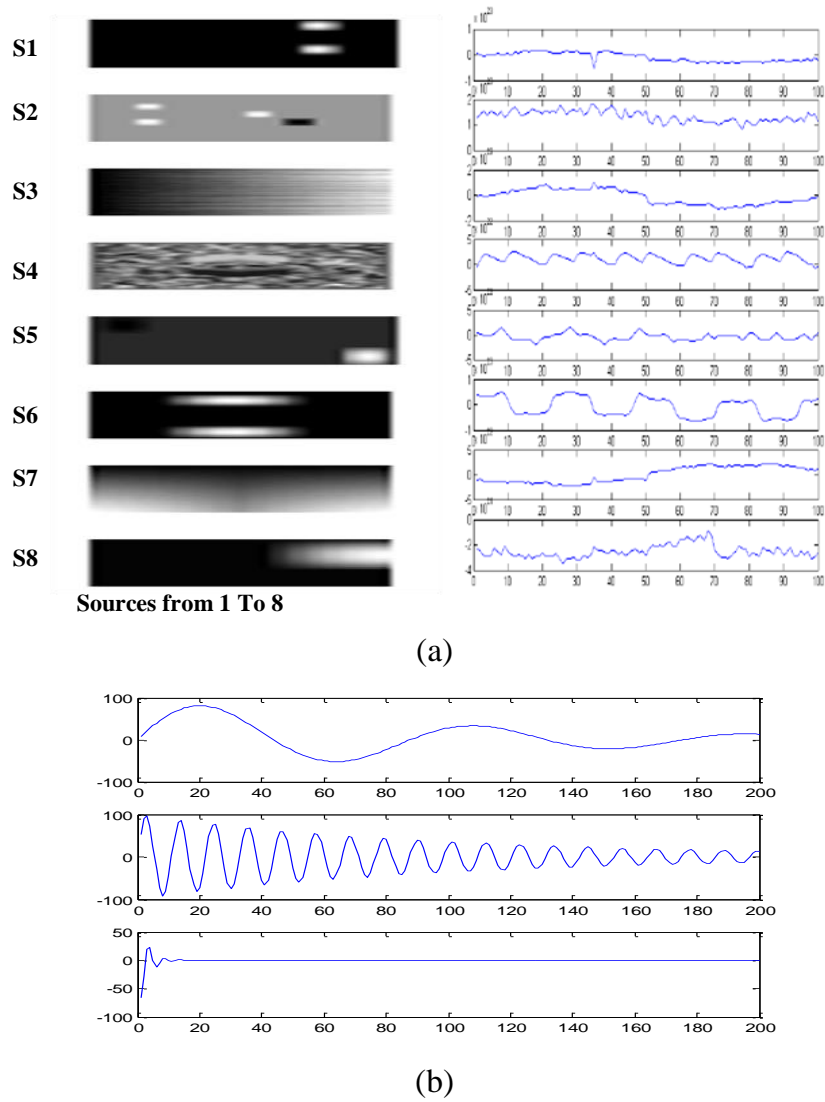


**Figure V-27 : Artificial fMRI and ERP data(a) Artificial fMRI data contains eight sources where each simulated source is of  $60 \times 60$  image with 100 point courses (b) the selected ERP simulation data generated by using( equa. V.24)**

The source  $S$  with a size of  $(8 \times 3339)$  has been obtained by mixing the different FMRI sources. In the next step, the Dempster method has been applied on these data to get the  $m_{fMRI}()$ . Then, the same algorithm has been applied on ERP dataset to compute  $m_{EEG}()$ . Once both  $m_{EEG}$  and  $m_{fMRI}$  have been obtained, the  $m_{EEG, fMRI}()$  have been computed by using the combination rule. The obtained  $m_{EEG, fMRI}()$  has been clustered via PHA method. In this process,  $(K=8)$  has been chosen according to the number of simulated data sources. The obtained results are presented in Figure V.28 where different slices have been clearly shown (mixed areas) in different sources. This figure presents the mixed activated areas detected by the proposed method. As it is clear in the first four slices on the left, the activated regions of the different sources ( $S1, S2, S5, S6$  and part of

S4) are depicted in figure V.28 (a) . Slices on the right show the activated areas of each source in (S4, S6 and S8). Comparing our results with those obtained with jointICA, it can be seen that jointICA detects only (S3,S4,S5,S6) sources (see Figure V.28(b)). Thus, the proposed approach has obviously shown its ability to yield a clear distinction between areas in terms of activation.

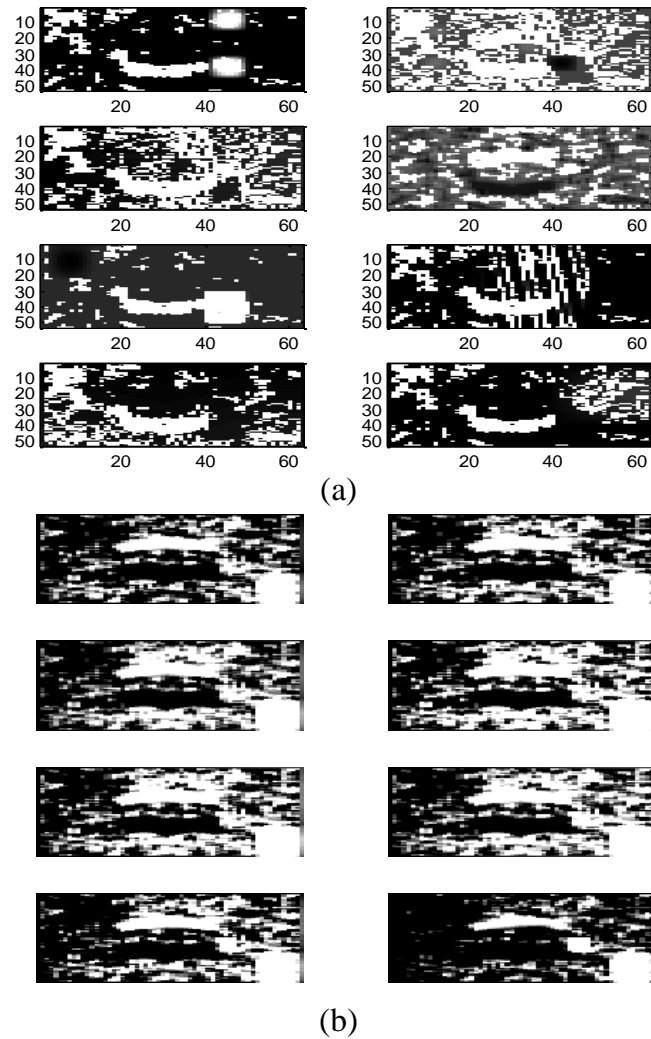


**Figure V-28: a) The obtained results by proposed method that show the mixed area in each slice**

Table V.5 describes the quantitative comparison between the introduced method and jointICA using the true activation rate (TAR) and false activation rate (FAR). It's clear from this table that each method achieves better result that is more than 90.25%. Also from this table the proposed method detects more accurately than jointICA for the sources (S1,S2, S6 ,S7, S8). Thus, jointICA outperforms the proposed method for sources (S3,S4,S5). Table V.6 shows the average of measures (TAR and FAR).

Table V-5: True and false activation rates by the proposed method and jointICA

Source		S1	S2	S3	S4	S5	S6	S7	S8
Proposed method	TAR%	97.25	93.50	98.25	90.75	98.50	96.75	92.75	91.75
	FAR	0.0275	0.0650	0.0175	0.0925	0.0150	0.0325	0.0725	0.0825
jointICA	TAR%	93.50	91.75	98.50	93.00	98.75	94.25	91.25	90.25
	FAR	0.0650	0.0825	0.0150	0.0700	0.0125	0.0575	0.0875	0.0975

Table V-6: Average of TAR and FAR of the proposed method and jointICA to the simulated dataset.

	AVG( TAR)	AVG( FAR)
Proposed method	94.93%	0.051
jointICA	93.87%	0.061

From the outcome, it can be concluded that the results are very motivating for identifying more activated areas. Thus, the introduced method can outperform better than the jointICA method in detecting more accurate activation for the simulated data.

### V.6.3.3 Real data

Besides simulation data, the current method has been evaluated also on a real fMRI and EEG dataset to assess its performance. As described in (Calhoun et al., 2006), this data was collected while participants were performing an auditory oddball. Prior to analysis, data goes through a series of preprocessing steps to identify and remove artifacts and validate model assumptions as well. Therefore, the fMRI slices require to be spatially realigned at first. However, spatial smoothing may cause unforeseen changes to occur into data. Thus, for better performance, spatial smoothing has been avoided. Then, the mean value has been subtracted from each of the time series and the variance has been normalized to a unit. The previous steps have been realized via SPM tools (Statistical Parametric Mapping). Once EEG signals are obtained, we extract the ERP from EEG. We apply the proposed method on each voxel. In this case, we compute  $m_{fMRI}$  and  $m_{EEG}$  then we fuse both fMRI and EEG data by employing the combination rule in order to get  $m_{EEG,fMRI}$ . This measure is used for extracting activated voxels. However, by using PHA clustering method, we proceed to change the max number of cluster (k) by increment and we observe the centroid (c) of cluster and the number of voxels in the target cluster. Then, we show the activated regions. The same process has been repeated till no new cluster will be generated. Table V.7 presents the results of  $m_{EEG,fMRI}$  clustering by PHA method. The plots depicted in Figure V.29 present the various numbers of voxels by max number of clusters.



Table V-7: Result of  $m_{EEG, fMRI}$  clustering by PHA method

Number max of cluster (k)	Number of voxels	Centre c
3	2235	0.0053
4	2184	0.0051
5	2184	0.0051
6	2184	0.0051
7	2184	0.0051
8	2184	0.0051
9	1378	0.0062
10	822	0.0069
11	783	0.0068
12	783	0.0068
13	783	0.0068
14	783	0.0068
15	783	0.0068

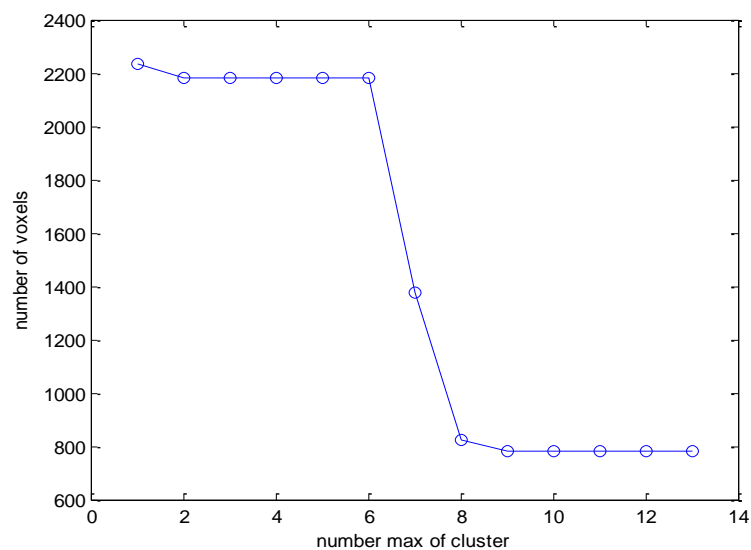
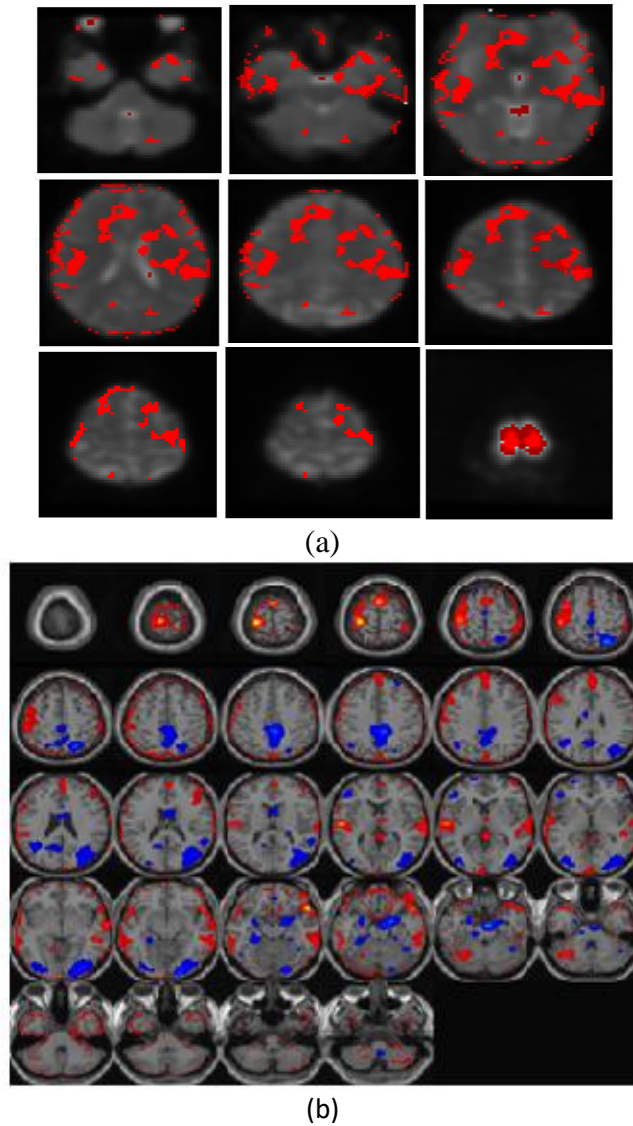


Figure V-29: Variation in the number of voxels by number max of clusters k

By varying the max number (K), false positive voxels may be obtained if k is small or some voxels may be neglected if (K) is great. Given this, a threshold should be selected for better distinction of activated voxels. Thus, the average of the centroids of the target clusters has been used. By computing the average of the centroids (c), we get 0.006. Figure V.30. (a) Illustrates slices that indicate activated regions while figure V.30. (b) depicts the activated areas for both components (red and blue). Qualitatively, it is clear that introduced method can detect activated region like jointICA method applied on the auditory data. For a quantitative comparison, the results obtained with the proposed

approach have been compared with those obtained with jointICA that has been applied to analyze simultaneous EEG-fMRI data as illustrated in Figure V.31 and Figure V.32.



**Figure V-30 : (a) Activated areas in some slices by proposed method (b) Activated areas in slices by jointICA method, provided in both color red and blue for each component**

As stated above in the current study, the proposed method depends on DS method that consists of two main components: The HRF model obtained by DS and  $m_{EEG, fMRI}()$  measure. For selecting activated voxels, PHA method must be used for clustering this measure.

To validate the efficiency of the introduced approach, a comparison between the proposed algorithm and jointICA has been performed. It should be noted that jointICA is performed on the basis of the t-test that uses a p-value or Z-threshold to map the activated voxels. Given that the definition of p-value is similar to that of the false activated position

rate in the jointICA, the p-value can be used as a metric for choosing thresholds. Thus, several plots have been generated for both true and false activation rates at different thresholds ( $m_{EEG,fMRI}$ , p-value). Consequently, the experiment has been performed by changing thresholds for computing the metrics. Figure V.31 depicts the variation of true and false activation rates according to  $m_{EEG,fMRI}()$  using the proposed algorithm. It seems obvious that the number of true activated voxels tends to be lower in true activation rate. However, the pace of false activation rate remains stable in the interval [0.001- 0.005], then it gradually decreases.

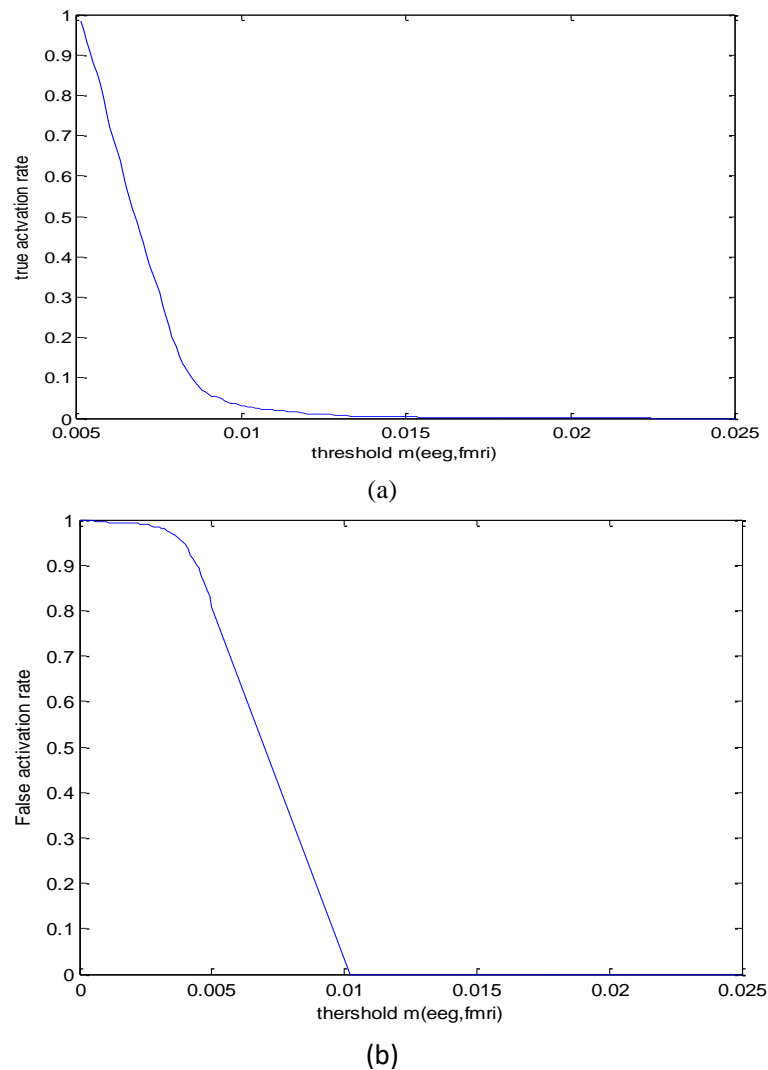


**Figure V-31 : Number of true positives (a) and false positives (b) using different thresholds ( $m_{EEG,fMRI}$ ).**

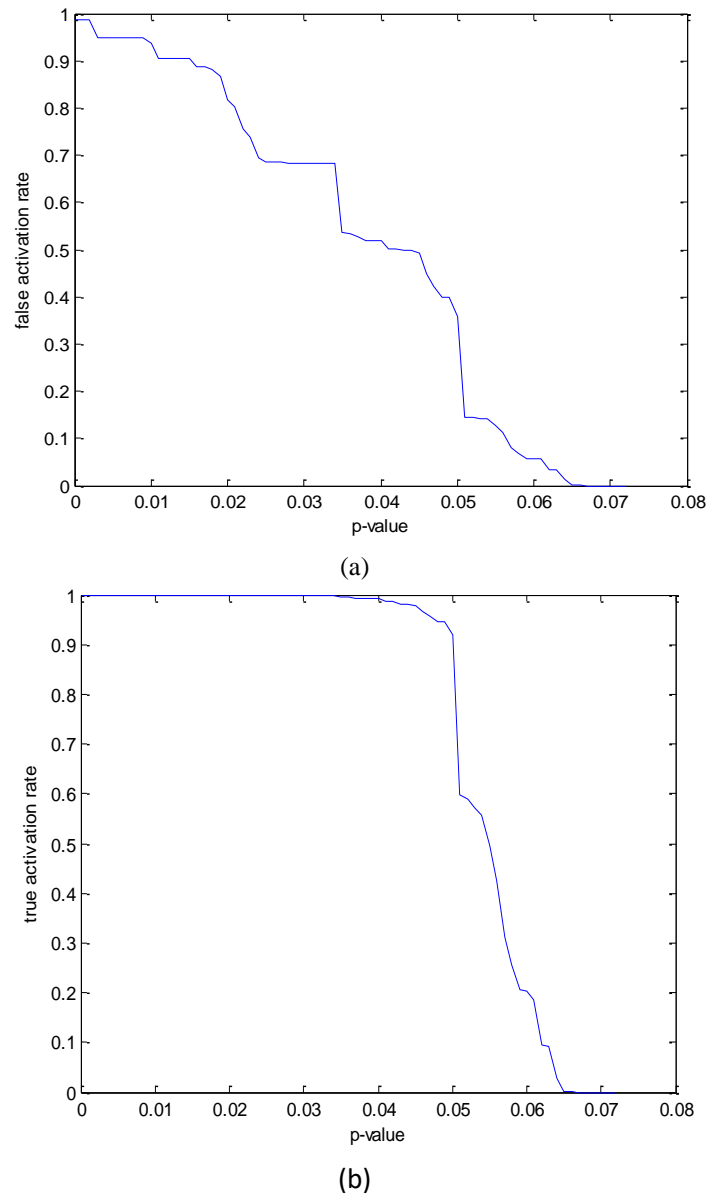


Figure V-32 The number of (a) false activation rate (b) by using several p-values

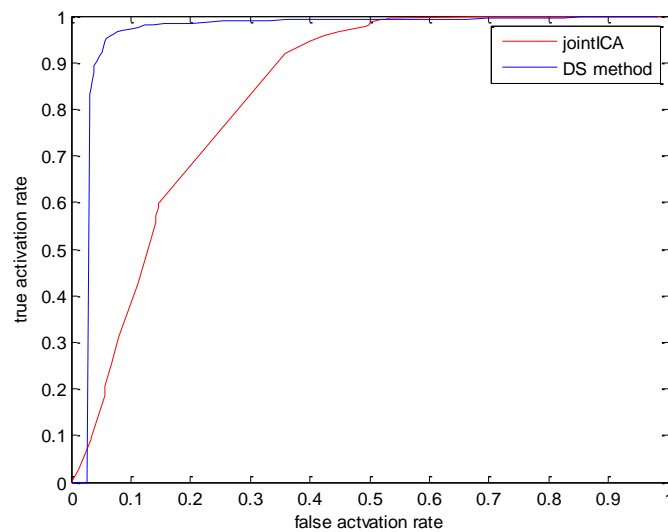


Figure V-33: ROC curves for the comparison of jointICA and the introduced method

Figure V.32 (a) shows that the true activation rate remains the same till the p-value reaches 0.05 where it starts to fall down gradually. Figure V.32 (b) illustrates that False Activation Rate continues to decrease gradually when the p-value increases and sometimes it remains fixed as in] 0.025, 0.035[. We have then specifically compared the obtained results with those yielded by using jointICA. The ROC curves for both methods are shown in Figure V-33 It is obviously observed that the ROC curve obtained by jointICA is much lower than that obtained by the proposed method. While joint-ICA provided few true positives with few false positives, the new method has detected more true positives without increasing the number of false position. However, the area under ROC curve for DS method is 0.877 and 0.733 for jointICA method. Therefore, this comparison reveals that the proposed algorithm provides a better performance in terms of identifying more true positives than jointICA.

## **V.7 Conclusion**

This work introduces a new analysis based on Dempster-Shafer theory that better separates activated voxels from fMRI time series by using basic belief assignment functions. Also, a new framework to identify activation areas in simultaneous EEG/fMRI data taking into account the application of combination rule.

For fMRI modality the proposed approach aims to extract activated areas from fMRI data sets. Mainly, information background is required about the hemodynamic response model at the beginning. The introduced method has been validated on a real auditory fMRI dataset as well as on an artificial dataset and its performance has been compared with GLM method. The obtained results have clearly shown the ability of belief measures to yield a better clustering of activated voxels.

From the outcome of this investigation, it is possible to conclude that the proposed framework can be employed in most fMRI data analysis methods. Also, the findings suggest that the theory of evidence can serve to understand the nature of data and to obtain relevant results that can be used and interpreted by neuroscientists.

The future work aims to use DS theory in analyzing fMRI-EEG data fusion to take advantage of both modalities in order to better study the brain activity and to reveal the mysterious secrets of this amazing organ.

Basically, the approach relies on DS theory and PHA method has been also employed to clustering the obtained measures. An extensive performance analysis has been provided with both artificial and real datasets. Compared to joint ICA, the obtained activation map confirmed the efficiency of the proposed algorithm for EEG-fMRI fusion in yielding a clear distinction between activated and non-activated areas. Although the focus has been placed on the analysis of auditory data, the introduced approach can be extended to explore various aspects of brain activity and to detect brain illnesses such as epilepsy.

# Final conclusion

---

Understanding the human brain activity requires knowledge about the temporal and spatial aspects of data processing. Functional Magnetic Resonance imaging (fMRI) and Electroencephalography (EEG) are the most pertinent techniques used for exploring the brain. In recent years, the combination of fMRI and EEG has become an issue of considerable interest in neuroscience and it has shown great promise for enabling the researchers to acquire a better comprehensive understanding of the neural activity. However, EEG/fMRI fusion is still a field of ongoing research.

The work described in this thesis has been directed towards developing and applying new technique that is able to fuse both EEG and fMRI modalities to take the advantages of spatial and temporal resolution. The proposed approach based on DS theory method has been applied on fMRI or EEG-fMRI where the focus has been placed on the analysis of auditory data.

At first, the current work provided a general description of the brain anatomy where the different main components of the brain were illustrated. Also, the different techniques used for analyzing brain function were briefly discussed in chapter one to give the reader a general view and introduce him to the subject of the thesis.

The EEG-fMRI fusion methods involve understanding in details each of the EEG and fMRI modalities that are used in exploring the neural activity. Given this, each of EEG and fMRI modalities were discussed separately in chapter two and three respectively. The main idea behind studying EEG and fMRI techniques is to study brain function and the relative advantages and disadvantages of these methods. In particular, an information background about the hemodynamic response model which is the key of the proposed method is required at the beginning. Then, chapter four explored the complementary information that the two techniques provide.

Finally, we introduced in chapter five our contribution to study brain activity that is based on Dempster-Shafer theory of evidence. First, we demonstrated that such theory

was applied on fMRI data (method & experimentation) starting by presenting the proposed model of HRF function and ending by detecting activated regions in brain. The experimental study clearly showed the ability of belief measures provided by DS theory to yield a better clustering of activated voxels.

From the outcome of this investigation, it is possible to conclude that the proposed framework can be employed in most fMRI data analysis methods. Also, the findings suggest that the theory of evidence can serve to understand the nature of data and to obtain relevant results that can be used and interpreted by neuroscientists. Second, the use of the rule of combination provided by DS theory in information fusion data was illustrated together with how to apply it on data coming from EEG and fMRI techniques in order to take advantage of both modalities for better studying the brain activity. The obtained activation map confirmed the efficiency of the proposed algorithm for EEG-fMRI fusion in yielding a clear distinction between activated and non-activated areas.

In the fascinating field of neuroscience, we seek to develop several methods to better explore the brain. As a future work, we focus on extending the introduced approach to explore various aspects of brain activity and to detect brain illnesses such as epilepsy. Also, we are conducting another research seeking to develop a new method based on information theory (mutual) for analyzing the EEG and fMRI data together.



## References

- Adrian, E. D. (1934). PAET 4, VOL. 57. THE BEBGEE EHYTHM: POTENTIAL CHANGES FEOM THE OCCIPITAL LOBES IN MAN.
- Aguirre, G. K., Zarahn, E., & D'esposito, M. (1998). The variability of human, BOLD hemodynamic responses. *Neuroimage*, 8(4), 360–369.
- Aubert, A., Costalat, R., & Valabrègue, R. (2001). Modelling of the coupling between brain electrical activity and metabolism. *Acta Biotheoretica*, 49(4), 301–326.
- Bahlmann, C., & Burkhardt, H. (2004). The writer independent online handwriting recognition system frog on hand and cluster generative statistical dynamic time warping. *IEEE Transactions on Pattern Analysis and Machine Intelligence*, 26(3), 299–310.
- Baillet, S., Mosher, J. C., & Leahy, R. M. (2001). Electromagnetic brain mapping. *Signal Processing Magazine, IEEE*, 18(6), 14–30.
- Bandettini, P. A., Wong, E. C., Hinks, R. S., Tikofsky, R. S., & Hyde, J. S. (1992). Time course EPI of human brain function during task activation. *Magnetic Resonance in Medicine*, 25(2), 390–397.
- Berger, H. (1929). {Ü}ber das elektrenkephalogramm des menschen. *European Archives of Psychiatry and Clinical Neuroscience*, 87(1), 527–570.
- Berthoz, A. (2002). *The brain's sense of movement*. Harvard University Press.
- Blamire, A. M., Ogawa, S., Ugurbil, K., Rothman, D., McCarthy, G., Ellermann, J. M., ... Shulman, R. G. (1992). Dynamic mapping of the human visual cortex by high-speed magnetic resonance imaging. *Proceedings of the National Academy of Sciences*, 89(22), 11069–11073.
- Bloch, F. (1946). Nuclear induction. *Physical Review*, 70(7–8), 460.
- Bogorodzki, P., Rogowska, J., & Yurgelun-Todd, D. A. (2005). Structural group classification technique based on regional fMRI BOLD responses. *Medical Imaging, IEEE Transactions on*, 24(3), 389–398.
- Bonmassar, G., Anami, K., Ives, J., & Belliveau, J. W. (1999). Visual evoked potential (VEP) measured by simultaneous 64-channel EEG and 3T fMRI. *Neuroreport*, 10(9), 1893–1897.
- Bonmassar, G., Schwartz, D. P., Liu, A. K., Kwong, K. K., Dale, A. M., & Belliveau, J. W. (2001). Spatiotemporal brain imaging of visual-evoked activity using interleaved EEG and fMRI recordings. *Neuroimage*, 13(6), 1035–1043.
- Born, A. P., Law, I., Lund, T. E., Rostrup, E., Hanson, L. G., Wildschjødzt, G., ... Paulson, O. B. (2002). Cortical deactivation induced by visual stimulation in human slow-wave sleep. *Neuroimage*, 17(3), 1325–1335.
- Broca, P. (1861). Perte de la parole, ramollissement chronique et destruction partielle du lobe ant{é}rieur gauche du cerveau. *Bull Soc Anthropol*, 2(1), 235–238.
- Brookings, T., Ortigue, S., Grafton, S., & Carlson, J. (2009). Using ICA and realistic BOLD models to obtain joint EEG/fMRI solutions to the problem of source localization. *Neuroimage*, 44(2), 411–420.
- Brooks, D. J. (1992). Exploring Brain Functional Anatomy with Positron Emission Tomography. *Journal of Anatomy*, 180(Pt 3), 557.
- Buračas, G. T., & Boynton, G. M. (2002). Efficient design of event-related fMRI experiments using M-sequences. *Neuroimage*, 16(3), 801–813.
- Buxton, R. B., & Frank, L. R. (1997). A model for the coupling between cerebral blood flow and oxygen metabolism during neural stimulation. *Journal of Cerebral Blood Flow & Metabolism*, 17(1), 64–72.
- Buzsáki, G., Kaila, K., & Raichle, M. (2007). Inhibition and brain work. *Neuron*, 56(5), 771–783.
- Cabeza, R., & Nyberg, L. (2000). Imaging cognition II: An empirical review of 275 PET and fMRI studies. *Journal of Cognitive Neuroscience*, 12(1), 1–47.
- Calhoun, V. D., & Adali, T. (2009). Feature-based fusion of medical imaging data. *Information Technology in Biomedicine, IEEE Transactions on*, 13(5), 711–720.
- Calhoun, V. D., Adali, T., Pearlson, G. D., & Kiehl, K. A. (2006). Neuronal chronometry of target detection: fusion of hemodynamic and event-related potential data. *Neuroimage*, 30(2), 544–553.
- Caparos, M., Louis-Dorr, V., Wendling, F., Maillard, L., & Wolf, D. (2006). Automatic lateralization of temporal lobe epilepsy based on scalp EEG. *Clinical Neurophysiology*, 117(11), 2414–2423.
- Caton, R. (1875). Electrical Currents of the Brain. *The Journal of Nervous and Mental Disease*, 2(4), 610.
- Changeux, J. P. (1983). *L'Homme neuronal*. Fayard, Paris; English edition: Neuronal man. *Pantheon New York*.
- Chee, M. W. L., Venkatraman, V., Westphal, C., & Siong, S. C. (2003). Comparison of block and event-related fMRI designs in evaluating the word-frequency effect. *Human Brain Mapping*, 18(3), 186–193.
- Chumbley, J. R., & Friston, K. J. (2009). False discovery rate revisited: FDR and topological inference using Gaussian random fields. *Neuroimage*, 44(1), 62–70.
- Correa, N., Adali, T., Li, Y.-O., & Calhoun, V. D. (2005). Comparison of blind source separation algorithms for FMRI using a new Matlab toolbox: GIFT. In *Acoustics, Speech, and Signal Processing, 2005*.

- Proceedings.(ICASSP'05). IEEE International Conference on* (Vol. 5, p. v--401).
- Cox, D. D., & Savoy, R. L. (2003). Functional magnetic resonance imaging (fMRI)“brain reading”: detecting and classifying distributed patterns of fMRI activity in human visual cortex. *Neuroimage*, 19(2), 261–270.
- Crouzeix-Cheylus, A. (2001). *Méthodes de localisation des générateurs de l'activité électrique cérébrale à partir de signaux électro-et magnéto-encéphalographiques*. Villeurbanne, INSA.
- Cuzzolin, F. (2008). A geometric approach to the theory of evidence. *Systems, Man, and Cybernetics, Part C: Applications and Reviews, IEEE Transactions on*, 38(4), 522–534.
- Czisch, M., Wehrle, R., Kaufmann, C., Wetter, T. C., Holsboer, F., Pollmächer, T., & Auer, D. P. (2004). Functional MRI during sleep: BOLD signal decreases and their electrophysiological correlates. *European Journal of Neuroscience*, 20(2), 566–574.
- Dale, A. M. (1999). Optimal experimental design for event-related fMRI. *Human Brain Mapping*, 8(2–3), 109–114.
- Dale, A. M., Liu, A. K., Fischl, B. R., Buckner, R. L., Belliveau, J. W., Lewine, J. D., & Halgren, E. (2000). Dynamic statistical parametric mapping: combining fMRI and MEG for high-resolution imaging of cortical activity. *Neuron*, 26(1), 55–67.
- Daunizeau, J., Grova, C., Marrelec, G., Mattout, J., Jbabdi, S., Péligrini-Issac, M., ... Benali, H. (2007). Symmetrical event-related EEG/fMRI information fusion in a variational Bayesian framework. *Neuroimage*, 36(1), 69–87.
- Daunizeau, J., Grova, C., Mattout, J., Marrelec, G., Clonda, D., Goulard, B., ... Benali, H. (2005). Assessing the relevance of fMRI-based prior in the EEG inverse problem: a Bayesian model comparison approach. *Signal Processing, IEEE Transactions on*, 53(9), 3461–3472.
- Daunizeau, J., Laufs, H., & Friston, K. J. (2009). EEG--fMRI information fusion: biophysics and data analysis. In *EEG-fMRI* (pp. 511–526). Springer.
- De Munck, J. C., Goncalves, S. I., Huijboom, L., Kuijter, J. P. A., Pouwels, P. J. W., Heethaar, R. M., & da Silva, F. H. L. (2007). The hemodynamic response of the alpha rhythm: an EEG/fMRI study. *Neuroimage*, 35(3), 1142–1151.
- de Oliveira Jordao, T. J. (2010). fMRI data analysis techniques and the self-organizing maps approach.
- Debener, S., Ullsperger, M., Siegel, M., & Engel, A. K. (2006). Single-trial EEG--fMRI reveals the dynamics of cognitive function. *Trends in Cognitive Sciences*, 10(12), 558–563.
- Deco, G., Jirsa, V. K., Robinson, P. A., Breakspear, M., & Friston, K. (2008). The dynamic brain: from spiking neurons to neural masses and cortical fields. *PLoS Comput Biol*, 4(8), e1000092.
- Deco, G., Jirsa, V., McIntosh, A. R., Sporns, O., & Kötter, R. (2009). Key role of coupling, delay, and noise in resting brain fluctuations. *Proceedings of the National Academy of Sciences*, 106(25), 10302–10307.
- Dempster, A. P. (1967). Upper and lower probabilities induced by a multivalued mapping. *The Annals of Mathematical Statistics*, 325–339.
- Eichele, T., Debener, S., Calhoun, V. D., Specht, K., Engel, A. K., Hugdahl, K., ... Ullsperger, M. (2008). Prediction of human errors by maladaptive changes in event-related brain networks. *Proceedings of the National Academy of Sciences*, 105(16), 6173–6178.
- Ferrier, D. (1875). The Croonian Lecture: experiments on the brain of monkeys (second series). *Philosophical Transactions of the Royal Society of London*, 165, 433–488.
- Finger, S. (2009). The birth of localization theory. *Handbook of Clinical Neurology*, 95, 117–128.
- Fisch, B. J., & Spehlmann, R. (1999). *Fisch and Spehlmann's EEG primer: basic principles of digital and analog EEG*. Elsevier Health Sciences.
- Friston, K., Harrison, L., Daunizeau, J., Kiebel, S., Phillips, C., Trujillo-Barreto, N., ... Mattout, J. (2008). Multiple sparse priors for the M/EEG inverse problem. *NeuroImage*, 39(3), 1104–1120.
- Friston, K. J., Holmes, A. P., Worsley, K. J., Poline, J.-P., Frith, C. D., & Frackowiak, R. S. J. (1994). Statistical parametric maps in functional imaging: a general linear approach. *Human Brain Mapping*, 2(4), 189–210.
- Friston, K. J., Jezzard, P., & Turner, R. (1994). Analysis of functional MRI time-series. *Human Brain Mapping*, 1(2), 153–171.
- Friston, K. J., Mechelli, A., Turner, R., & Price, C. J. (2000). Nonlinear responses in fMRI: the Balloon model, Volterra kernels, and other hemodynamics. *NeuroImage*, 12(4), 466–477.
- Friston, K. J., Zarahn, E., Josephs, O., Henson, R. N. A., & Dale, A. M. (1999). Stochastic designs in event-related fMRI. *Neuroimage*, 10(5), 607–619.
- George, J. S., Aine, C. J., Mosher, J. C., Schmidt, D. M., Ranken, D. M., Schlitt, H. A., ... Belliveau, J. W. (1995). Mapping function in the human brain with magnetoencephalography, anatomical magnetic resonance imaging, and functional magnetic resonance imaging. *Journal of Clinical Neurophysiology*, 12(5), 406–431.
- Gibbs, F. A., & Gibbs, E. L. (1946). The electroencephalographic pattern of encephalitis. *Archives of Neurology and Psychiatry*, 55, 166.
- Gilmore, R. L. (1994). American-electroencephalographic-society guidelines in electroencephalography,

- evoked-potentials, and polysomnography. *Journal of Clinical Neurophysiology*, 11(1), 1–142.
- Gjedde, A. (2001). Brain energy metabolism and the physiological basis of the hemodynamic response. In *Functional Magnetic Resonance Imaging*. Oxford University Press.
- Goldman, R. I., Stern, J. M., Engel Jr, J., & Cohen, M. S. (2002). Simultaneous EEG and fMRI of the alpha rhythm. *Neuroreport*, 13(18), 2487.
- Goodwin, J. E., & Hall, G. E. (1939). The human electroencephalogram and its clinical significance. *Canadian Medical Association Journal*, 41(2), 146.
- Gotman, J., & Pittau, F. (2011). Combining EEG and fMRI in the study of epileptic discharges. *Epilepsia*, 52(s4), 38–42.
- Gu, J., & Jin, X. (2006). A simple approximation for dynamic time warping search in large time series database. *Intelligent Data Engineering and Automated Learning--IDEAL 2006*, 841–848.
- Hämäläinen, M., Hari, R., Ilmoniemi, R. J., Knuutila, J., & Lounasmaa, O. V. (1993). Magnetoencephalography—theory, instrumentation, and applications to noninvasive studies of the working human brain. *Reviews of Modern Physics*, 65(2), 413.
- Hari, R., & Kujala, M. V. (2009). Brain basis of human social interaction: from concepts to brain imaging. *Physiological Reviews*, 89(2), 453–479.
- Horwitz, B., Friston, K. J., & Taylor, J. G. (2000). Neural modeling and functional brain imaging: an overview. *Neural Networks*, 13(8), 829–846.
- Ives, J. R., Warach, S., Schmitt, F., Edelman, R. R., & Schomer, D. L. (1993). Monitoring the patient's EEG during echo planar MRI. *Electroencephalography and Clinical Neurophysiology*, 87(6), 417–420.
- Jun, S. C., George, J. S., Kim, W., Paré-Blagoev, J., Plis, S., Ranken, D. M., & Schmidt, D. M. (2008). Bayesian brain source imaging based on combined MEG/EEG and fMRI using MCMC. *NeuroImage*, 40(4), 1581–1594.
- Kevin, W., Doug, W., Matthias, S., & Gerhard, S. (2008). Correspondence of visual evoked potentials with fMRI signals in human visual cortex. *Brain Topography*, 21(2), 86–92.
- Khotanlou, H. (2008). *3D brain tumors and internal brain structures segmentation in MR images*. T{é}l{é}com ParisTech.
- Kruggel, F., Wiggins, C. J., Herrmann, C. S., & von Cramon, D. Y. (2000). Recording of the event-related potentials during functional MRI at 3.0 Tesla field strength. *Magnetic Resonance in Medicine*, 44(2), 277–282.
- Kwong, K. K., Belliveau, J. W., Chesler, D. A., Goldberg, I. E., Weisskoff, R. M., Poncelet, B. P., ... Turner, R. (1992). Dynamic magnetic resonance imaging of human brain activity during primary sensory stimulation. *Proceedings of the National Academy of Sciences*, 89(12), 5675–5679.
- Lange, N., & Zeger, S. L. (1997). Non-linear Fourier Time Series Analysis for Human Brain Mapping by Functional Magnetic Resonance Imaging. *Journal of the Royal Statistical Society: Series C (Applied Statistics)*, 46(1), 1–29.
- Laufs, H., Krakow, K., Sterzer, P., Eger, E., Beyerle, A., Salek-Haddadi, A., & Kleinschmidt, A. (2003). Electroencephalographic signatures of attentional and cognitive default modes in spontaneous brain activity fluctuations at rest. *Proceedings of the National Academy of Sciences*, 100(19), 11053–11058.
- Lauterbur, P. C. (1973). Image formation by induced local interactions: examples employing nuclear magnetic resonance.
- Lei, X., Qiu, C., Xu, P., & Yao, D. (2010). A parallel framework for simultaneous EEG/fMRI analysis: Methodology and simulation. *Neuroimage*, 52(3), 1123–1134.
- Lei, X., Valdes-Sosa, P. A., & Yao, D. (2012). EEG/fMRI fusion based on independent component analysis: integration of data-driven and model-driven methods. *Journal of Integrative Neuroscience*, 11(3), 313–337.
- LeVan, P., Tyvaert, L., Moeller, F., & Gotman, J. (2010). Independent component analysis reveals dynamic ictal BOLD responses in EEG-fMRI data from focal epilepsy patients. *Neuroimage*, 49(1), 366–378.
- Liu, Z., & He, B. (2008). fMRI-EEG integrated cortical source imaging by use of time-variant spatial constraints. *NeuroImage*, 39(3), 1198–1214.
- Lövblad, K.-O., Thomas, R., Jakob, P. M., Scammell, T., Bassetti, C., Griswold, M., ... Warach, S. (1999). Silent functional magnetic resonance imaging demonstrates focal activation in rapid eye movement sleep. *Neurology*, 53(9), 2193.
- Lu, Y., & Wan, Y. (2013). PHA: A fast potential-based hierarchical agglomerative clustering method. *Pattern Recognition*, 46(5), 1227–1239.
- Malonek, D., & Grinvald, A. (1996). Interactions between electrical activity and cortical microcirculation revealed by imaging spectroscopy: implications for functional brain mapping. *Science*, 272(5261), 551.
- Martínez-Montes, E., Valdés-Sosa, P. A., Miwakeichi, F., Goldman, R. I., & Cohen, M. S. (2004). Concurrent EEG/fMRI analysis by multiway partial least squares. *NeuroImage*, 22(3), 1023–1034.
- Masterton, R. A. J., Harvey, A. S., Archer, J. S., Lillywhite, L. M., Abbott, D. F., Scheffer, I. E., & Jackson, G.

- D. (2010). Focal epileptiform spikes do not show a canonical BOLD response in patients with benign rolandic epilepsy (BECTS). *Neuroimage*, 51(1), 252–260.
- Matthews, P. M., & Jezzard, P. (2004). Functional magnetic resonance imaging. *Journal of Neurology, Neurosurgery & Psychiatry*, 75(1), 6–12.
- Mattout, J., Phillips, C., Penny, W. D., Rugg, M. D., & Friston, K. J. (2006). MEG source localization under multiple constraints: an extended Bayesian framework. *NeuroImage*, 30(3), 753–767.
- McKie, S., & Brittenden, J. (2005). (ii) Basic science: magnetic resonance imaging. *Current Orthopaedics*, 19(1), 13–19.
- Meyer, F. G., & Chinrungrueng, J. (2005). Spatiotemporal clustering of fMRI time series in the spectral domain. *Medical Image Analysis*, 9(1), 51–68.
- Mohammed, A. N., Taha, T. E., & Faragallah, O. S. (2014). A Comparison of Joint ICA and Parallel ICA Multimodal Fusion Methods in Schizophrenia. *International Journal of Computer Applications*, 95(9).
- Moosmann, M., Ritter, P., Krastel, I., Brink, A., Thees, S., Blankenburg, F., ... Villringer, A. (2003). Correlates of alpha rhythm in functional magnetic resonance imaging and near infrared spectroscopy. *Neuroimage*, 20(1), 145–158.
- Niedermeyer, E. (1997). Alpha rhythms as physiological and abnormal phenomena. *International Journal of Psychophysiology*, 26(1–3), 31–49.
- Niedermeyer, E., & da Silva, F. H. L. (2005). *Electroencephalography: basic principles, clinical applications, and related fields*. Lippincott Williams & Wilkins.
- Niennattrakul, V., & Ratanamahatana, C. A. (2007). On clustering multimedia time series data using k-means and dynamic time warping. In *Multimedia and Ubiquitous Engineering, 2007. MUE'07. International Conference on* (pp. 733–738).
- Ogawa, S., Lee, T.-M., Kay, A. R., & Tank, D. W. (1990). Brain magnetic resonance imaging with contrast dependent on blood oxygenation. *Proceedings of the National Academy of Sciences*, 87(24), 9868–9872.
- Ogawa, S., Tank, D. W., Menon, R., Ellermann, J. M., Kim, S. G., Merkle, H., & Ugurbil, K. (1992). Intrinsic signal changes accompanying sensory stimulation: functional brain mapping with magnetic resonance imaging. *Proceedings of the National Academy of Sciences*, 89(13), 5951–5955.
- Otsu, N. (1975). A threshold selection method from gray-level histograms. *Automatica*, 11(285–296), 23–27.
- Penny, W. D., Holmes, A. P., & Friston, K. J. (2003). Random effects analysis. *Human Brain Function*, 2, 843–850.
- Petersen, S. E., & Dubis, J. W. (2012). The mixed block/event-related design. *Neuroimage*, 62(2), 1177–1184.
- Pflieger, M. E., & Greenblatt, R. E. (2001). Nonlinear analysis of multimodal dynamic brain imaging data. *Int. J. Bioelectromagnetism*, 3.
- Phillips, C., Mattout, J., Rugg, M. D., Maquet, P., & Friston, K. J. (2005). An empirical Bayesian solution to the source reconstruction problem in EEG. *NeuroImage*, 24(4), 997–1011.
- PIDOUX, B. (2007). Des {é}lectrodes contre les tics. *La Recherche*, (410), 66–67.
- Portas, C. M., Krakow, K., Allen, P., Josephs, O., Armony, J. L., & Frith, C. D. (2000). Auditory processing across the sleep-wake cycle: simultaneous EEG and fMRI monitoring in humans. *Neuron*, 28(3), 991–999.
- Purcell, E. M., Torrey, H. C., & Pound, R. V. (1946). Resonance absorption by nuclear magnetic moments in a solid. *Physical Review*, 69(1–2), 37.
- Raichle, M. E. (2009). A brief history of human brain mapping. *Trends in Neurosciences*, 32(2), 118–126.
- Raichle, M. E., & Mintun, M. A. (2006). Brain work and brain imaging. *Annu. Rev. Neurosci.*, 29, 449–476.
- Raichle, M. E., & Snyder, A. Z. (2007). A default mode of brain function: a brief history of an evolving idea. *Neuroimage*, 37(4), 1083–1090.
- Roy, C. S., & Sherrington, C. S. (1890). On the regulation of the blood-supply of the brain. *The Journal of Physiology*, 11(1–2), 85.
- Sakoe, H., & Chiba, S. (1978). Dynamic programming algorithm optimization for spoken word recognition. *IEEE Transactions on Acoustics, Speech, and Signal Processing*, 26(1), 43–49.
- Salek-Haddadi, A., Lemieux, L., Merschhemke, M., Friston, K. J., Duncan, J. S., & Fish, D. R. (2003). Functional magnetic resonance imaging of human absence seizures. *Annals of Neurology*, 53(5), 663–667.
- Sands, M. J., & Levitin, A. (2004). Basics of magnetic resonance imaging. In *Seminars in vascular surgery* (Vol. 17, pp. 66–82).
- Sanei, S., & Chambers, J. A. (2013). *EEG signal processing*. John Wiley & Sons.
- Sato, J. R., Rondinoni, C., Sturzbecher, M., de Araujo, D. B., & Amaro, E. (2010). From EEG to BOLD: brain mapping and estimating transfer functions in simultaneous EEG-fMRI acquisitions. *NeuroImage*, 50(4), 1416–1426.
- Schabus, M., Dang-Vu, T. T., Albouy, G., Balteau, E., Boly, M., Carrier, J., ... others. (2007). Hemodynamic cerebral correlates of sleep spindles during human non-rapid eye movement sleep. *Proceedings of the National Academy of Sciences*, 104(32), 13164–13169.
- Scherg, M., & Von Cramon, D. (1986). Evoked dipole source potentials of the human auditory cortex.

- Electroencephalography and Clinical Neurophysiology/Evoked Potentials Section*, 65(5), 344–360.
- Schocken, S., & Hummel, R. A. (1993). On the use of the Dempster Shafer model in information indexing and retrieval applications. *International Journal of Man-Machine Studies*, 39(5), 843–879.
- Shafer, G., & others. (1976). *A mathematical theory of evidence* (Vol. 1). Princeton university press Princeton.
- Shellhaas, R. A., Soaita, A. I., & Clancy, R. R. (2007). Sensitivity of amplitude-integrated electroencephalography for neonatal seizure detection. *Pediatrics*, 120(4), 770–777.
- Smets, P., & Kennes, R. (1994). The transferable belief model. *Artificial Intelligence*, 66(2), 191–234.
- Sokoloff, L. (1977). Relation between physiological function and energy metabolism in the central nervous system. *Journal of Neurochemistry*, 29(1), 13–26.
- Sorenson, J. A., & Wang, X. (1996). ROC methods for evaluation of fMRI techniques. *Magnetic Resonance in Medicine*, 36(5), 737–744.
- Spinelli, L. (1999). *Analyse spatiale de l'activité électrique corticale: nouveaux développements*. Université Joseph-Fourier-Grenoble I.
- Steinberg, A. N., Bowman, C. L., & White, F. E. (1999). Revisions to the JDL data fusion model. In *AeroSense '99* (pp. 430–441).
- Sturzbecher, M. J., Tedeschi, W., Cabella, B. C. T., Baffa, O., Neves, U. P. C., & De Araujo, D. B. (2008). Non-extensive entropy and the extraction of BOLD spatial information in event-related functional MRI. *Physics in Medicine and Biology*, 54(1), 161.
- Trujillo-Barreto, N. J., Martinez-Montes, E., Melie-Garcia, L., & Valdes-Sosa, P. (2001). A symmetrical Bayesian model for fMRI and EEG/MEG neuroimage fusion. *Int. J. Bioelectromagn*, 3(1), 1998–2000.
- Valdes-Sosa, P. A., Sanchez-Bornot, J. M., Sotero, R. C., Iturria-Medina, Y., Aleman-Gomez, Y., Bosch-Bayard, J., ... Ozaki, T. (2009). Model driven EEG/fMRI fusion of brain oscillations. *Human Brain Mapping*, 30(9), 2701–2721.
- Van Essen, D. C., & Deyoe, E. A. (1995). Concurrent processing in the primate visual cortex. *The Cognitive Neurosciences*, 383–400.
- van Geuns, R.-J. M., Wielopolski, P. A., de Bruin, H. G., Rensing, B. J., van Ooijen, P. M. A., Hulshoff, M., ... de Feyter, P. J. (1999). Basic principles of magnetic resonance imaging. *Progress in Cardiovascular Diseases*, 42(2), 149–156.
- Yager, R. R. (2001). Dempster--Shafer belief structures with interval valued focal weights. *International Journal of Intelligent Systems*, 16(4), 497–512.
- Yao, J., & Dewald, J. P. A. (2005). Evaluation of different cortical source localization methods using simulated and experimental EEG data. *Neuroimage*, 25(2), 369–382.

## ***Abstract:***

Electroencephalogram (EEG) and functional magnetic resonance imaging (fMRI) are two very effective noninvasive techniques for revealing a detailed mapping of brain activity. The fusion of such multimodal data has gradually become a major area of interest in many researches. Simultaneous EEG-fMRI recording has been extensively used in several fields, especially in the field of medical imaging and neuroimaging where researchers have developed numerous methods to study the brain activity. EEG-fMRI fusion permits to provide a better insight of the brain with a good spatiotemporal resolution.

In this thesis, we are interested in the different models of exploration of the brain activity and EEG-fMRI data fusion methods. Our research focuses on the development and application of new techniques that will be able to analyze EEG and fMRI data simultaneously.

In line with this scope, we have developed a theoretical framework, for fusing these two modalities, based on Dempster shafer theory commonly known as belief theory or the theory of evidence. This theory permits; on the one hand, to study the cerebral activity by using fMRI data and on the other hand to develop a new approach based on symmetric methods for the analysis of the EEG-fMRI multimodal data. We can sum up the main contribution of this thesis as follows:

1. To analyze the functional Magnetic Resonance Imaging (fMRI) data, we have proposed a new method based on Dynamic Time Warping (DTW) and where detestation of cerebral activities is made by a segmentation of the image by the so-called technique of PHA (*Potential-Based Hierarchical Agglomerative*).
2. A second method has been proposed to map the brain bu using the Dempster-Shafer theory (DS) that is considered as an efficient theoretical framework for the analysis and representation of uncertain data. Dempster-Shafer permits to mark the activated voxels in fMRI images. The activated brain regions linked to a given stimulus are detected by using the belief measure ( $bel()$ ) as a metric for evaluating the activity of voxels in question . The comparison of the proposed method with the t-test and the GLM method has clearly shown its ability to precisely detect the activated voxels.
3. Finally, EEG-fMRI data fusion permits to obtain a better knowledge of the cerebral activity due to the high spatiotemporal resolution provided and for which we have proposed a theoretical fusion framework based on the Dempster Shafer theory allowing to take the two EEG and fMRI modalities simultaneously. In the simulation phase, artificial data and real auditory data have been used to assess the performance of the proposed approach. In addition, true and false activation rates (TAR, FAR) and Receiver Operating Characteristic (ROC) curves have been used to compare with the jointICA method. The obtained results have clearly shown the effectiveness of the introduced approach to reveal the activated areas of the brain.

**Keywords**— EEG-fMRI data fusion; symmetric as-symmetric approach; BOLD, HRF; Dempster Shafer theory; Dynamic Time Warping; PHA method; fMRI; GLM; t-test;jointICA; OTSU method;

## Résumé

L'électroencéphalogramme (EEG) et l'imagerie par résonance magnétique fonctionnelle (IRMf) sont deux techniques non invasives très efficaces servant à révéler une cartographie détaillée de l'activité cérébrale. La fusion des données multimodales est progressivement devenue un domaine d'intérêt majeur dans de nombreuses recherches. L'enregistrement simultané d'EEG-IRMf a été largement utilisé dans plusieurs domaines, en particulier dans le domaine de l'imagerie médicale et la neuroimagerie où les chercheurs ont développé beaucoup d'outils et de méthodes afin d'étudier l'activité cérébrale. La fusion EEG-IRMf permet une meilleure connaissance du cerveau avec une bonne résolution spatiotemporelle.

Dans cette thèse, nous nous sommes intéressés aux différents modèles d'exploration de l'activité cérébrale ainsi qu'aux méthodes de fusion des données EEG-IRMf. Notre recherche concerne principalement le développement et l'application de nouvelles techniques qui seront en mesure d'analyser les données EEG et IRMf simultanément. Pour cela nous avons développé un cadre théorique, pour la fusion de ces deux modalités, basé sur la théorie Dempster Shafer appelée communément théorie des croyances ou théorie de l'évidence. Cette théorie nous a servie, d'une part, à l'étude de l'activité cérébrale en utilisant des données d'IRMf et d'autre part, à élaborer une nouvelle approche basée sur les méthodes symétriques pour l'analyse des données multimodales EEG-IRMf. Nous pouvons résumer les principales contributions de cette thèse comme suit :

- 1- Afin d'analyser les données d'imagerie par résonance magnétique fonctionnelle (IRMf), nous avons proposé une nouvelle méthode basée sur la distance d'alignement temporel dynamique (*Dynamic Time Warping : DTW*) et où la détection d'activités cérébrales se fait via une segmentation de l'image par la technique dite dePHA (*Potential-Based Hierarchical Agglomerative*).
- 2- Une deuxième méthode a été proposée pour cartographier le cerveau par usage de la théorie de Dempster-Shafer (DS) considérée comme cadre théorique efficace pour l'analyse et la représentation des données incertaines. Cette dernière nous a permis de marquer les voxels activés dans les images IRMf. Les zones du cerveau activées liées à un stimulus externe sont détectées en utilisant la mesure de croyance ( $bel()$ ) comme une métrique pour évaluer l'activité des voxels en question. La comparaison de la méthode proposée avec le t-test et la méthode GLM a clairement montré sa capacité à bien détecter correctement les voxels activés.
- 3- Enfin, la fusion des données EEG-IRMf nous a permis d'obtenir une meilleure connaissance de l'activité cérébrale du cerveau en raison de la résolution spatiotemporelle élevée qui en découle et pour laquelle nous avons proposé un cadre théorique de fusion basé sur la théorie de Dempster Shafer permettant de prendre les deux modalités EEG et IRMf simultanément. Dans la phase de simulation, des données artificielles et données auditives réelles ont été utilisées pour évaluer la performance de l'approche proposée. En outre, les taux d'activation vrais et faux (TAR, FAR) et courbe ROC (*Receiver Operating Characteristic*) ont été utilisés pour établir une comparaison avec la méthode de *jointICA*. Les résultats obtenus montrent clairement l'efficacité de l'approche introduite pour révéler les zones actives du cerveau.

## ملخص:

رسم تخطيط الكهربي للدماغ (EEG) والتصوير بالرنين المغناطيسي الوظيفي (fMRI) هما تقنيات فعالة جدا تستعمل للكشف عن رسم خرائط مفصلة لنشاط الدماغ. أصبح دمج البيانات متعددة الوسائط تدريجيا مجالا رئيسيا من مجالات الاهتمام في العديد من الدراسات. وقد استخدم تسجيل في وقت واحد EEG-الرنين المغناطيسي الوظيفي على نطاق واسع في العديد من المجالات، وخاصة في مجال التصوير الطبي والتشخيص التصويري للأعصاب حيث طور الباحثون العديد من الأدوات والأساليب لدراسة نشاط الدماغ. يوفر EEG-الرنين المغناطيسي الوظيفي معرفة أفضل للدماغ مع دقة تحديد المنطقة الناشطة.

في هذه الأطروحة، نحن مهتمون في نماذج مختلفة من استكشاف نشاط الدماغ وطرق دمج من البيانات EEG-الرنين المغناطيسي الوظيفي. أبحاثنا تتعلق أساسا تطوير وتطبيق تقنيات جديدة من شأنها أن تكون قادرة على تحليل EEG والبيانات الرنين المغناطيسي الوظيفي في وقت واحد. لهذا قمنا بتطوير إطار نظري للاندماج بين البيانات، على أساس نظرية ديمبستر شافر يسمى عادة نظرية الاعتقاد أو نظرية الأدلة. عملت هذه النظرية لنا، أولا، لدراسة نشاط الدماغ باستخدام بيانات الرنين المغناطيسي الوظيفي، وثانيا، لوضع نهج جديد يستند إلى أساليب متناظرة لتحليل البيانات المتعدد الوسائط EEG-الرنين المغناطيسي الوظيفي. يمكننا تلخيص المساهمات الرئيسية لهذه الرسالة على النحو التالي:

- 1- من أجل تحليل البيانات التصوير بالرنين المغناطيسي الوظيفي (الرنين المغناطيسي الوظيفي)، اقترحنا طريقة جديدة تقوم على الوقت الديناميكي واريبنغ (دتو) وحيث يكره أنشطة الدماغ مصنوعة من خلال تجزئة البيانات من قبل ما يسمى بتقنية (PHA (Potential-Based Hierarchical Agglomerative)).
- 2- تم اقتراح طريقة ثانية لتخطيط المخ باستخدام نظرية ديمبستر-شافر (DS) كإطار نظري فعال لتحليل وتمثيل البيانات غير المؤكدة. هذا الأخير سمح لنا للاحتفال فوزيلس تفعيلها في الصور الرنين المغناطيسي الوظيفي. تم الكشف عن مناطق المخ النشطة المرتبطة التحفيز الخارجي باستخدام بيل (Bel()) قياس كمقياس لتقييم نشاط فوزيلس في السؤال. وأظهرت المقارنة بين الطريقة المقترحة مع اختبار T-test- وطريقة GLM بوضوح قدرته على الكشف عن voxels التي تم تفعيلها بشكل صحيح.
- 3- وأخيرا، مزيج من البيانات EEG-الرنين المغناطيسي الوظيفي سمح لنا للحصول على فهم أفضل للدماغ بسبب القرار المكانية والزمانية عال من نشاط الدماغ الناتجة عن ذلك، والتي اقترحنا إطارا نظريا على أساس الاندماج نظرية ديمبستر شافر السماح لاتخاذ اثنين EEG وطرق الرنين المغناطيسي الوظيفي في وقت واحد. وفي مرحلة المحاكاة، استخدمت بيانات اصطناعية وبيانات سمعية حقيقية لتقييم أداء النهج المقترح. بالإضافة إلى ذلك، تم استخدام معدلات تفعيل صحيحة وكاذبة (FAR، TAR) ومنحنيات تشغيل الخصائص (ROC) منحنيات لمقارنة مع طريقة jointICA. و تبين النتائج التي تم الحصول عليها بوضوح فعالية النهج الذي أدخل للكشف عن المناطق النشطة من الدماغ.